DOCTORAL SCHOOL
UNIVERSITY *MEDITERRANEA* OF REGGIO CALABRIA

DIPARTIMENTO DI INGEGNERIA CIVILE, ENERGIA,
AMBIENTE E MATERIALI (DICEAM)

PHD IN
CIVIL, ENVIRONMENTAL AND SAFETY ENGINEERING

PARTNERSHIP BETWEEN
UNIVERSITY *MEDITERRANEA* OF REGGIO CALABRIA
UNIVERSITY OF MESSINA

S.S.D. ING-IND/31
XXXIII Cycle

BRAIN SOURCE LOCALIZATION BASED ON LOW RESOLUTION ELECTROMAGNETIC TOMOGRAPHY (LORETA)

CANDIDATE
SERENA DATTOLA
Serena Dattola

ADVISOR
Prof. Ing. FABIO LA FORESTA

COORDINATOR
Prof. FELICE ARENA
Felice Arena

REGGIO CALABRIA, FEBRUARY 2021

SERENA DATTOLA

BRAIN SOURCE LOCALIZATION BASED ON LOW RESOLUTION ELECTROMAGNETIC TOMOGRAPHY (LORETA)

Acknowledgements

First of all, I would like to express my gratitude to my advisor Prof. Fabio La Foresta. I have really appreciated his valuable suggestions, encouragement and confidence in me throughout these years.

Besides my advisor, I would like to thank Prof. Francesco Carlo Morabito, whose experience and wisdom were an example to me.

I would also like to thank my precious "travel companions" of Neurolab team, who supported and endured me every day. In particular, a special thanks goes to Dr. Nadia Mammone for her valuable help, insightful advice and moral support.

All of you have been a second family to me and have deeply contributed to both my professional and personal growth.

Moreover, I would like to thank all the doctors and researchers of IRCCS Centro Neurolesi Bonino Pulejo Messina (Italy) for providing the EEG datasets, processed in my research activity.

Finally, I would like to thank the reviewers and members of my PhD doctoral committee for reading and reviewing this thesis.

Contents

List of Tables

List of Figures

I

Introduction

The brain is the most complex organ of the human body. Billion of nerve cells, the neurons, transmit and receive information from other neurons. Therefore, this massive information exchange creates a functionally interconnected network, which is responsible for every process that regulates our body.

During the last century, the development of several brain imaging techniques has provided new tools for capturing information about the structure and functions of the brain, useful in both clinical applications and cognitive neuroscience. Among these techniques, one of the most popular is electroencephalography (EEG), which records brain electric activity by means of electrodes placed on the scalp. EEG is widely employed because it is a non-invasive tool, easy-to-use, portable and relatively low cost. For years EEG has been recorded by a few number of electrodes according to the International 10-20 system. Nowadays, the limited spatial resolution of standard EEG can be improved using High-Density EEG (HD-EEG) systems, which include up to 256 electrodes.

The localization of brain sources from EEG data is a very important matter to understand brain physiology and highlight any alterations in the presence of pathological conditions. Source localization consists in solving the so-called EEG inverse problem. Over the years, researchers have developed many methods for solving it.

In particular, this thesis focuses on the LORETA (Low Resolution Electromagnetic Tomography) method, which is one of the most accurate technique for brain source localization. Specifically, the first objective of the present work is to employ LORETA for investigating three different neurological diseases: Alzheimer's Disease (AD), gliotic lesions and stroke. The second objective is to compare the results obtained applying LORETA to standard EEG and HD-EEG.

I.1 Thesis outline

The structure of this thesis can be summarized as follows:

- **Chapter 1**: this chapter describes the basics of the anatomy of the human brain and its main functions. Then, the electroencephalography is described and both standard EEG and HD-EEG montages are shown.
- **Chapter 2**: this chapter introduces the EEG inverse problem and its resolution. In particular, the chapter focuses on the description of the LORETA method and the most recent algorithms belonging to this family of inverse solutions (sLORETA and eLORETA). Finally, a literature review of the findings about LORETA applied to HD-EEG is presented.
- **Chapter 3**: this chapter describes the activity research, conducted during the PhD course, by means of LORETA, applied to both standard EEG and HD-EEG data. Specifically, first the studies that investigate the brain active source reconstruction and the functional connectivity in Alzheimer's disease are presented. Then, an application of LORETA in the case of gliotic lesions is described. Finally, a study about stroke is reported.
- **Chapter 4**: this chapter addresses conclusions and future developments.

I.2 List of publications

The studies described in this thesis have been published in different journals. The list of all publications produced during the PhD course is provided below.

Journals

- Dattola, S., & La Foresta, F. (2020). An eLORETA Longitudinal Analysis of Resting State EEG Rhythms in Alzheimer's Disease. Applied Sciences, 10(16), 5666.
- Formica, C., De Salvo, S., Micchìa, K., La Foresta, F., Dattola, S., Mammone, N., ... & Bramanti, A. (2020). Cortical Reorganization after Rehabilitation in a Patient with Conduction Aphasia Using High-Density EEG. Applied Sciences, 10(15), 5281.
- Dattola, S., Morabito, F. C., Mammone, N., & La Foresta, F. (2020). Findings about LORETA Applied to High-Density EEG—A Review. Electronics, 9(4), 660.
- La Foresta, F., Morabito, F. C., Marino, S., & Dattola, S. (2019). High-density EEG signal processing based on active-source reconstruction for brain network analysis in alzheimer's disease. Electronics, 8(9), 1031.

Book chapters

- Dattola, S., Inuso, G., Mammone, N., Bonanno, L., De Salvo, S., Morabito, F. C., & La Foresta, F. eLORETA Active Source Reconstruction Applied to HD-EEG in Alzheimer's Disease. In Progresses in Artificial Intelligence and Neural Systems (pp. 575-583). Springer, Singapore.
- Dattola, S., La Foresta, F., Bonanno, L., De Salvo, S., Mammone, N., Marino, S., & Morabito, F. C. (2020). Effect of Sensor Density on eLORETA Source Localization Accuracy. In Neural Approaches to Dynamics of Signal Exchanges (pp. 403-414). Springer, Singapore.
- Mammone, N., De Salvo, S., Marino, S., Bonanno, L., Ieracitano, C., Dattola, S., ... & Morabito, F. C. (2020). Estimating the Asymmetry of Brain Network Organization in Stroke Patients from High-Density EEG Signals. In Neural Approaches to Dynamics of Signal Exchanges (pp. 475-483). Springer, Singapore.
- Inuso, G., La Foresta, F., Mammone, N., Dattola, S., & Morabito, F. C. (2017, June). Evolution Characterization of Alzheimer's Disease Using eLORETA's Three-Dimensional Distribution of the Current Density and Small-World Network. In Italian Workshop on Neural Nets (pp. 155-162). Springer, Cham.

1

Electroencephalography

1.1 Introduction

Brain imaging refers to several techniques which map the structure and functions of the brain, used for investigations in cognitive neuroscience and clinical applications. These techniques include, among others, positron emission tomography (PET), single photon emission computer tomography (SPECT), functional magnetic resonance imaging (fMRI), magnetoencephalography (MEG) and electroencephalography (EEG). Imaging techniques differ according to several factors, such as spatial and temporal resolution, invasiveness and cost [1]. In particular, EEG is a non-invasive diagnostic tool which records the electrical signals, generated by neurons, from electrodes placed on the head surface. For its non-invasiveness and its relatively low cost, over the years EEG has become a powerful instrument successfully employed in different fields, such as neurosurgery, neurology, and cognitive science. As the results reported in this thesis are based on EEG data processing, this Chapter provides an overview of the brain anatomy and its main function (Section 1.2), and describes electroencephalography (Section 1.3).

1.2 Anatomy of the brain

The brain is the main organ of the central nervous system and is located inside the skull. The nervous tissue is made up of about 86 billion neurons, organized in a very complex network. The brain consists of three structures: the cerebrum, the cerebellum and the brain stem (Figure 1.1).

The *cerebrum* is separated from the other parts of the brain by a horizontal plane going through the upper surface of the cerebellum. It represents the largest part of the brain and is responsible for extremely complex functions, including processing information from the sense organs (sight, hearing, taste, touch, smell), producing language, and controlling movement. Emotions, reasoning and learning also originate in the cerebrum. The cerebrum is divided by the longitudinal fissure into the left and right cerebral hemispheres. The corpus callosum connects the two hemispheres. Each hemisphere controls the opposite side of the body and is divided into four main lobes: frontal, temporal, parietal, and occipital (Figure 1.1). Each lobe is related to different brain functions. In particular:

- Frontal lobe: its main functions are related to body movements, language, planning and problem-solving skills, behavioural and emotional control.
- Parietal lobe: it combines the sensory information such as touch, temperature and pain from the skin. It is also involved in language processing and spatial perception.
- Occipital lobe: it includes most of the anatomical regions of the visual cortex so it is involved in visual-spatial processing, colour recognition and motion perception.
- Temporal lobe: it controls auditory and visual memories, language comprehension, speech and emotion association.

The outer layer of the cerebrum is the *cerebral cortex*. Its thickness is between 2 and 4 mm – it is thinner in the primary sensory areas and thicker in the motor and associative areas. The characteristic folded structure of the cortex increases the surface area and thus the space available. Each fold is referred to as a "gyrus", and each groove between the folds as a "sulcus". The *Brodmann map* is the most used cortical map, which divided the cortex into 52 areas on the basis of the cytoarchitectural organization of neurons (Figure 1.2).

The *cerebellum* is located just below the brain. It is involved in the coordination of movements, equilibrium, the ability to maintain an upright position and correct posture, and the ability to pay attention.

The *brain stem* includes the midbrain, the pons and the medulla oblongata, and connects the brain and the cerebellum with the spinal cord. It regulates many automatic functions, including breathing, heartbeat, digestion, thermoregulation, sleep-wake cycles, involuntary stimuli (sneezing, coughing, vomiting).

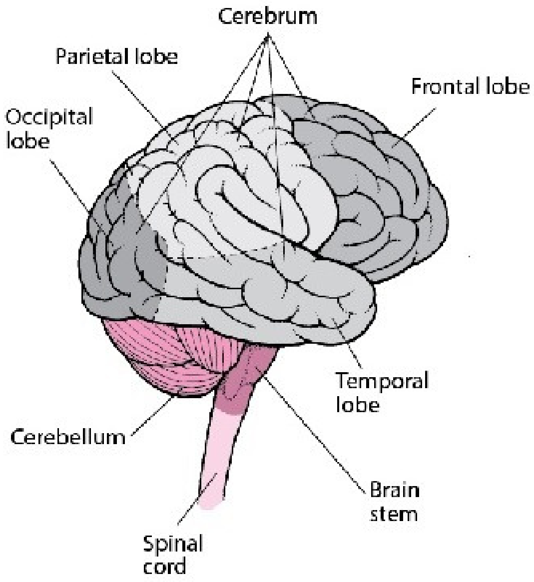

Fig. 1.1: Overview of the brain.

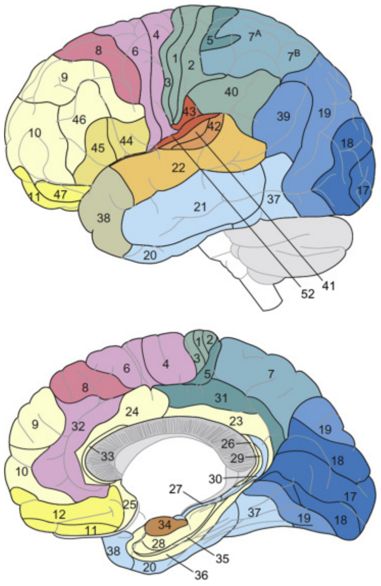

Fig. 1.2: Brodmann areas. (Source: Adapted by Bernard J. Baars from M. Dubin, with permission; drawn by Shawn Fu.)

1.3 Electroencephalography

Electroencephalography is a technique used for recording the brain electrical activity from electrodes placed on the scalp. It was introduced by Hans Berger, who recorded the first human EEG in 1929, and described for the first time the alpha and beta waves [2]. EEG measures the potentials generated by large populations of neurons in the brain. The electrical activity can be spontaneous, the consequence of a stimulus or caused by the execution of any task. In order to generate a measurable EEG, a large number of simultaneously active neurons are needed. The electric potentials generated by neurons can be represented by dipoles. The EEG signal recorded by a single electrode does not only arise from the electrical activity of the regions underlying it—in fact, it detects the contribution of all sources, due to the conductivity of the scalp and the tissues. Consequently, the use of a realistic head model is fundamental to making EEG analysis more accurate [3]. For its non-invasiveness and its relatively low cost, over the years EEG has become a valuable tool for studying the brain. Because of its excellent temporal resolution, on the order of milliseconds, EEG is well-suited to analyze the dynamics of brain functions; on the other hand, EEG has a modest spatial resolution.

EEG pre-processing is a very important step in EEG signal analysis. The EEG is affected by unwanted components, called artifacts, which can have a physiological origin (eye artifacts, muscle artifacts) or derive from instrumentation (movement of cables, material used as a conductive gel between the electrodes and the scalp). Therefore, after the signal acquisition, the various types of artifacts have to be identified and removed by means of rejection methods based on automatic or visual detection [4]. Another crucial issue concerns the reference electrode. As it is known, the EEG consists of a relative measurement, not an absolute one, because it detects the potential differences between two points. The properties of the reference, determined by its physical position or by the calculation method, affects the EEG measurements [5, 6]. When a large number of electrodes is employed, it would be advisable to use the average reference, according to which the signal of each electrode, acquired in physical reference, is referred to a virtual value resulting from the average of the signals coming from all the electrodes [7].

1.3.1 EEG rhythms

The EEG signal band ranges from about 1 to 50 Hz, although the largest amount of information content is typically found within 30 Hz. The signal amplitude is between 10 and 100 μV. The EEG frequency band is usually divided into sub-bands (delta (δ), theta (θ), alpha (α), beta (β)), which are related to specific physiological and functional states of the brain (Figure 1.3) [8]:

- δ band (0.5–4 Hz): delta waves are the slowest waves. They are normally present in babies. Delta rhythm is also detected in adults affected by certain brain disorders (brain lesions, encephalopathies, epilepsy). Moreover, delta waves are typical of non-REM sleep (slow-wave sleep);
- θ band (4–8 Hz): theta waves are dominant in young children and also occurs in the first stage of sleep (in healthy subjects);
- α band (8–13 Hz): alpha waves appear in waking and resting state conditions. They differ in slow (8–9 Hz), intermediate (9–11.5 Hz) and fast (11.5–13 Hz) alpha waves, with an average voltage of 40–50 μV. Alpha rhythms are commonly observed in the posterior brain region;
- β band (13–32 Hz): beta waves are dominant in a subject with open eyes during intense brain activity. Beta waves are also present in alert state and in REM sleep. Beta rhythm is divided into slow beta (13.5–18 Hz) and fast beta (18.5–32 Hz), with a voltage of about 10–15 μV.

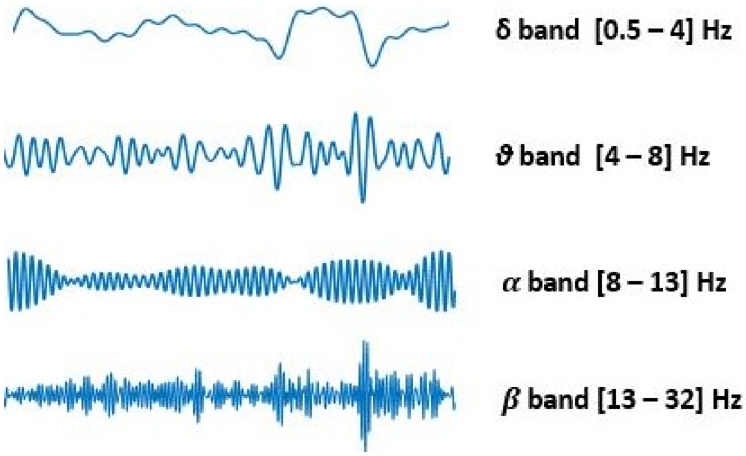

Fig. 1.3: EEG sub-bands.

1.3.2 EEG montages

The two following subsections describe the most commonly used systems for the electrode arrangement on the scalp.

Low-density EEG

For years, the position of the electrodes on the head surface was set according to the International 10–20 System [9]. Electrode placement is based on four reference points on the head surface: nasion, inion, left and right preauricular points. “10–20” refers to the distance between adjacent electrodes, that is 10% or 20% of the length inion-nasion and left-right preauricular points. The use of percentages instead of fixed distances allows to preserve the correspondence between the electrodes and the underlying brain areas, whatever the size of the head [10]. Each location site is associated with letters and numbers. Fp, F, C, P and O denote the frontopolar, frontal, central, parietal and occipital areas, respectively. Even numbers indicate the right hemisphere, odd numbers the left one, and “z” identifies the midline (Figure 1.4). The maximum electrodes number is 21.

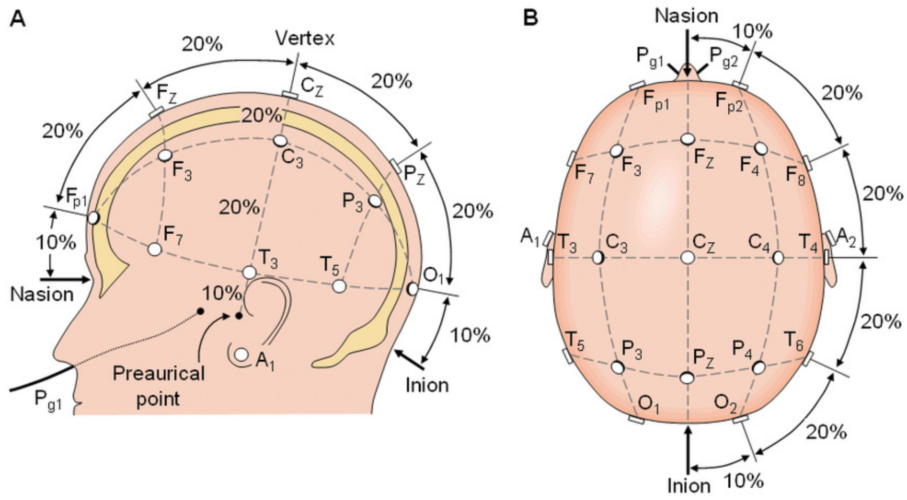

Fig. 1.4: Electrode location on the scalp according to the 10–20 system [10]. (**A**) Lateral view of the skull. (**B**) Superior view of the skull.

High-density EEG (HD-EEG)

Over the years, the sampling of the scalp potential has been a matter broadly discussed by many researchers [11]. A correct spatial sampling, in fact, is essential to avoid aliasing and mislocalization of the sources [12]. In 1985, Chatran et al. proposed the 10–10 system, which is made up of 81 electrodes [13]. It was obtained adding 60 supplementary electrodes to the 21 of the 10–20 system (Figure 1.5a). After some modifications it became the standard of the American Clinical Neurophysiology Society and the International Federation of Clinical Neurophysiology. Later, the results of several studies showed that the interelectrode distance should be between 1 cm and 3 cm, which implies the use of at least 100 electrodes [14–16]. Therefore, a further extension of the 10–10 system was introduced, the so-called 10-5 system, which consists of 345 electrode locations [17] (Figure 1.5b). However, today the EEG acquisition systems on the market include no more than 256 electrodes.

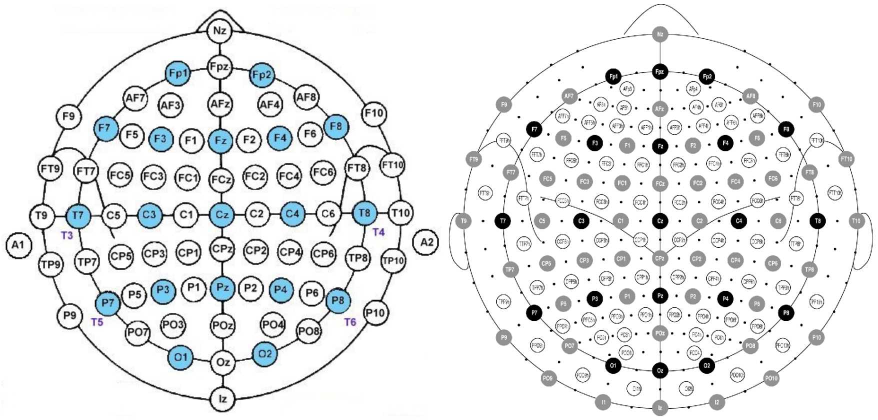

(a) (b)

Fig. 1.5: (**a**) Electrode positions in the 10–10 system; light blue circles denote the 10-20 electrode positions. (**b**) Electrode positions in the 10-5 system; dots indicate the positions added to the 10–10 system.

2

EEG Source Localization

2.1 Introduction

Estimating the location of sources generating the electric signals is a key issue for diagnosing pathological conditions in the brain. As for the clinical applications, EEG source localization has been widely used in epilepsy, for detecting the epileptogenic zones generating seizures. The localization of brain sources is also the first step for functional connectivity analysis, useful for monitoring the evolution of neurodegenerative disorders, such as Alzheimer's Disease. Moreover, EEG source localization has become a common procedure for detecting the brain areas activated as a result of performing specific tasks. Finally, although to a lesser extent, psychiatric disorders have been investigated by means of EEG source localization methods.

Reconstructing the distribution of the current density starting from EEG measurements is termed as EEG inverse problem. During the last two decades, LORETA (Low Resolution Electromagnetic Tomography) has been one of the most employed algorithm for the brain source localization, turning out to be a promising tool in several clinical fields. In Section 2.2 the formulation of the EEG inverse problem and the LORETA method are presented. Section 2.3 provides a literature overview of the results achieved by applying LORETA to HD-EEG.

2.2 EEG inverse problem

The localization of active brain sources is a very important matter concerning the EEG. This issue is termed as EEG inverse problem. Generally speaking, the inverse problem consists of two phases, namely an estimation problem and an evaluation problem: it can be considered as a combination of what needs to be estimated and the relationship between the estimated models and the real ones. The activation of a configuration of known brain sources generates a well-defined electric and magnetic field. Therefore, it is possible to predict the potential differences recorded on the scalp from the current densities of the sources. This is the so-called forward problem, which provides a unique solution. On the other hand, the inverse problem is an ill-posed problem: it does not produce a unique solution because more than one combination of simultaneously active sources can generate the same electric field on the head surface. Therefore, in order to estimate the locations of the sources from the potential differences on the scalp, some biophysical and mathematical constraints must be imposed [18]. Regardless of the method employed, over the years the improvement in source localization accuracy using HD-EEG systems has been proved by several studies [19–21]. Moreover, analyzing simulated EEG data, it was shown that the accuracy in source localization was better when the sensors were distributed on the whole head surface (not only the superior head regions) [22].

The algorithms for solving the EEG inverse problem can be classified in two main groups—parametric and non parametric methods [23]. The parametric methods assume that the EEG signals arise from a small number of point sources, whose location and orientation are unknown: in this case the number of dipoles is chosen a priori (*Equivalent Current Dipole* approach).

Over the years, these kind of algorithms are being replaced by the introduction of the non parametric methods, which assume that several sources with fixed positions are distributed across the brain volume (*Distributed Source Models* approach). Among the latter methods, the minimum norm estimate was the first one which produced an instantaneous, distributed, discrete, linear solution, but it showed a misplacement of deep source onto the outermost cortex [24]. The issue of large localization errors was solved with the introduction of the Low Resolution Electromagnetic Tomography (LORETA) [25].

2.2.1 LORETA

LORETA, introduced in 1994, represented an innovative method in the field of high temporal resolution neuroimaging, since it allowed a three-dimensional reconstruction of the brain electrical activity distribution and proposed a linear solution to the inverse problem, valid from the neurophysiological point of view [25]. The brain volume is divided in a three-dimensional grid, made up of 2394 voxels at 7 mm spatial resolution. LORETA uses a three-shell spherical head model registered to the Talairach human brain atlas [26]. Each source has a fixed position on a grid point (voxel) and is defined by a current density vector with unknown components. The intensity and direction of the electrical activity at each point determine the electromagnetic field measured on the scalp. The solution space is restricted to grey matter and hippocampus. From a physiological point of view, the solution takes into consideration that neighboring neurons have a higher probability of being simultaneously active. Hence, the model assumes that nearby points have a certain probability of being synchronized (in terms of orientation and intensity) as compared with points distant from each other. Among the possible infinite reconstructions of the active generators, starting from a set of data recorded on the scalp, LORETA chooses the smoothest. Mathematically, this is performed by using a discrete spatial Laplacian operator. As a consequence, LORETA has a relatively low spatial resolution since produces blurred images, maintaining the location of the maximal activity, but with a certain amount of dispersion. Nevertheless, its average localization error is only one grid unit. Compared to other methods for solving the inverse problem, LORETA has shown a greater accuracy in localizing deep neuronal sources [27].

The general inverse problem can be expressed as [28]

$$\min_J F_W \tag{2.1}$$

with

$$F_W = \|\mathbf{\Phi} - \mathbf{KJ}\|^2 + \alpha \mathbf{J}^T \mathbf{WJ} \tag{2.2}$$

where $\mathbf{\Phi} \in R^{N_E x 1}$ is the vector of the electric potential differences measured at N_E electrodes with respect to a single common reference electrode; $\mathbf{K} \in R^{N_E x (3N_V)}$ is the lead field matrix corresponding to N_v voxels; $\mathbf{J} \in R^{(3N_V)x1}$ is the current density; $\alpha > 0$ is the Tikhonov regularization parameter [29]. It is assumed that the EEG measurements and the lead field are average reference transformed.

The solution is

$$\hat{\mathbf{J}}_{\mathbf{W}} = \mathbf{T}_{\mathbf{W}} \mathbf{\Phi} \tag{2.3}$$

where $\mathbf{T}_{\mathbf{W}}$ is the pseudoinverse, given by

$$\mathbf{T}_W = \mathbf{W}^{-1} \mathbf{K}^T (\mathbf{K} \mathbf{W}^{-1} \mathbf{K}^T + \alpha \mathbf{H})^+ \tag{2.4}$$

The matrix $\mathbf{H}$ is the average reference operator. For LORETA, the matrix $\mathbf{W}$ denotes the squared spatial discrete Laplacian operator.

2.2.2 sLORETA

A few years later, the authors of LORETA proposed a new method, called Standardized Low Resolution Electromagnetic Tomography (sLORETA), based on the noise normalized current density approach [30]. This method no longer uses the Laplacian operator and is based on the standardization of the current density [31]. In particular, the current density estimation is obtained using the minimum norm solution and is standardized by means of its variance. In this case, unlike the Dale method [30], the variance considers not only the noise caused by the EEG measurements but also the biological noise deriving from the actual sources. So, the electric potential variance is

$$\mathbf{S}_{\mathbf{\Phi}} = \mathbf{K}\mathbf{S}_{\mathbf{J}}\mathbf{K}^T + \mathbf{S}_{\mathbf{\Phi}}{}^{Noise} \tag{2.5}$$

where $\mathbf{S}_{\mathbf{\Phi}}{}^{Noise}$ is the variance of the noisy measurements and $\mathbf{S}_{\mathbf{J}}$ is the variance of the current density. According to the Bayesian point of view, the actual source variance, that is the current density variance (prior), is equal to the identity matrix. Therefore, the variance of the estimated current density can be written as

$$\mathbf{S}_{\hat{\mathbf{J}}} = \mathbf{T}\mathbf{S}_{\mathbf{\Phi}}\mathbf{T}^T = \mathbf{T}(\mathbf{K}\mathbf{K}^T + \alpha\mathbf{H})\mathbf{T}^T = \mathbf{K}^T[\mathbf{K}\mathbf{K}^T + \alpha\mathbf{H}]^+\mathbf{K} \tag{2.6}$$

Finally, sLORETA is given by the estimates of standardized current density power:

$$\sigma_v^T \sigma_v = \hat{j}_v^T [S_{\hat{j}}]_v^{-1} \hat{j}_v \tag{2.7}$$

where $[S_{\hat{j}}]_v$ is the vth 3×3 diagonal matrix in $[S_{\hat{j}}]$.

In sLORETA a more realistic head model is used, applying the boundary elements method (BEM) to the MNI152 template [32]. Unlike LORETA, the brain volume consists of 6239 voxels at 5 mm spatial resolution. The simulations showed that sLORETA has zero localization error in ideal (no-noise) conditions and the lowest localization error as compared with the minimum norm and the Dale methods in the presence of measurement and biological noise [31].

2.2.3 eLORETA

The need to further reduce the localization error led to the formulation of the Exact Low Resolution Electromagnetic Tomography (eLORETA) algorithm. eLORETA introduced a weight matrix which takes the deeper sources into account in a more adequate way [33]. The eLORETA solution is computed by Equation (2.4), where the weight matrix $\mathbf{W}$ has the following expression:

$$\mathbf{W}_v = [\mathbf{K}_v^T(\mathbf{K}\mathbf{W}^{-1}\mathbf{K}^T + \alpha\mathbf{H})^+\mathbf{K}_v]^{1/2} \tag{2.8}$$

The matrix $\mathbf{W}_v \in R^{3\times 3}$ is the vth diagonal subblock of $\mathbf{W}$. eLORETA is a genuine inverse solution with zero localization error in the presence of measurement and structured biological noise.

eLORETA outperforms sLORETA in terms of resolution and localization error, as reported in [34]. In particular, seventeen subjects underwent a visual stimulus and the corresponding ERP data were collected by 25 electrodes. The active source reconstruction was performed with both sLORETA and eLORETA methods. The comparison between the resulting images at four different time instants showed that eLORETA removes less significant sources and generates less blurred images as compared with sLORETA.

2.3 LORETA applied to HD-EEG: a review

Recently, high-density montages have been employed for recording the EEG signals, in order to improve the low spatial resolution deriving from the traditional EEG systems. The next subsections focus on the LORETA method applied to HD-EEG, classifying the results according to their clinical application.

2.3.1 Event-Related Potentials (ERP)

Event-Related Potentials (ERPs) are electrical signals time locked to sensory, motor or cognitive stimuli, which reflect the timing of the information processing in the brain. ERP waveforms (components), described on the basis of their amplitude and latency, provide useful information about sensory, cognitive and emotional processes both in healthy and brain-injured subjects. In this section we focused on the results about the localization of ERP neuronal sources in healthy subjects.

In the study reported in Reference [35], ten healthy subjects performed a visual task, which consisted in discriminating between a perspective drawing of an object existing in the 3D world (possible object) and perspective drawing of an object which can not exist in the 3D world (impossible object). The EEG were recorded by 72 channels. A significant difference between possible and impossible conditions in current density was found in the right inferior fusiform gyrus, suggesting that this region is involved in cognitive processes of discrimination between spatially possible and impossible objects.

The word repetition effects on the implicit memory were investigated in Reference [36]. Thirteen healthy subjects underwent a lexical decision task, in which word and nonword (speech sounds without meaning in Korean) were visualized on a computer monitor. Some of the words were repeated after 1–5 intervening words. The ERP elicited during the task were recorded by 128 electrodes and the ERP sources were reconstructed by LORETA, using a realistic head model based on individual MRI. The statistical analysis revealed that the sources produced by old words (i.e., repeated words) showed a significant current density reduction, in comparison to the new words, in the left inferior frontal gyrus, suggesting that the activity of the left inferior frontal area is associated with word repetition effects. The study in Reference [37] focused on the anticipatory neural responses to heat stimuli and the modulation of brain activity caused by the expectation of pain. Before receiving laser heat stimuli at three different intensities (low, medium or high), fifteen healthy subjects visualized a cue word that predicted the heat intensity (certain expectation) or not (uncertain expectation). The source reconstruction, starting from 61-channel EEGs, showed that the uncertain condition, compared to the certain condition, produced a greater activation in the left dorsolateral prefrontal cortex (DLPFC), posterior cingulate cortex, left (contralateral) inferior parietal cortex and right superior frontal gyrus (SFG), which are associated with attentional function (including somatosensory and pain functions). Conversely, there was an increased activity for the certain condition (relative to the uncertain condition) in the left inferior frontal and inferior temporal cortex, and right anterior prefrontal cortex, involved in prospective memory functions.

Lamm explored the N2 ERP component, associated with cognitive control, in two works. In the first one [38], seventeen children executed a go/no-go task with two different stimuli deriving from non-affectively (neutral) charged pictures and affectively charged pictures. The LORETA reconstruction, performed on 64-channel EEGs, showed that the DLPFC, a region related to cognitive control, was more active in the affectively charged picture condition as compared to the neutral picture condition. In the second study [39], the author explored the behavioral inhibition (BI) in 106 seven-years old children. In this case, children performed a go/no-go task presenting only neutral pictures. The analysis of the estimated sources, starting from 64-channel EEGs, revealed that BI produced a greater activity in the DLPFC and the dorsal anterior cingulate cortex (dorsal ACC).

Meyer and colleagues studied the brain activity involved in semantic processing [40]. The source localization of responses to stimuli, represented by semantically congruent and incongruent audiovisual speech and body actions, was computed starting from 128-channel EEGs of eleven subjects. The analysis of results revealed that the sources, reconstructed for different time windows, were located in the occipital/posterior temporal area in the early activation (before 120 ms after stimulus). From 180 to 420 ms, the activation involved different regions simultaneously, including the inferior frontal, superior temporal, parasagittal and superior parietal areas. This outcome was consistent with models which place parallel processing of complex action sequences in frontal, temporal and parietal areas. Late activity (after 460 ms) was mainly concentrated in the inferior-frontal areas.

Tremblay and Vannasing studied the differences between the development of the parvocellular (P) and magnocellular (M) visual system of 33 healthy preterm and 41 fullterm infants [41]. More specifically, the participants underwent visual stimuli for investigating the visual evoked potentials, in particular the N1 and P1 components. The EEG were recorded by 128 electrodes at 12 months of age. In response to stimuli which stimulated preferentially the M system, a greater activity was detected in the dorso-parietal region in fullterm infants, corresponding to a mature M pathways response, as compared to preterm babies. On the contrary, there was no difference in brain sources between the groups for the P system. These outcome suggested a normal development of the P pathway in the preterms, whereas the M system was not yet mature at 12 months of age. The study explained in Reference [42] explored the age and gender differences obtained from three ERP components: the mismatch negativity (MMN), the P300 and the N400. 27 young adults and 18 elderly underwent an oddball task and HD-EEG were acquired by 256 electrodes. There was a statistically significant age-related difference in lantencies and amplitude of the MMN and the P300. From the source reconstruction done by sLORETA, in the case of P300 emerged that the maximum current density is in the frontal lobe for the young subjects whereas it is in the temporal lobe for the elderly group. There was also a decreased activity with aging. As for the gender analysis, in the young group the MMN and the P300 component maximum current density is similar for both gender, even if it is located in the frontal lobe in female and in the temporal lobe in male. Finally, as for the N400 component, females have almost the half maximum intensity as compared to age matched males. Tsolaki and colleagues explored neural activation during emotion processing [43]. The study involved 22 adult females, 11 young and 11 elderly. Images of facial expressions of fear and anger were presented to the participants while a 256-channel system was recording their EEG. The analysis of the N170 ERP component revealed a significantly higher amplitude in the elderly for both emotions, especially at the occipito-temporal sites. The brain source localization, conducted using sLORETA, showed that during the N170 component, for both emotions, the maximum current density of the difference wave between the young and the elderly subjects is located in the same brain region, that is the limbic area. These findings indicated a deficit in the limbic area due to aging during the emotional processing. Table 2.1 summarizes the main features of each above-mentioned study.

Table 2.1: Overview of the included papers about event-related potentials (ERPs).

Event-Related Potentials						
Author	**ERP Component**	**Method**			**Number of EEG Electrodes**	**Head Model**
		LORETA	**sLORETA**	**eLORETA**		
Shigemura (2004) [35]	0–500 ms	✓			72	template
Kim (2006) [36]	200–500 ms	✓			128	individual
Brown (2008) [37]	P2	✓			61	template
Lamm (2012) [38]	N2	✓			64	template
Lamm (2014) [39]	N2	✓			64	template
Meyer (2013) [40]	N400	✓			128	template
Tremblay (2014) [41]	N1, P1	✓			128	template
Tsolaki (2015) [42]	MMN, P300, N400		✓		256	template
Tsolaki (2017) [43]	N170		✓		256	template

2.3.2 Epilepsy

Epilepsy is a neurological disorder caused by abnormal electrical activity of brain cells and characterized by recurrent seizures. Epilepsy can be classified into two main categories—focal (partial) or generalized. In the first one, seizures derived from alterations in a limited brain area; in the second one, both hemispheres are involved [44]. From the physiological point of view, epilepsy is associated with increased neuronal synchronization. Therefore, the brain areas showing a rising activity may have ictogenic property.

In the event of drug resistant focal epilepsy, the resective surgery is a valid therapeutic option. In this case, the accurate localization of the epileptogenic zone to be removed is a crucial issue. Recently, HD-EEG have improved the noninvasive evaluation of epilepsy, confirmed by several studies.

Wang et al. studied the generators of the interictal spikes [45]. From the analysis of 7 patients, the authors proved that using a high-density montage with 76 electrodes, the epileptogenic zones generating seizures were localized more accurately than a 31-electrode EEG system. The localization error was defined as the shortest distance between the LORETA maximum source strength and the resected zones. Moreover, they investigated how the head modeling affected the high-density source localization. They compared a realistic boundary element method head model and a three-shell spherical head model. The results showed that the first one provided a statistically significant lower localization error. These findings were confirmed by the surgical resection outcome. In Reference [46] the authors considered four electrode configurations (32, 64, 96 and 128) for studying five epileptic pediatric patients. The outcome showed that the localization error of the epileptogenic foci decreased when the number of electrodes increased. In particular, the most significant improvement was observed when going from 32 to 64 electrodes. The study explained in Reference [47] investigated the attention impairment in temporal lobe epilepsy (TLE). Ten patients and ten healthy subjects underwent an oddball paradigm while a 128-channel system was acquiring their EEG. The source reconstruction of the P3b component was performed by LORETA using a head model based on individual MRIs for each subject. The analysis of results revealed a statistically significant lower current density for TLE patients in the temporal areas and, to a lesser extent, in the frontal regions, as compared to controls, in both auditory and visual oddball paradigms. The temporal and frontal areas are involved in attentional processes, so TLE might cause a dysfunction of the attention system, as these results suggest. Birot and colleagues [48] based their research on the study of the interictal epileptiform discharges. Thirty-eight patients with pharmacoresistant focal epilepsy were selected. They underwent HD-EEG (128 or 256 electrodes) and intracranial recordings. The authors compared the localization accuracy of the irritative zones deriving from three different head models: a Locally Spherical Model with Anatomical Constraints (LSMAC), a Boundary Element Model and a Finite Element Model, all of them obtained from the individual MRI of the patients. Thirty-two subjects underwent surgical resection of the supposed epileptogenic zones. For the 23 patients with a post-operative positive outcome (Engel class I and II), at least in the 74% of cases the source maxima were within the resected zone. Moreover, the authors computed the distance between the source estimated by LORETA and the irritative zone defined by the intracranial recordings. The results showed that the position of source maxima is very similar for all head model (in 10% of cases the maximum is at the exact same position). A statistical test confirmed that there was not a statistical significant difference between the distributions of distance across the head model. So this study proved that the choice of one of the above-mentioned head model does not significantly affect presurgical evaluation and clinical decision making. In Reference [49], the authors considered forty-three patients with TLE, who underwent resective surgeries. In order to acquire the EEG signals a 256-channel montage was used. The authors analyzed the localization accuracy of the epileptogenic zone evaluated by means of LORETA and other noninvasive methods (MRI, PET, cEEG, and semiology). The evaluation was carried out by comparing results with resections that eliminated or significantly reduced seizures. The outcome obtained with LORETA showed the best sensitivity and specificity. The study also revealed that the probability of postoperative seizure freedom when the interictal epileptic discharges arose from one single source was significantly better than the case of multiple sources. Moreover, it was more likely that patients were seizure-free after surgery when the localized sources were within the resected zones as compared to sources outside resection (94.1% vs. 33.3%). These findings suggested that source localization of the epileptogenic zone by LORETA could be a good instrument for presurgical planning. Akdeniz [50] studied 15 patients with drug-resistant focal epilepsy by means of 64 electrodes. As the above-mentioned papers, the author used individual head model obtained from MRI images. 9 patients of 15 showed lesions on MRI; for the other 6, intracranial recordings were also performed for the presurgical evaluation. The epileptogenic zone localized by LORETA agreed with the resected area for 13 patients, who were seizure-free after surgery. For the remaining two patients, an epileptogenic zone next to the resected area was found, denoting that the epileptogenic zone had not been resected completely. This outcome was supported by the fact that both subjects had seizures, although fewer, even after surgery. Fifteen patients affected by intractable focal epilepsy took part in the study proposed in Reference [51]. The recordings were made using 256 electrodes, except for one patient for whom 128 electrodes were used. The analysis of results was based on the concordance of the interictal and ictal source localization and the surgical outcome, using individual head model (LSMAC). Starting from the 8 patients who underwent resection surgery, the seizure onset zone was correctly localized in 5 of 6 patients who turned out to be seizure-free after surgery. For the sixth one (128 electrodes) the localized ictal source was outside the resected zone. This could suggest the need of a greater number of electrodes for achieving a correct localization. As for the comparison between interictal and ictal localization, they were sublobar concordant in 9 of 14 patients and agreed with MRI scans. For additional 4 patients there was partially concordance because the interictal analysis showed more than one solution: in these cases the ictal source corresponded with one of the detected interictal source. In total there was concordance in 93% of cases. Kuo et al. [52] examined 84 seizures in 12 patients with medically resistant epilepsy. Their aim was the localization of the seizure onset zone by means of sLORETA starting from 256-channel EEG. The accuracy of results were tested by comparing them according to one or more of the following clinical criteria: epileptogenic lesions assessed from MRI imaging, seizure onset detected in intracranial EEG and successful surgical outcomes. For the source localization from HD-EEG individual head modeling were used, whereas the others source analysis were carried out with the atlas head model. The number of seizure onsets localized was 56 out of 84. For the lateralization measure, the results from HD-EEG were more accurate than results from the 19-channel 10-20 EEG (100% vs. 50%). This trend was also confirmed for the sublobar concordance (90% vs. 40%).

Finally, the seizure localization resulting from HD-EEG with ictal onset was better than that deriving from the clinical interpretation of the interictal spikes (IIS). Table 2.2 summarizes the main features of each above-mentioned study.

Table 2.2: Overview of the included papers about epilepsy.

Epilepsy					
Author	**Method**			**Number of EEG Electrodes**	**Head Model**
	LORETA	**sLORETA**	**eLORETA**		
Bocquillon (2009) [47]	✓			128	individual
Wang (2011) [45]	✓			76, subset: 31	individual
Birot (2014) [48]	✓			256, 128	individual
Sohrabpour (2015) [46]		✓		128, subset: 96, 64, 32	individual
Feng (2016) [49]	✓			256	template
Akdeniz (2016) [50]	✓			64	individual
Nemtsas (2017) [51]	✓			256, 128	individual
Kuo (2018) [52]		✓		256	individual

2.3.3 Alzeheimer's disease

Alzheimer's Disease (AD) is a neurodegenerative disorder which is the most common cause of dementia. The first stage of the disease, called Mild Cognitive Impairment (MCI), is a transition state between normal aging and dementia. However, the MCI symptoms, above all memory problems, do not alter the everyday life significantly. As the disease advances, people are no more able to take care of themselves. An early diagnosis is essential but extremely hard because the first stage condition is often mistaken for normal aging. Most of the studies about LORETA and AD considered low density montage EEG. The few works carried out on HD-EEG are reported below.

The study conducted in Reference [53] explored the effect of cognitive and physical training on the deterioration of brain processes. Seventy MCI patients were divided into five equally populated groups: long lasting memory (LLM), physical training (PT), cognitive training (CT), active control (AC) and passive control (PC). LLM performed physical and cognitive exercises, PT underwent only physical training, CT carried out only cognitive tasks, AC group watched a documentary and answered a questionnaire, and PC were not involved in any activity. The EEG were recorded before and after the completion of the procedure (8 weeks), using 57 electrodes. eLORETA computed the active source reconstruction for delta, theta, alpha, beta 1 and beta 2 bands. In order to perform the statistical analysis, the statistical non-parametric mapping method was employed, implemented in an eLORETA software package. From the comparison between the reconstructed sources before and after the procedure within each group arose that there were statistically significant differences only for the LLM group, for all frequency bands except for the alpha band. In particular, the cortical activity decreased in precuneus extending in the posterior cingulate cortex. As for delta and theta decrease, it can be considered as a positive outcome on brain neuroplasticity, which could decelerate the neurodegeneration processes. Therefore, results showed that combined physical and cognitive training maintains or improves cognitive functions.

The analysis of the ERP components could be a useful tool for an early diagnosis of AD. In Reference [54], the authors examined two ERP components, the MMN and the P300, for detecting the cognitive decline. The study involved three groups of subjects: 21 healthy elderly, 21 mild cognitive impairment, and 21 mild AD. The EEG were recorded by a 256-channel system during the execution of the 2-tone oddball task. The localization of active sources, performed by sLORETA, revealed that the highest difference in the amplitude between controls and MCI and controls and AD for both MMN and P300 is similar in MCI and AD and is in the same Brodmann area (BA 11) in the frontal lobe, independently of the stage of the disease. This research was the first one which explored MMN and P300 using LORETA applied to HD-EEG for studying Alzheimer's disease. Gu and colleagues [55] carried out a study which combined ERP and sLORETA, too. Their study dealt with amnestic mild cognitive impairment (aMCI), which can be divided into two groups: single domain aMCI (sd-aMCI) and multiple-domain aMCI (md-aMCI). They considered 85 subjects: 46 healthy elderly controls and 39 aMCI (26 sd-aMCI and 13 md-aMCI patients). 64-channel EEG were recorded while the subjects were performing two tasks related to visuospatial working memory (VSWM task) and executive function (Go/Nogo tasks). Two ERP components were considered and analysed: N200 and P300. As for VSWM task, the results revealed no significant differences in source activation between sd-aMCI and controls during P300 time range. However, the P300 amplitude in md-aMCI decreased as compared to sd-aMCI patients. Moreover, for md-aMCI there was a hypoactivation in the right middle frontal gyrus (BA 8) during P300 time range, compared to sd-aMCI. These outcome confirmed that md-aMCI showed more serious deficits in updating operation of working memory, compared to sd-aMCI patients. sLORETA source reconstruction also detected a hypoactivation for md-aMCI in the right medial frontal gyrus (BA 9) compared to controls, and in the right SFG (BA 10) compared to sd-aMCI, in both Nogo and Go task during N200 time range. Finally, md-aMCI showed less activation in the right SFG (BA 8) compared to sd-aMCI in Go task during P300 time range.

In [56], the authors explored the alteration of networks in AD. Differently from the majority of previous studies, EEGs were recorded in an open eyes state. A 64-channel system was employed for detecting the EEGs from 21 AD patients and 26 controls. Using eLORETA, the power spectrum was computed for each subject, for the total band and for each of the classic five frequency bands. The only significant difference was the increase in power for theta band. Then, starting from the reconstructed sources, a functional connectivity analysis was conducted over 40 regions of interest (ROIs) for theta band, computing the phase locking factor between each pair of ROIs. Results showed that the small-worldness of networks decreased in AD and was positively correlated with MMSE language subscore, suggesting that modifications in AD networks topology are mostly associated with language deficits. It was also found that the reduction of the small-worldness was a consequence of increased path lengths, mainly localized to the temporal lobes. Moreover, the authors investigated the relationship between functional and effective connectivity: the results suggested that changes in functional connectivity derived from a reduced effective connectivity between the temporal lobes and other anatomical regions of the brain. Table 2.3 summarizes the main features of each above-mentioned study.

Table 2.3: Overview of the included papers about Alzheimer's disease.

Alzheimer's Disease					
Author	**Method**			**Number of EEG Electrodes**	**Head Model**
	LORETA	**sLORETA**	**eLORETA**		
Styliadis (2015) [53]			✓	57	template
Tsolaki (2017) [54]		✓		256	template
Gu (2019) [55]		✓		64	template
Tait (2019) [56]			✓	64	template

2.3.4 Depression

Major depressive disorder (MDD) is a mental disorder characterized by a lasting feeling of sadness or a lack of interest in outside stimuli. It has a recurrent nature, so people experience, on average, five to nine major depressive episodes in their lifetime. If not correctly treated, depression can significantly affect the quality of life. Over the years, LORETA has been widely employed for detecting alterations in the brain activity of MDD subjects. As for HD-EEG, the papers examined are the following.

In Reference [57], Pizzagalli and colleagues studied the activity within the rostral anterior cingulate cortex, a region involved in action regulation. They considered 17 subjects with high BDI (Beck Depression Inventory) scores and 17 subjects with low BDI scores (controls). A 128-channel system recorded the EEGs in resting state (with both eyes open and closed) before the execution of the Eriksen Flanker task. LORETA reconstructed the cortical current density distribution of theta (6.5–8 Hz) and gamma (36.5–44 Hz) bands. Results showed that high BDI subjects had significantly lower accuracy after incorrect than correct trials, and a statistically significant reduction of the pre-task gamma current density within the affective (rostral) but not cognitive (dorsal) ACC subdivision, as compared to low BDI. Therefore, the lower activity within the ACC in depressed subjects may cause abnormal responses to errors. Conversely, for low BDI subjects, pre-task gamma within the affective ACC subdivision was a predictor of the post-error adjustments effect. In Reference [58], the authors focused on depression in adolescence. Female adolescents, 36 healthy controls (HC) and 23 MDD, were enrolled and executed the facial recognition task: four basic emotional facial expressions (happy, sad, fearful, angry) were presented in different intensity, ranging from 10% (low intensity) to 100% (high intensity). In addition, EEGs were recorded in resting state by 128 electrodes, not simultaneously with the emotion identification. The cortical current density was estimated by LORETA, for the theta (6.5–8.0 Hz) and low alpha (8.5–10 Hz) bands in the DLPFC, a region related to the emotion processes biases in MDD. The results revealed that MDD subjects exhibited a greater accuracy in the identification of sad faces and worse accuracy in the identification of happy faces, especially low-intensity happy faces, as compared to HC. There were no significant differences between groups for both fearful and angry expression. Moreover, LORETA analysis showed greater theta and alpha current density in MDD versus HC, particularly in the left DLPFC. Finally, it was also found that greater left DLPFC theta and alpha activity was correlated with a reduced accuracy for happy emotion identification. The same author examined depressed female adolescents in Reference [59], too. Thirty HC and twenty-two MDD subjects completed the self-referential encoding task while ERP were recorded with a 128-channel system. The above-mentioned task included 80 trials consisting of 40 positive and 40 negative words. In order to analyse the cognitive-affective processes related to self-referential processing, P1, P2 and late positive potential (LPP) responses to positive and negative words were examined. It was also estimated the cortical current density by LORETA. Results showed that depressed subjects endorsed, recalled, and recognised more negative words and fewer positive words, as compared to the healthy group. Moreover, MDD showed greater P1 amplitudes following negative words, which is associated with a more negative self-view and greater self-criticism. As for the late LPP, a greater amplitude following negative versus positive words in depressed group was observed too; conversely, the healthy females displayed the opposite trend. For both P1 and LPP, LORETA showed less current density to negative words in the inferior frontal gyrus in MDD versus HC. In addition to the inferior frontal gyrus, for P1, reduced activity was detected in the depressed group within the anterior cingulate and medial temporal gyrus, whereas for LPP in the middle temporal gyrus. The referred-to group differences were all statistically significant. These findings indicated that the P1 and LPP reflect self-referential processing biases in female adolescents with depression. Whitton and colleagues [60] examined 26 patients with remitted major depressive disorder (rMDD) and 34 control subjects with no history of depression. ERPs were recorded during the execution of a probabilistic reward task by means of a 128-channel system. The objective was to study the reward learning systems in rMMD subjects. The source localization was carried out by LORETA for eight ROIs, defined from two meta-analysis of reward-related fMRI studies. Results showed a decrease in reward-related ERP amplitudes and a reduced reward-related activation in the ACC and the pregenual ACC for rMMD group, as compared to controls. These outcome implied that the reward learning deficits detected in acute MDD persisted into full remission and that these impairments could derive from abnormalities in the neural processes involved in reward feedback monitoring. In Reference [61], the authors investigated the resting state functional connectivity in 65 subjects with MDD compared to 79 healthy controls; moreover, 30 rMDD subjects were considered for a secondary analysis. The cortical activity was reconstructed by the eLORETA method applied to 128-channel EEGs. The functional connectivity was computed by the lagged phase synchronization parameter, using a tool implemented in the eLORETA software. The analysis was conducted considering ROIs belonging to the default mode network (DMN) and the frontoparietal network (FPN) for several frequency bands. A statistical analysis was used for investigating the group differences in within- and between-network connectivity. Significant differences were found between the HC and MDD groups within-DMN connectivity in beta 2 band (18.5–21 Hz) and between the DMN and FPN connectivity in beta 1 band (12.5–18 Hz). In addition, results revealed that both indices of connectivity were lower in rMDD group as compared to MDD, whereas the rMDD and HC did not differ. These findings showed that depression is characterized by greater within-DMN and DMN–FPN phase synchronization in the high-frequency band, which normalizes to some extent in remitted subjects but is associated with a more recurrent depressive illness course. Table 2.4 summarizes the main features of each above-mentioned study.

Table 2.4: Overview of the included papers about depression.

Depression					
Author	**Method**			**Number of EEG Electrodes**	**Head Model**
	LORETA	**sLORETA**	**eLORETA**		
Pizzagalli (2006) [57]	✓			128	template
Auerbach (2015) [58]	✓			128	template
Auerbach (2015) [59]	✓			128	template
Whitton (2016) [60]	✓			128	template
Whitton (2018) [61]			✓	128	template

2.3.5 Stroke

Stroke is defined by the World Health Organization as a clinical syndrome, with a vascular origin, consisting of rapidly developing clinical signs of focal or global disturbance of cerebral function lasting more than 24 hours or leading to death. The papers in literature about LORETA and stroke are few. As for HD-EEG, just three works were found.

The study proposed in Reference [62] explored the closed-open eyes alpha reactivity phenomenon from 64-channel EEGs of 32 healthy subjects and a patient with acute ischemic stroke. The comparison between open eyes and closed eyes conditions in healthy subjects revealed that there was a statistical significant higher activation in the bilateral posterior cortical regions, where the primary visual cortex is located. In some cases, lower activations were also found in the anterior and thalamic regions. As for the stroke patient, there was a significant decrease in reactivity in the damaged hemisphere, as compared to normal subjects. It was also detected a reactivity reduction in the undamaged hemisphere. The research in Reference [63] involved 10 stroke patients with a coordination impairment of the upper limb and 5 healthy controls. The participants executed an upper extremity reaching task while a 64-channel system was acquiring their EEGs. The objective was the estimation of the cortical activity related to both movement preparation and motor execution. The source localization was carried out by LORETA and the contralesional/lesional activation ratio (CTLR) for both groups was computed and compared. CTLR is the ratio of activation in the right or non-lesion hemisphere versus left or lesioned hemisphere. The results showed that the CTLR for the primary motor cortices was significantly higher for stroke as compared to the controls in the planning phase, but not in the execution phase. In the stroke group, the CTLR was significantly higher in the planning than execution phase in the Brodmann area 4, whereas for the controls the CTLR for both phases were similar. As it is expected, these findings revealed that stroke patients have an abnormally high brain activity, specifically in the contralesional hemisphere. In fact, because of damage in the cortical network, a greater effort was needed to execute the motor task for stroke patients. In Reference [64], 160-channel EEGs from 10 adults with chronic, hemiparetic stroke and 8 adults without neurological injury were examined during the execution of a motor task for exploring the mechanisms underlying the so-called “flexion synergy”. An individual head model was created from MRI and used for reconstructing the cortical activity by means of LORETA. In controls group, the cortical activity was mainly observed in the hemisphere contralateral to the arm being examined, regardless of the shoulder abduction load. In stroke patients, contralesional cortical activity quickly and progressively rose in premotor and primary motor cortices as shoulder abduction loading, and the synergy expression increased too. Conversely, the subjects without neurological injury showed a decreased cortical activity in these regions as shoulder abduction loading increased. These findings can be interpreted as an adaptive strategy of recruiting contralesional motor resources for preserving low-level function at the cost of fine motor control. Table 2.5 summarizes the main features of each above-mentioned study.

Table 2.5: Overview of the included papers about stroke.

Stroke					
Author	**Method**			**Number of EEG Electrodes**	**Head Model**
	LORETA	**sLORETA**	**eLORETA**		
Cuspineda (2009) [62]	✓			64	individual
Fang (2015) [63]	✓			64	template
Mcpherson (2018) [64]	✓			160	individual

2.3.6 Schizophrenia

Schizophrenia is a chronic mental disorder characterized by psychotic behaviors, deficits of normal responses to emotions and cognitive impairment. ERPs have been widely employed for investigating schizophrenia. In particular, the studies reported here analyzed the MMN and the P300 components.

In Reference [65], the authors investigated the source localization of the MMN, produced by an auditory deviant stimulus. A 128-channel system was used for recording the EEGs from 14 schizophrenic patients and 14 controls. The MMN source reconstruction by LORETA was performed after matching the electrode positions with individual MRI. The statistical parametric mapping revealed a significant decrease of

MMN current density for patients group in the left superior temporal gyrus and the left inferior parietal lobule. A similar study (individual head model, 128 electrodes) was conducted in Reference [66], but in this case the P300 component was examined. The statistical analysis showed a P300 current density reduction for schizophrenic patients in the left medial temporal area and in the left inferior parietal area, whereas in the left prefrontal and right orbitofrontal the current density increased. It was also found that current density in the left parietotemporal area was negatively correlated with the Positive and Negative Syndrome Scale (PANSS) total scores, a scale which measures the symptom severity of schizophrenia. Wang and colleagues [67] explored the P300 component, too. Thirteen patients and twenty controls were enrolled and performed the auditory oddball paradigm. A high-density system made up of 128 electrodes was employed for recording the EEGs. The source reconstruction estimated by LORETA showed that the neural generators in healthy subjects extended over the cortex, including bilateral frontal, parietal and temporal lobes. LORETA analysis also revealed a statistically significant reduction in the P300 current density in patients group as compared to controls. In particular, the aforementioned decrease was detected in the left fronto-temporal cortex, as reported in previous studies. A few years later, the same author conducted a study with the same method but, unlike his previous research, drug-naive first episode schizophrenia patients were considered, using just 64 electrodes for recording the EEGs [68]. The source distribution in controls was consistent with the outcome of Wang's previous study. As for the comparison between the two groups, there was a statistically significant reduced P300 current density in the patient group especially over the left insula, left superior temporal gyrus and left postcentral gyrus. Moreover, the P300 current density over the aforementioned brain regions showed an inverse correlation with the patients' total PANSS scores. Table 2.6 summarizes the main features of each above-mentioned study.

Table 2.6: Overview of the included papers about schizophrenia.

Schizophrenia					
Author	**Method**			**Number of EEG Electrodes**	**Head Model**
	LORETA	**sLORETA**	**eLORETA**		
Park (2002) [65]	✓			128	individual
Pae (2003) [66]	✓			128	individual
Wang (2003) [67]	✓			128	template
Wang (2010) [68]	✓			64	template

2.3.7 Conclusions

The main information about the papers included in Section 2.3 are summarized in Table 2.7 and Figures 2.1-2.2.

Table 2.7: Overview of the included papers.

Clinical Application	**Publications**	**Method**		
		LORETA	**sLORETA**	**eLORETA**
ERPs	[35] – [43]	7	2	-
Epilepsy	[45] – [52]	6	2	-
AD	[53] – [56]	-	2	2
Depression	[57] – [61]	4	-	1
Stroke	[62] – [64]	3	-	-
Schizophrenia	[65] – [68]	4	-	-

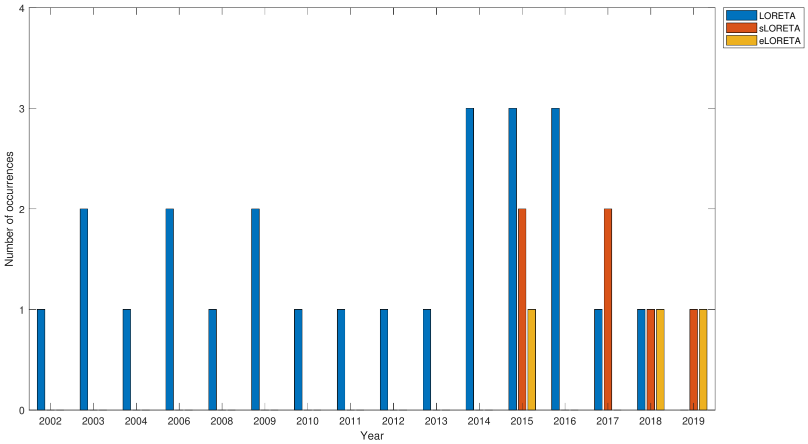

Fig. 2.1: Bar graph of LORETA, sLORETA and eLORETA application by year.

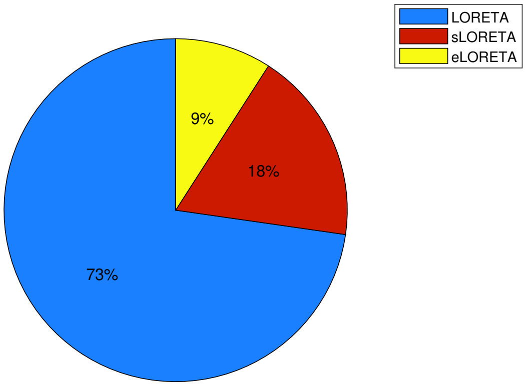

Fig. 2.2: Percentage use of LORETA, sLORETA and eLORETA.

3

Clinical Applications of LORETA

3.1 Introduction

This chapter focuses on the description of the research activity conducted during the PhD course. In particular, LORETA was used for investigating three different neurological diseases: Alzheimer's disease (Section 3.2), gliosis (Section 3.3) and stroke (Section 3.4). The subsection 3.1.1 provides a preliminary description of the statistical tools used in the analysis reported in the following sections.

3.1.1 Statistical tools

Three different statistical tests and several boxplots were employed in the research studies. They are described below.

The *Wilcoxon rank sum test* is a nonparametric test for two populations when samples are independent [69]. It does not assume that the samples are normally distributed. It tests the null hypothesis that data in population x and population y are samples from continuous distributions with equal medians, against the alternative that they are not.

The *Kruskal-Wallis test* is an extension of the Wilcoxon rank sum test to more than two groups [70]. It compares the medians of the groups of data to determine if the samples come from different populations with the same distribution.

The *Tukey's Honestly Significant Difference test* is a multiple comparison test used for comparing more than two means [71]. Specifically, it determines the individual means which are significantly different from a set of means. Typically, it is performed after a previous analysis has shown that significant difference exists, for determining where the difference exists.

A *boxplot* is a standardized method of displaying the summary statistics for a dataset [72]. In particular, boxplots are useful for comparing distributions across groups. The spacings between the different parts of the box indicate the degree of dispersion and skewness in the data. The boxplot is made up of the following components:

- the *median* is the middle value of the dataset and is represented by the line that divides the box into two parts;
- the *first quartile* is the bottom of the box and represents the 25th percentile of the data; the *third quartile* is the top of the box and represents the 75th percentile of the data. The distance between the bottom and top of the box is the interquartile range (IQR);
- the *whiskers* are lines extending below and above the box up to the minimum and maximum data values, respectively;
- the *outliers* are data values beyond the whisker length. Specifically, an outlier is a value that is more than 1.5 times the interquartile range away from the bottom or top of the box.

Figure 3.1 shows the above-mentioned components of a boxplot.

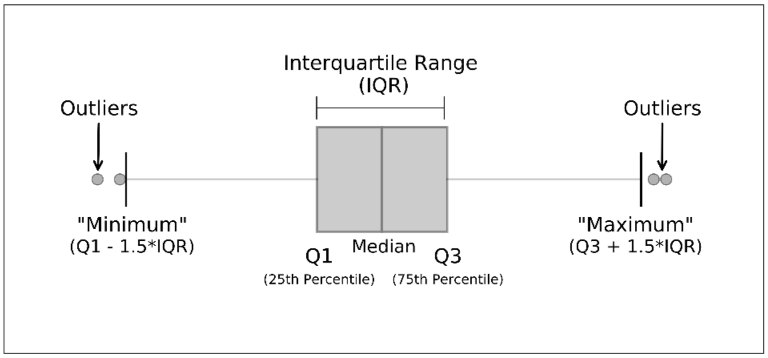

Fig. 3.1: Components of a boxplot.

3.2 Applications of LORETA in Alzheimer's disease

3.2.1 Alzheimer's disease

Alzheimer's disease (AD) is a brain disorder causing a progressive decline in cognitive functions. The diagnosis of the disease is based, initially, on the evaluation of neuropsychological and behavioral symptoms related to disorders of memory, language, and visual-spatial perception [73].

There are four stages which characterize the evolution of the disease. In the first stage, called Mild Cognitive Impairment (MCI), the subject shows short-term memory loss and difficulty in remembering even words of daily use. These symptoms, however, do not substantially affect everyday life. This condition is not always irreversible because not all MCI subjects convert to AD—it happens for 50–60% of them. During the next two stages (Mild and Moderate AD) the patient shows difficulty in recognizing relatives and friends, and suffers from spatial and temporal disorientation. Moreover, the first behavioral changes appear, such as anxiety, insomnia, and personality changes. During the last stage—Severe AD—the patient no longer recognizes anyone, does not understand words, and has difficulty in dressing, eating, and swallowing. The subject is completely dependent on caregivers. Death occurs because of the further worsening of these symptoms [74–76]. To date, there is no cure for Alzheimer's disease, but several medications are used for delaying the onset of the symptoms and improving the patient's quality of life. Therefore, early diagnosis of AD is very important because the medications are effective only if taken during the first stage. However, the diagnosis is hard because the first symptoms are often mistaken for normal aging [77].

3.2.2 LORETA cross-sectional and longitudinal studies in Alzheimer's disease: a review

Several studies have proven that the EEG frequency bands are affected by AD in a specific way. In particular, the spectral analysis shows a "slowing" of EEG signals in MCI and AD patients: the power increases in low frequencies (delta and theta) and decreases in higher frequency (alpha and beta), compared to normal elderly (Nold) [78–83].

Over the years, LORETA has been widely employed for studying the spectral power density of EEG signals in AD. Babiloni carried out several studies about this topic. In [84], the results showed that the power in alpha 1 declined in AD in the central, parietal, temporal, and limbic lobes as compared to Nold. Alpha 1 power in the occipital lobe was lower when the disease was at a more severe stage. There was also an "anteriorization" of alpha 1 rhythm, as the power decreased much more in the parieto-occipital area than in the frontal one. As for the theta band, there was no significant difference between mild AD and Nold. This study was extended in [85], as it included also MCI. The findings revealed that, in comparison to Nold and mild AD groups, MCI group had intermediate power in delta (occipital area) and alpha 1 (parietal, occipital, temporal, and limbic areas) bands and greater power in alpha 2 (occipital area) band. In [86], the correlation between the disease and the hippocampal volume was explored. For the alpha 1 band, the activity was maximum in MCI with greater hippocampal volume, intermediate in MCI with smaller hippocampal volume, and minimum in AD. The study conducted in [87] showed that for MCI and AD subjects, posterior delta and alpha EEG rhythms do not decline when white matter vascular lesion increased. In [88], it was found a positive correlation between the gray matter volume and the alpha 1 power, and a negative correlation with delta power in MCI and AD. Canuet and colleagues [89] reported a significant reduction of alpha 1 activity in the parieto-occipital regions for AD as compared to healthy subjects. In [90], the authors found a positive correlation between the severity of the disease and delta power, and a negative correlation with alpha 1 power. The study in [91] showed a greater power in delta band in large areas, including the frontal lobe, in AD in comparison to controls. All the above-mentioned papers refer to cross-sectional studies. In literature, there are only three longitudinal studies that applied LORETA. In [92], the EEG power of a group of MCI patients was evaluated during a follow-up of approximately 14 months. Twenty-four subjects converted to AD, whereas 45 subjects remained stable. The results showed that the EEG power for delta (temporal area), theta (temporal, parietal, and occipital areas) and alpha 1 (central, temporal, parietal, occipital, and limbic areas) bands was significantly higher in MCI who converted to AD, as compared to MCI stable. The remaining two works were carried out by Babiloni and colleagues. In [93], a group of MCI patients were examined about 1 year after the first EEG recording. The subjects were divided into three groups, according to their MMSE score variation, as "stable", "decreased" and "increased". The only significant difference was detected for the alpha 1 band: the temporal, parietal, and occipital power density was greater in the stable group than in the decreased and increased groups, suggesting that preserved resting cortical activity at alpha band is related to a long-term stable cognitive function in MCI subjects. Resting state EEG of a mild AD group was investigated in [94]. The second recordings were carried out after 1 year. The alpha rhythm was characterized by a widespread power decrease as well as the temporal, parietal and occipital beta 1 band. It was also shown an increased power of delta sources in all brain areas except for the central region.

3.2.3 An eLORETA longitudinal analysis of resting state EEG rhythms in Alzheimer's disease

This subsection includes a longitudinal study based on the computation of the power current density, employing the eLORETA algorithm, in MCI patients. In particular the research involved eight subjects, who were diagnosed with MCI at time T0 and mild AD at time T1 (four months later). Five patients out of eight showed an increasing power in delta and theta bands. Seven patients exhibited a lower activation in alpha 1 and beta 2 bands. Finally, six patients revealed a decreased power in alpha 2 and beta 1 bands.

The subsection is organized as follows: first the methodology is described; then, information about patients and EEG recordings are provided; finally the experimental results are presented and discussed.

Methodology

The computation of the power current density was conducted by means of the eLORETA algorithm implemented in the LORETA-KEY software (v20200414). The power current density was evaluated by eLORETA for each patient, at time T0 and T1, for the following frequency sub-bands: delta (0.5–4 Hz), theta (4–8 Hz), alpha 1 (8–10.5 Hz), alpha 2 (10.5–13 Hz), beta 1 (13–18 Hz), and beta 2 (18–30 Hz). The comparison between the values at T0 and T1 was carried out by grouping the eLORETA solutions by frontal, occipital, parietal and temporal lobes.

Subjects

Eight amnestic MCI patients (four males and four females) were enrolled by a team of experts at the IRCCS Centro Neurolesi Bonino-Pulejo of Messina (Italy). The subjects underwent a series of examination at time T0 and at time T1 (four months later). The doctors agreed that patients converted from MCI (at T0) to AD (at T1) on the basis of the Montreal Cognitive Assessment (MoCA) scores. The study excluded the subjects suffering from epilepsy, neurological or psychiatric diseases related to cognitive impairment, traumatic brain injuries, systemic diseases. Subjects who took psychoactive drugs were also excluded. The study followed a clinical protocol approved by the the local Ethics Committee (Prot. E29/16). The patients or their caregivers were notified of the procedure and signed an informed consent form. The demographic data of the subjects are reported in Table 3.1.

Table 3.1: Demographic data of the recruited subjects.

Patient ID	**Gender**	**Age**
Pt 03	M	68
Pt 32	M	78
Pt 41	M	78
Pt 51	F	72
Pt 71	F	79
Pt 164	M	76
Pt 180	F	78
Pt 184	F	69

EEG data

The EEG signals were acquired in resting state with eyes closed but the subjects were awake. The data were recorded using a Brain-Quick System (Micromed) from nineteen channels, according to the international 10–20 system: Fp1, Fp2, F3, F4, C3, C4, P3, P4, O1, O2, F7, F8, T3, T4, T5, T6, Fz, Cz and Pz, with linked earlobe (A1-A2) reference. The artifactual segments were detected and marked by the doctors during the EEG acquisition. Those segments were not considered for the analysis. The sampling rate was 256 Hz. It was applied a notch filter at 50 Hz. Data were transformed to a common average reference montage and divided into artifact-free non-overlapping epochs of 256 samples (1s).

Results

The methodology explained in Section 3.2.3 was applied to the EEG recordings and produced the following results. The EEG preprocessing and the grouping of power current density values according to the four regions of interest were executed with Matlab (R2018a). A statistical analysis was carried out for determining whether the differences between values at T0 and T1 were significant. For this purpose, the Wilcoxon rank sum test [69] was performed under the null hypothesis that, for each patient, the medians of the current density values at time T0 do not differ from those at time T1. The significance level was set at 5%, which means that there is a 5% risk of concluding that a difference exists when there is no actual difference. So, the difference between T0 and T1 is statistically significant when the *p*-value is less than 0.05. Tables 3.2–3.4 report the p-values resulting from the statistical analysis for each sub-band and each region of interest. F. L., O. L., P. L. and T. L. stand for Frontal Lobe, Occipital Lobe, Parietal Lobe, Temporal Lobe, respectively. The p-values statistically significant which are consistent with the expected results are highlighted in gray. Patient 03 shows a widespread increase of power density in delta and theta bands, and a decrease in alpha 1 (parietal region) and beta 2 (temporal lobe) bands. Patient 32 exhibits a greater activation of delta sources in all regions; an increasing power in theta band in the occipital, parietal and temporal lobes; a lower activity in alpha 1, alpha 2, and beta 1 bands in the frontal lobe, and in beta 2 band in the frontal and occipital lobes. Patient 41 shows a greater power in delta (occipital and parietal areas) and theta (occipital and temporal regions) bands, and a lower activation in alpha 1 (frontal lobe), alpha 2 (frontal, parietal and temporal lobes), beta 1 and beta 2 bands in all lobes. Patients 51 and 71 reveal a widespread decrease of power density for alpha 1, alpha 2, beta 1 and beta 2 bands. As for patient 164, the results are the same except for the parietal lobe in alpha 1 band: in this case the power density increases. Patient 180 displays a widespread greater power in delta and theta bands. Patient 184 shows an increased activation in delta (temporal lobe) and theta (parietal and temporal lobes) bands; the power density decreases in the frontal and occipital regions for alpha 1 and alpha 2 bands, in the occipital lobe for beta 1 band, in the frontal, occipital and parietal lobe for beta 2 band. The bar graph in Figure 3.2 summarizes the statistically significant results highlighted in gray in Tables 3.2–3.4. The graph reveals that most significant variations were detected in higher frequency bands. In particular, six patients show a decreasing power density in alpha 1 and alpha 2 (frontal lobe) bands, in addition to beta 2 (frontal and occipital lobes) band. As for delta and theta bands, the power density increases in four subjects at most, except for the temporal lobe in theta band: in this case, the increase is detected in five patients. Figures 3.3–3.10 show the boxplots of the power density values of each patient at time T0 and T1, for each frequency sub-band and each region of interest. From the analysis of the results, the hypothesis is that the outcome not consistent with previous findings are due to the passage from MCI to a mild AD condition. Therefore, the not yet severe stage of the disease, together with the inter-subject variability, could lead to the above-mentioned discrepancy of some outcome.

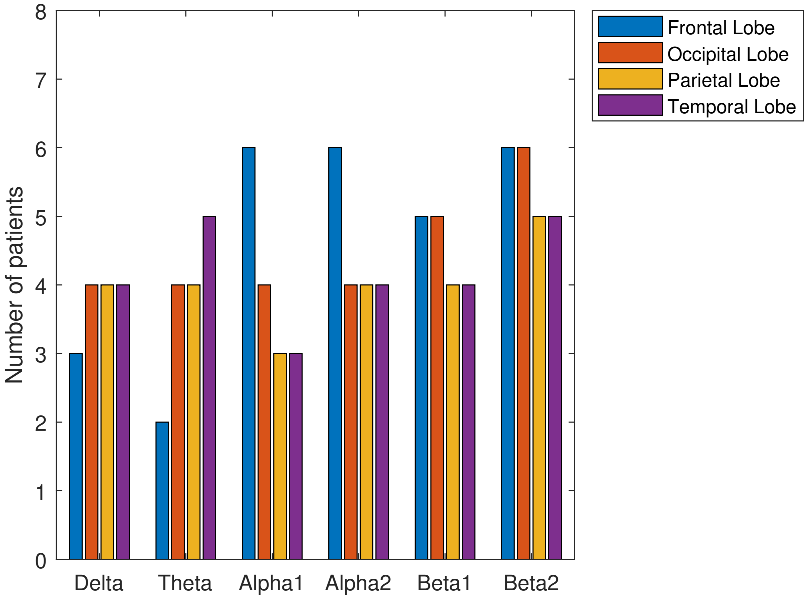

Fig. 3.2: Bar graph of the statistically significant results highlighted in gray in Tables 3.2–3.4.

Pt 03

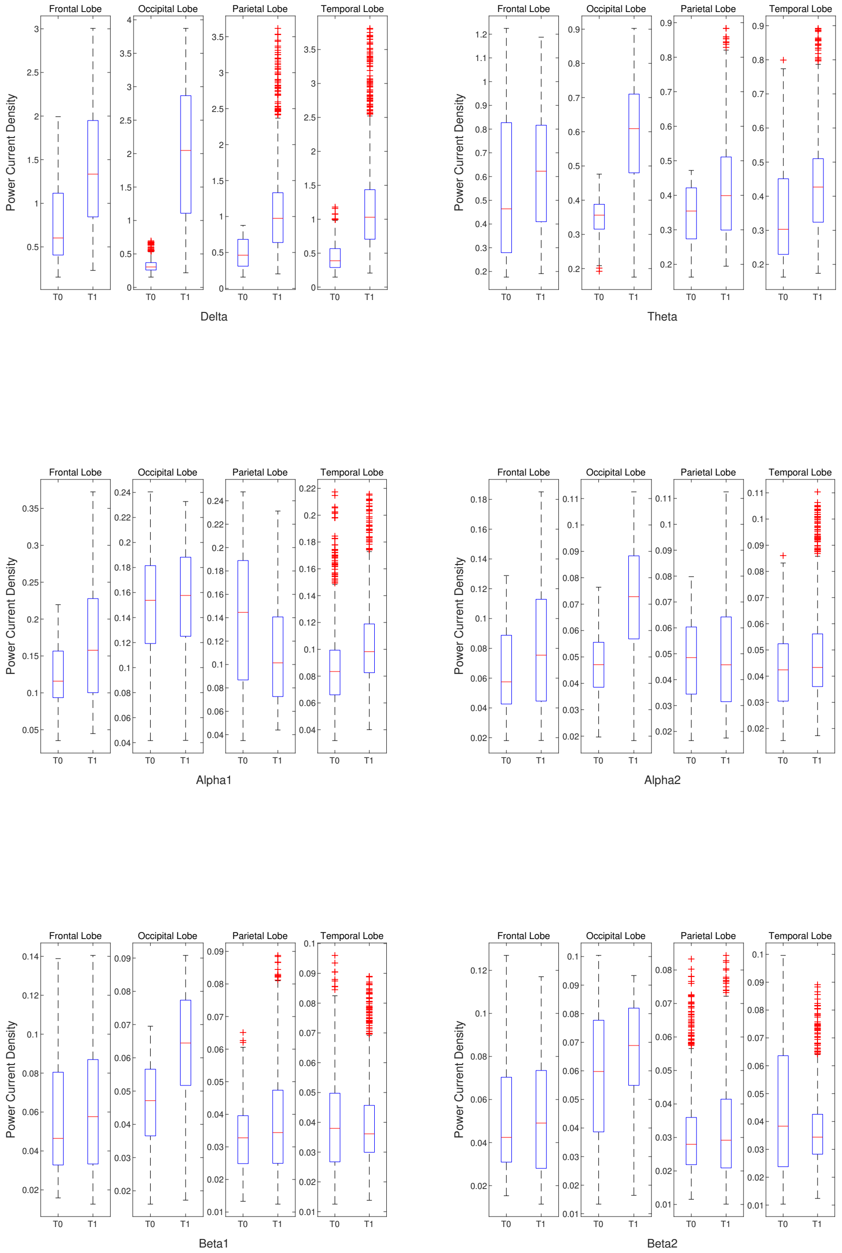

Fig. 3.3: Boxplot of the power current density of patient 03 at time T0 and T1 for each frequency sub-band and each region of interest (frontal, occipital, parietal, and temporal).

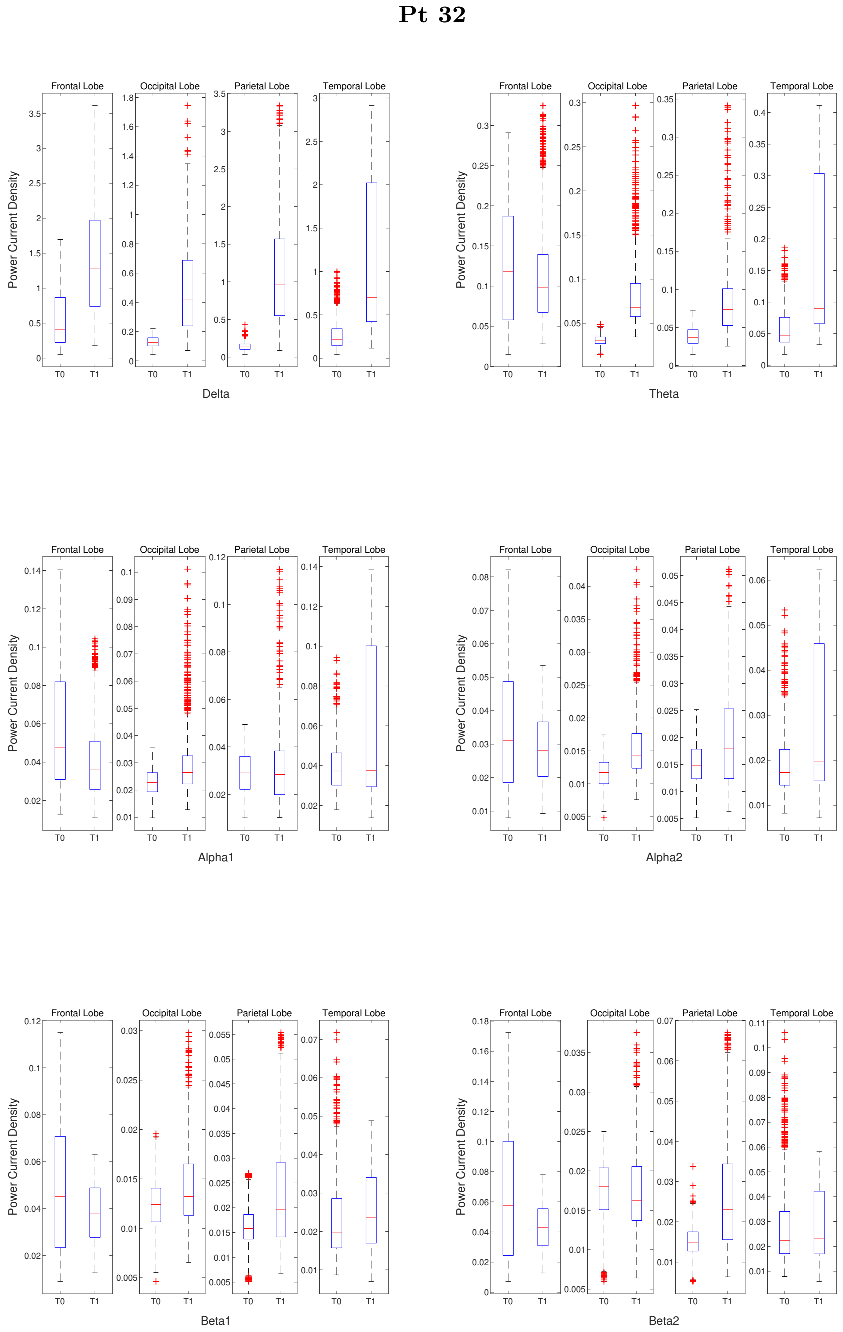

Fig. 3.4: Boxplot of the power current density of patient 32 at time T0 and T1 for each frequency sub-band and each region of interest (frontal, occipital, parietal, and temporal).

Pt 41

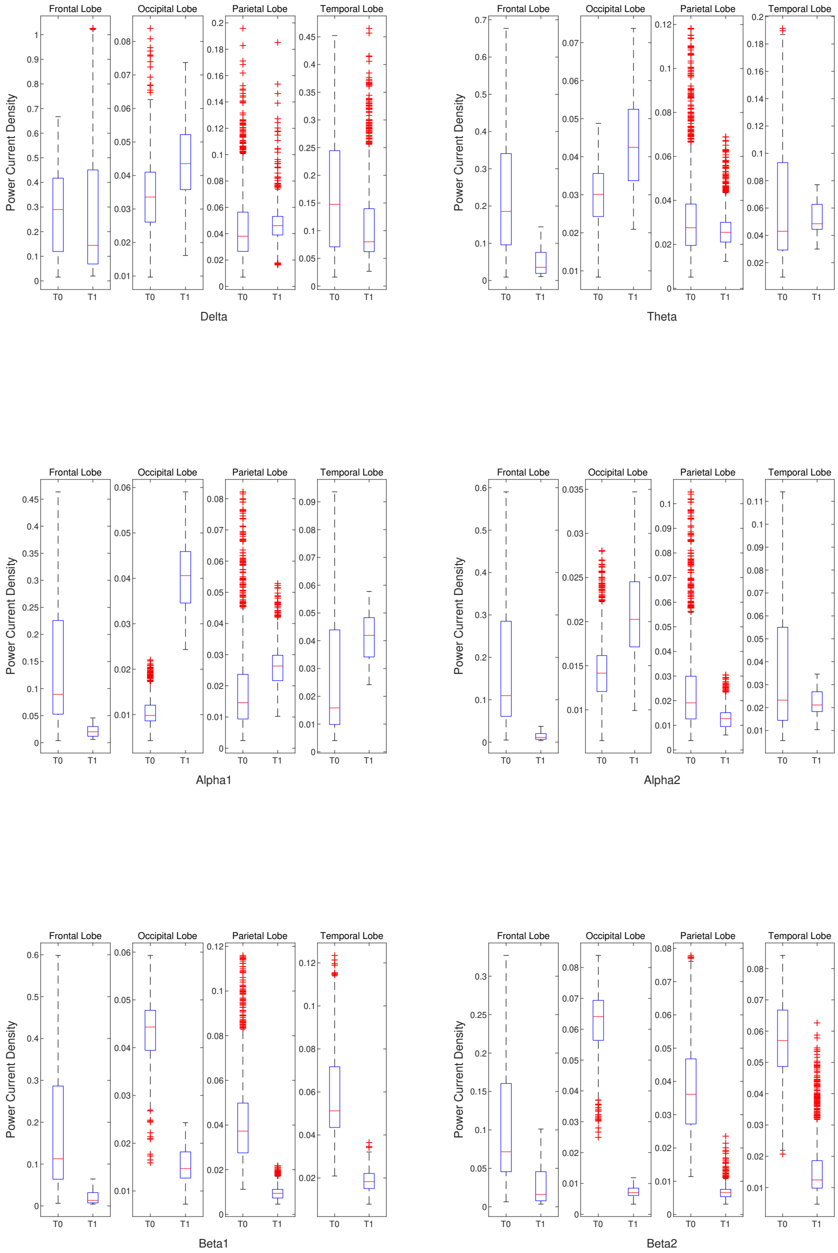

Fig. 3.5: Boxplot of the power current density of patient 41 at time T0 and T1 for each frequency sub-band and each region of interest (frontal, occipital, parietal, and temporal).

Pt 51

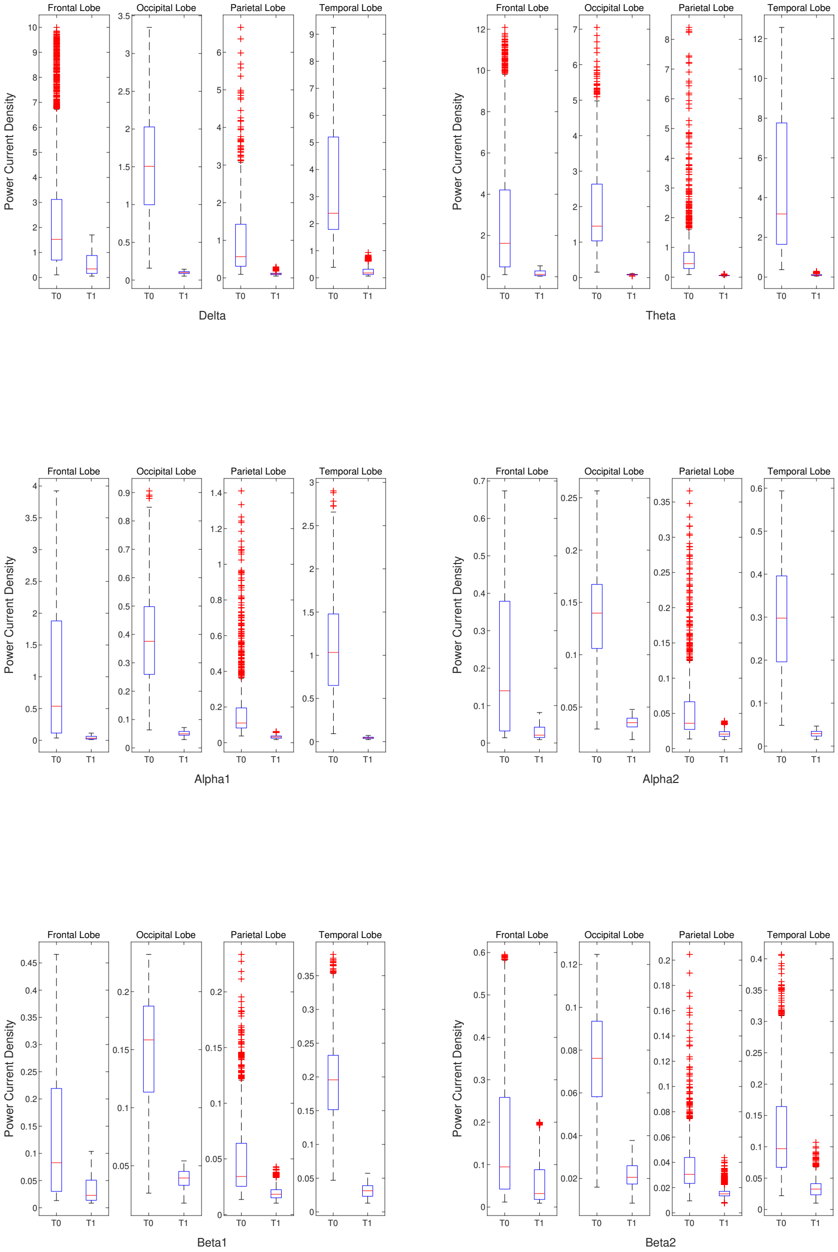

Fig. 3.6: Boxplot of the power current density of patient 51 at time T0 and T1 for each frequency sub-band and each region of interest (frontal, occipital, parietal, and temporal).

Pt 71

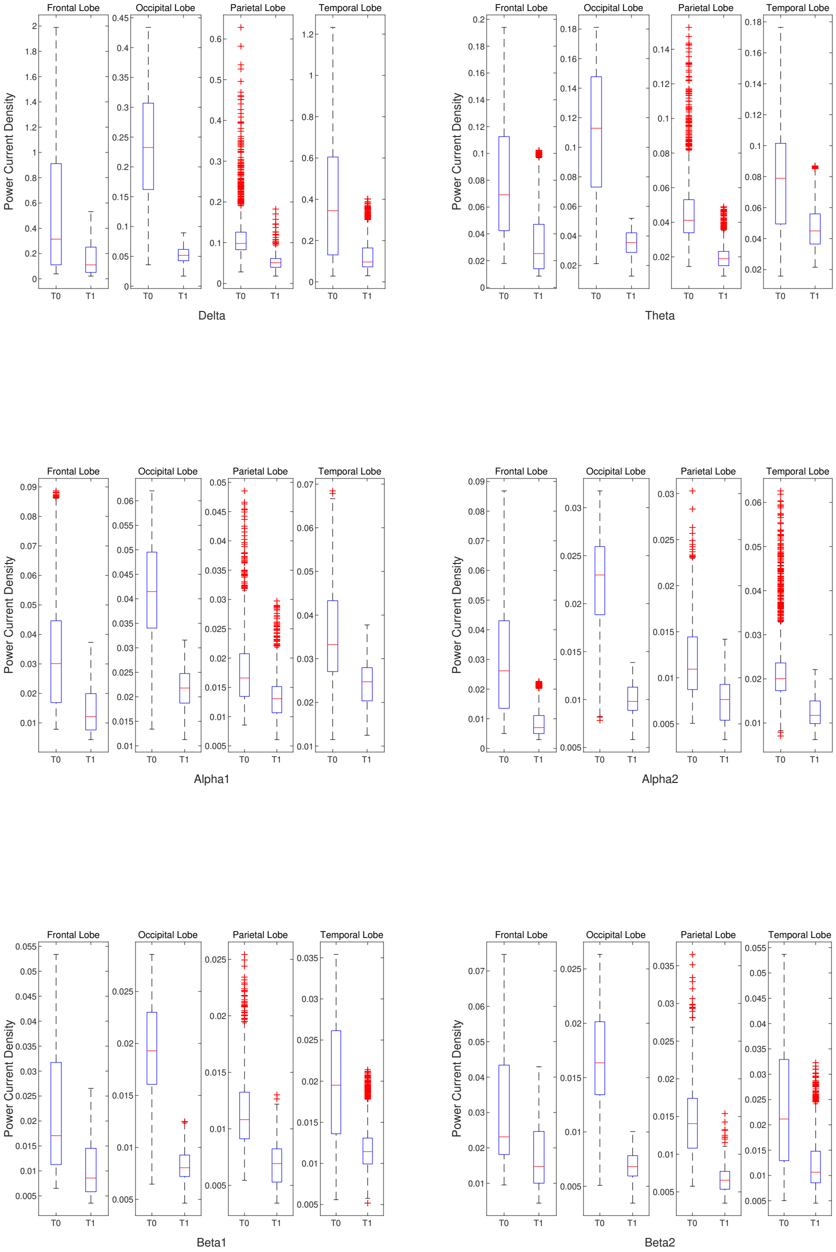

Fig. 3.7: Boxplot of the power current density of patient 71 at time T0 and T1 for each frequency sub-band and each region of interest (frontal, occipital, parietal, and temporal).

Pt 164

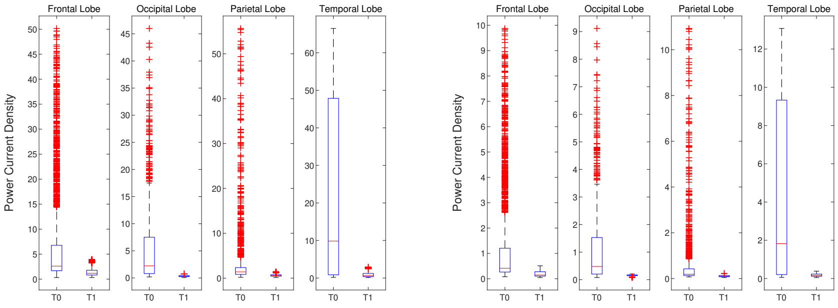

Delta Theta

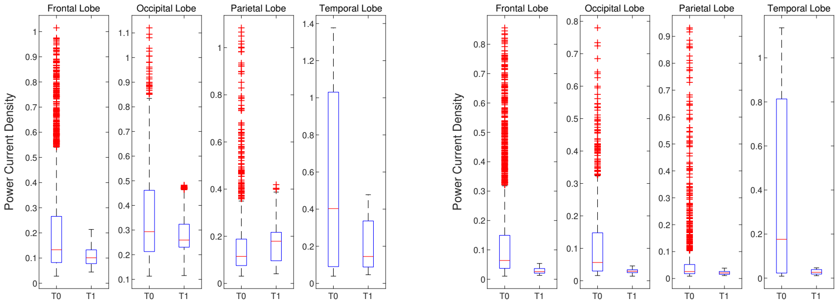

Alpha1 Alpha2

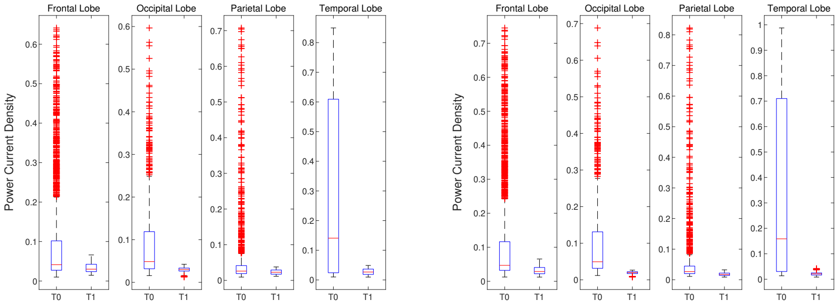

Beta1 Beta2

Fig. 3.8: Boxplot of the power current density of patient 164 at time T0 and T1 for each frequency sub-band and each region of interest (frontal, occipital, parietal, and temporal).

Pt 180

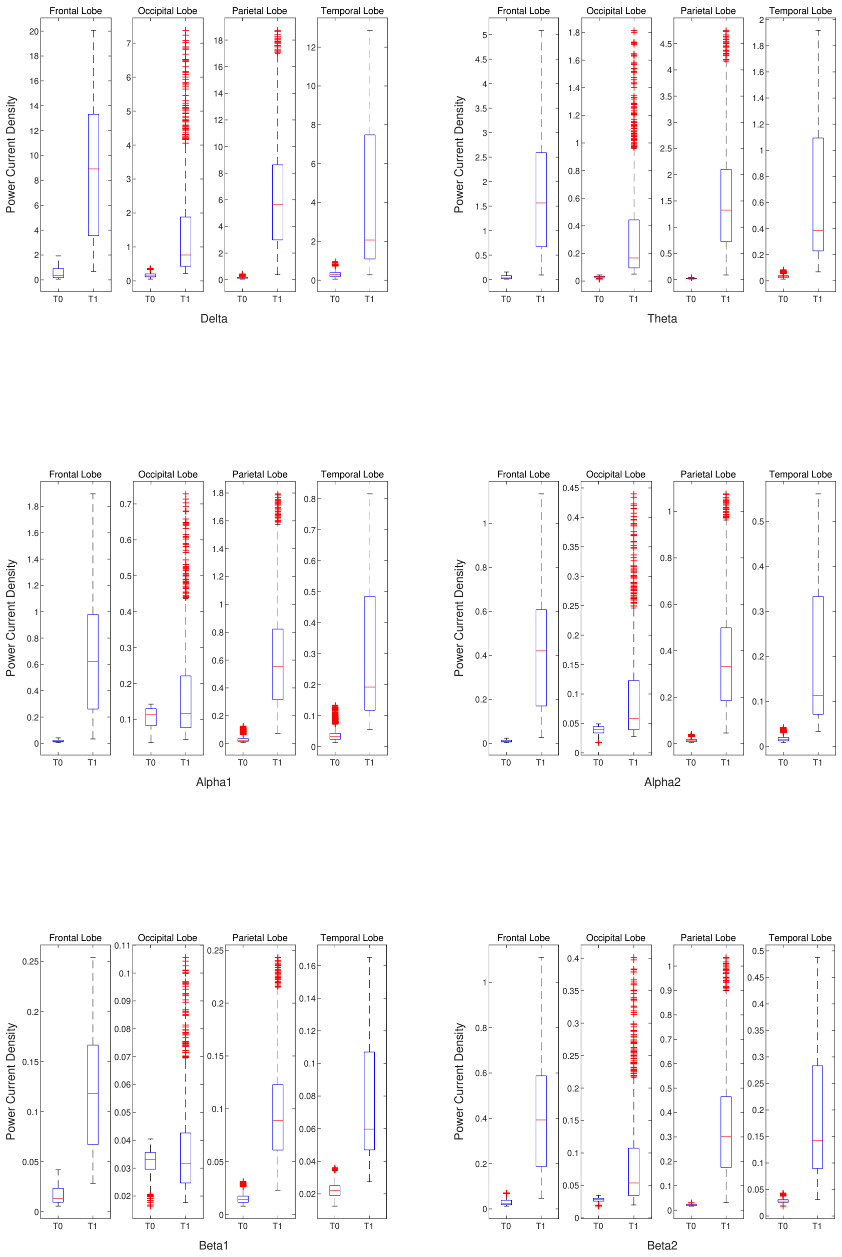

Fig. 3.9: Boxplot of the power current density of patient 180 at time T0 and T1 for each frequency sub-band and each region of interest (frontal, occipital, parietal, and temporal).

Pt 184

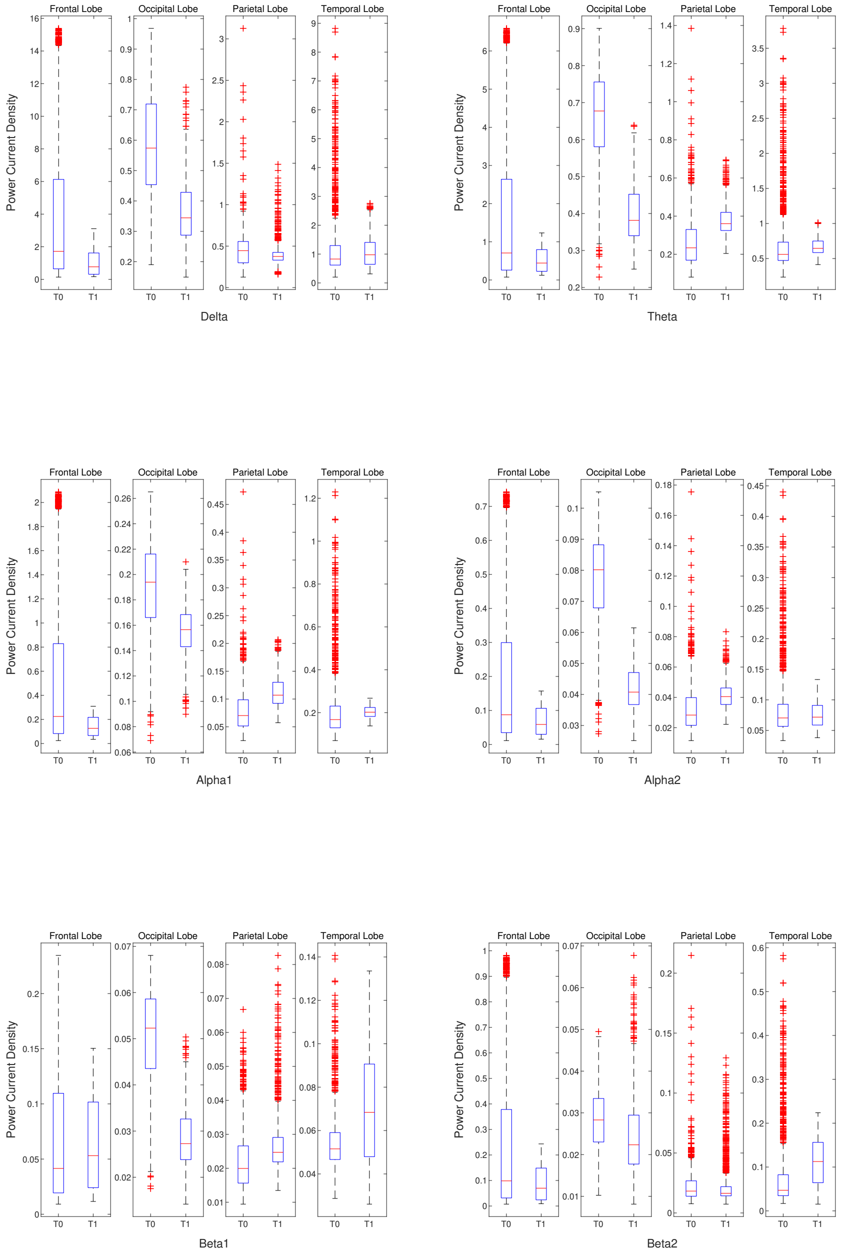

Fig. 3.10: Boxplot of the power current density of patient 184 at time T0 and T1 for each frequency sub-band and each region of interest (frontal, occipital, parietal, and temporal).

Table 3.2: p-values resulting from the Wilcoxon rank sum test for delta and theta sub-bands.

Patient ID	Delta				Theta			
	F. L.	**O. L.**	**P. L.**	**T. L.**	**F. L.**	**O. L.**	**P. L.**	**T. L.**
Pt 03	8.75×10^{-222}	1.12×10^{-235}	2.82×10^{-180}	7.55×10^{-264}	1.54×10^{-23}	1.49×10^{-161}	5.13×10^{-13}	4.16×10^{-48}
Pt 32	2.38×10^{-301}	6.10×10^{-207}	0	2.12×10^{-240}	2.73×10^{-8}	2.90×10^{-244}	1.82×10^{-234}	2.54×10^{-160}
Pt 41	3.22×10^{-14}	2.78×10^{-55}	2.37×10^{-18}	3.382×10^{-29}	0	6.27×10^{-101}	8.97×10^{-6}	5.55×10^{-5}
Pt 51	0	4.60×10^{-250}	0	0	0	4.60×10^{-250}	0	0
Pt 71	8.15×10^{-184}	2.31×10^{-232}	4.56×10^{-303}	1.37×10^{-148}	7.94×10^{-319}	5.59×10^{-222}	6.23×10^{-309}	1.13×10^{-134}
Pt 164	3.87×10^{-261}	9.26×10^{-214}	4.17×10^{-210}	1.55×10^{-147}	0	1.39×10^{-168}	4.16×10^{-189}	2.62×10^{-171}
Pt 180	0	2.66×10^{-242}	0	0	0	4.60×10^{-250}	0	0
Pt 184	1.05×10^{-126}	7.47×10^{-124}	7.11×10^{-15}	3.80×10^{-4}	1.15×10^{-44}	3.22×10^{-187}	4.31×10^{-131}	6.08×10^{-30}

Table 3.3: p-values resulting from the Wilcoxon rank sum test for alpha 1 and alpha 2 sub-bands.

Patient ID	Alpha 1				Alpha 2			
	F. L.	**O. L.**	**P. L.**	**T. L.**	**F. L.**	**O. L.**	**P. L.**	**T. L.**
Pt 03	7.81×10^{-70}	0.0511	3.42×10^{-38}	1.23×10^{-47}	4.07×10^{-27}	4.38×10^{-111}	0.4836	8.77×10^{-8}
Pt 32	2.30×10^{-63}	7.24×10^{-36}	0.6518	2.06×10^{-15}	3.78×10^{-14}	2.45×10^{-69}	3.65×10^{-27}	2.24×10^{-33}
Pt 41	0	4.60×10^{-250}	1.37×10^{-97}	5.93×10^{-88}	0	2.07×10^{-118}	8.614×10^{-90}	5.95×10^{-5}
Pt 51	0	8.09×10^{-250}	0	0	0	5.44×10^{-242}	4.74×10^{-242}	0
Pt 71	1.69×10^{-302}	4.72×10^{-206}	5.86×10^{-90}	1.25×10^{-150}	0	2.97×10^{-225}	1.63×10^{-164}	1.55×10^{-248}
Pt 164	1.46×10^{-61}	5.18×10^{-7}	2.09×10^{-18}	2.84×10^{-18}	5.62×10^{-317}	5.06×10^{-81}	1.50×10^{-39}	6.83×10^{-74}
Pt 180	0	1.81×10^{-9}	0	0	0	1.32×10^{-75}	0	0
Pt 184	1.45×10^{-68}	4.03×10^{-92}	2.72×10^{-127}	1.16×10^{-31}	4.80×10^{-42}	1.28×10^{-217}	2.05×10^{-90}	0.7671

Table 3.4: p-values resulting from the Wilcoxon rank sum test for beta 1 and beta 2 sub-bands.

Patient ID	Beta 1				Beta 2			
	F. L.	**O. L.**	**P. L.**	**T. L.**	**F. L.**	**O. L.**	**P. L.**	**T. L.**
Pt 03	0.0015	5.75×10^{-79}	8.44×10^{-9}	0.8607	0.4786	1.66×10^{-11}	0.0279	4.77×10^{-6}
Pt 32	1.02×10^{-21}	8.53×10^{-13}	7.93×10^{-40}	5.12×10^{-11}	1.17×10^{-34}	0.0037	3.85×10^{-105}	0.0128
Pt 41	0	9.77×10^{-248}	0	0	0	4.60×10^{-250}	0	0
Pt 51	7.31×10^{-268}	3.02×10^{-228}	6.65×10^{-241}	0	1.83×10^{-191}	6.56×10^{-229}	9.64×10^{-273}	1.41×10^{-321}
Pt 71	6.83×10^{-260}	6.19×10^{-232}	6.19×10^{-232}	1.02×10^{-176}	1.58×10^{-196}	9.14×10^{-229}	0	3.09×10^{-141}
Pt 164	2.77×10^{-80}	4.62×10^{-87}	3.14×10^{-19}	1.23×10^{-68}	3.13×10^{-181}	8.86×10^{-214}	1.23×10^{-132}	2.67×10^{-279}
Pt 180	0	0.4370	0	0	0	1.84×10^{-149}	0	0
Pt 184	0.0016	5.54×10^{-200}	2.60×10^{-55}	6.59×10^{-45}	1.45×10^{-33}	1.05×10^{-26}	2.67×10^{-4}	1.47×10^{-78}

Conclusions

This work proposed a longitudinal study involving eight patients who converted from MCI to AD after four months. The novelty is that the spectral power analysis was carried out by means of eLORETA algorithm, which should provide a better source localization accuracy compared to LORETA. The previous works, both cross-sectional and longitudinal, were all carried out using LORETA [84–94]. The time period of follow-up was relatively short, so the condition at time T1 should be considered as slight worse in comparison with MCI condition at time T0. Finally, unlike the three longitudinal studies reported in [92–94], whose results are at group level, this work wants to investigate whether resting state EEG sources can be a marker to follow the progression of the disease in a single AD subject. In our study, five patients (03, 32, 41, 180, and 184) out of eight showed an increasing power in delta and theta bands. All patients, except for 180, exhibited a lower activation in alpha 1 and beta 2 bands. Finally, all patients, except for 03 and 180, revealed a decreased power in alpha 2 and beta 1 bands. Most of the findings are consistent with those of previous studies. On the other hand, the discrepancy of some outcomes could be related to the not yet severe stage of the disease at time T1. This topic needs to be further explored. As for the future development, it could be interesting to apply the eLORETA method to HD-EEG, which should improve the source localization accuracy. In addition, it would be advisable to test the method on a larger number of patients for the validation of results. In order to further confirm the better performance of eLORETA as compared to both LORETA and sLORETA, as already proved in [33, 34], a comparative methodological study could be carried out. Moreover, as in recent years several new algorithms for solving the EEG inverse problem have been developed, a comparison between them and eLORETA would be essential for testing the eLORETA effectiveness [95]. Finally, the combination of source reconstruction with complex network analysis could also provide a further instrument for a better understanding of the evolution of the disease. In conclusion, this study represents a first step for more detailed investigations, in order to make the analysis of power current density a valid tool for evaluating the cognitive decline in AD.

3.2.4 eLORETA active-source reconstruction applied to HD-EEG in Alzheimer's disease

The purpose of this study is the computation of the brain electrical activity by the eLORETA method for three groups of subjects: CNT (healthy subjects), MCI patients and AD patients. The analysis of the results suggests that EEG of MCI and, even more, of AD is characterized by an increasing power in delta and theta bands as compared with CNT. Moreover, it has been shown that the greater source activation involves Brodmann areas typically affected by this pathology and is consistent with it.

The subsection is organized as follows: first the methodology is explained; then, information about patients and EEG recordings are provided; finally the experimental results are presented and discussed.

Methodology

In this study, the active source reconstruction was computed by the LORETA-KEY software (v20181107), using the eLORETA algorithm. Three groups of subjects were involved: CNT, MCI and AD. The brain electrical activity of each subject was reconstructed for the frequency sub-bands delta (0.5–4 Hz) and theta (4–8 Hz). The average current density of each group was obtained by averaging the current density of all subjects belonging to the given group.

HD-EEG recordings and preprocessing

EEG signals were acquired by the 256-channel HydroCel Geodesic Sensor Net, belonging to the Geodesic EEG System (GES). The electrodes are arranged so that their interdistance is the shortest distance between two points on the surface of a sphere. In such a way, the sampling of the electrical field is optimized [96]. The high-density montage is shown in Figure 3.11. The electrode impedance was kept <50 kΩ, according to EGI guidelines. The reference electrode was Cz, placed in the middle of the head surface. The data were recorded at IRCCS Centro Neurolesi Bonino-Pulejo of Messina (Italy). The study involved three groups of subjects: 12 CNT, 23 MCI and 16 AD. The demographic data of the subjects are reported in Table 3.5. The EEGs were detected in an eye-closed resting state with sampling rate of 250 Hz. The EEGs were band-pass filtered between 1 and 40 Hz and cleaned from artifacts by visual inspection. Only 173 channels from the starting 256 were considered because the recordings from the sensors placed on the face and the neck were too noisy. Finally, the EEG recordings were average referenced and segmented into artifact-free non-overlapping epochs of 250 samples [5].

Table 3.5: Demographic data for each group of subjects.

Patients	**Female**	**Male**	**Age**
CNT	7	5	62±5
MCI	13	10	69±8
AD	11	5	74±11

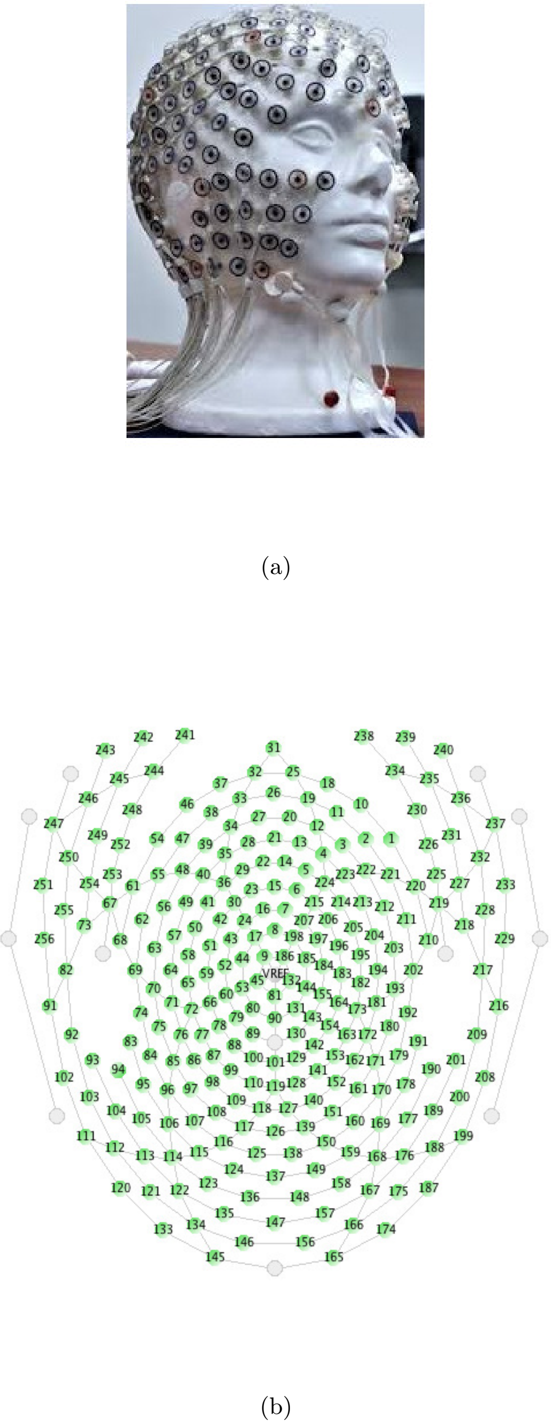

Fig. 3.11: HD-EEG acquisition system: (**a**) The 256-channel HydroCel Geodesic Sensor Net; (**b**) 2D representation of the 256-channel HydroCel Geodesic Sensor Net montage.

Results

EEG frequency bands have a specific biological significance and can be associated to different states of brain functioning. As reported in subsection 3.2.2, AD patients are characterized by a "slowing" of their EEG, that is an increase of power for the lower frequency bands (delta and theta). Therefore, eLORETA analysis of the above-mentioned frequency sub-bands can be used for determining which brain regions are activated during different states. The brain electrical activity of each subject was reconstructed for the frequency sub-bands delta (0.5–4 Hz) and theta (4–8 Hz). The average current density of each group was obtained by averaging the current density of all subjects belonging to the given group. The results are shown in Figures 3.12-3.13. As for the delta rhythm, in MCI the most activated area is the Brodmann area 38 of the right hemisphere, in the temporal lobe (Figure 3.12b); in AD there is a greater activation in Brodmann area 21 of both hemispheres, in the temporal lobe too (Figure 3.12c). Both MCI and AD show an increase of power spectrum as compared with CNT (Figure 3.12a). As for the theta rhythm, also in this case, in MCI and AD there is a greater activation of the temporal lobe areas in comparison to CNT (Figure 3.13a). In particular, in MCI the maximum current density value is in Brodmann area 38 of the right hemisphere (Figure 3.13b), whereas in AD it is in Brodmann area 37 of the right hemisphere (Figure 3.13c).

Brodmann area 21 is associated with language and complex sounds processing. Brodmann area 37 is involved in lexico-semantic associations (i.e. associated words with visual percepts). Brodmann area 37 seems to be also participating in some memory circuitries, especially when visual information is involved. Clinical observations have proved that damage in Brodmann area 37 usually results in word-finding difficulties and semantic paraphasias. Brodmann area 38 is involved in language processes, emotion, executive functions and memory. This is one of the earliest areas affected by Alzheimer's disease. These results are consistent with the hallmarks of Alzheimer's disease reported in literature.

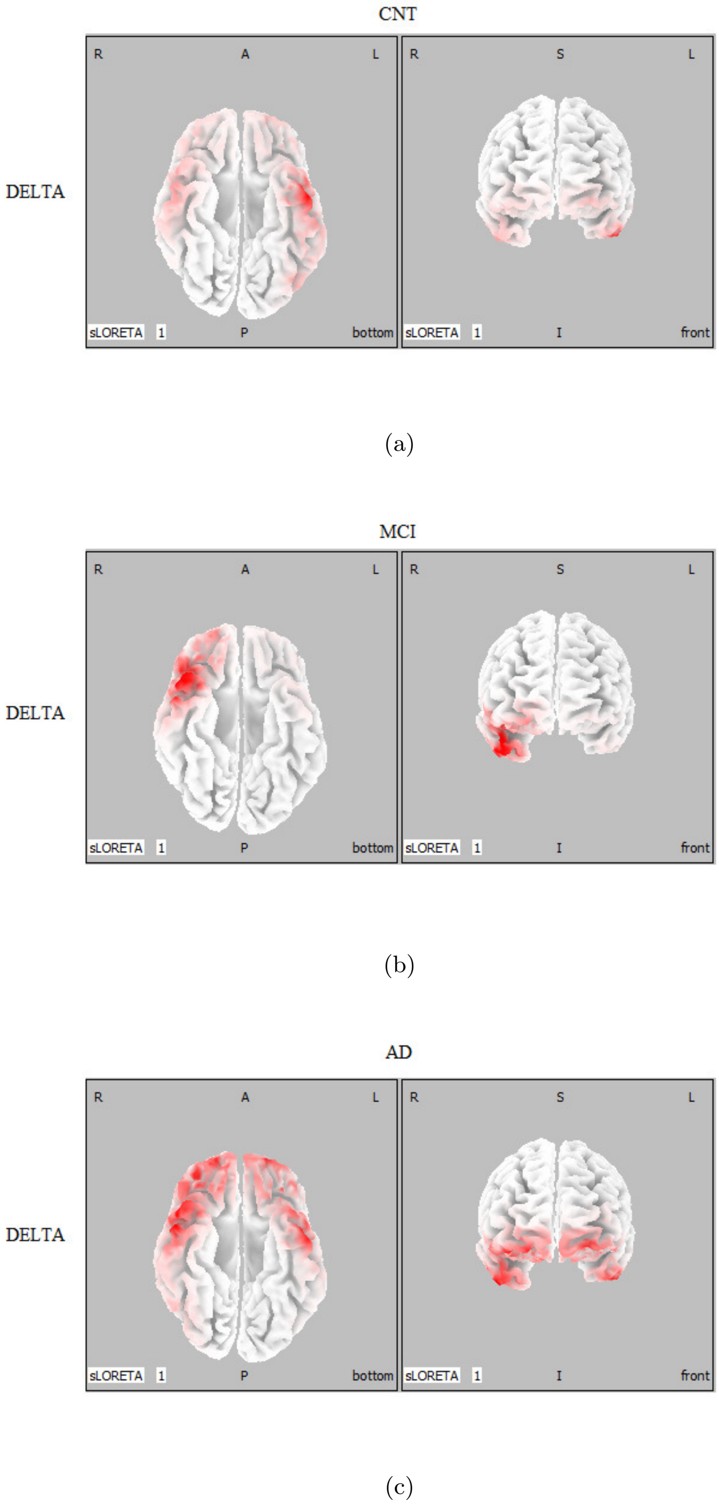

(a)

(b)

(c)

Fig. 3.12: Active source distribution in delta band for (**a**) CNT, (**b**) MCI and (**c**) AD. On the left: a bottom view of the brain cortex. On the right: a front view of the brain cortex.

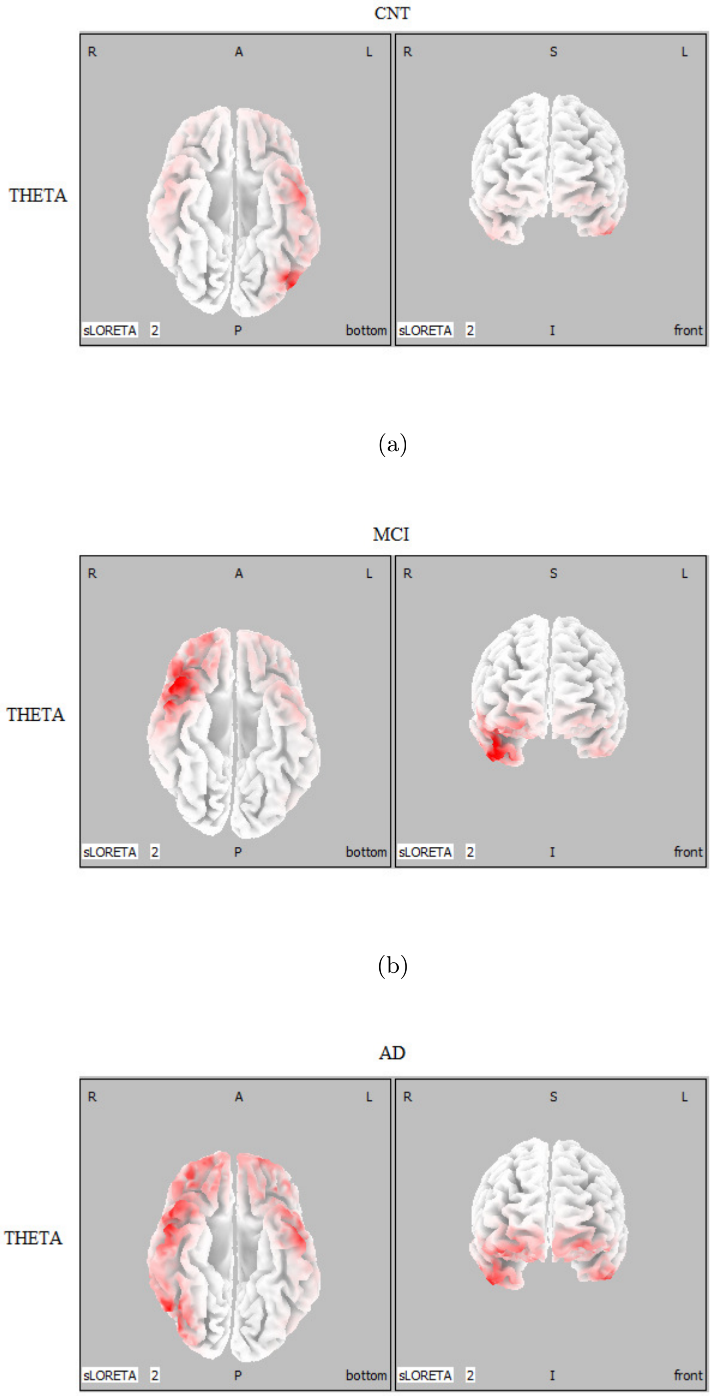

(a)

(b)

(c)

Fig. 3.13: Active source distribution in theta band for (**a**) CNT, (**b**) MCI and (**c**) AD. On the left: a bottom view of the brain cortex. On the right: a front view of the brain cortex.

Conclusions

This work provided a reconstruction of the brain active sources by means of the eLORETA method applied to HD-EEG. The study involved three groups of subjects: 12 CNT, 23 MCI and 16 AD. The current density estimation was carried out for delta and theta rhythms because they are two critical frequency bands in Alzheimer's disease. eLORETA computation of current density distribution revealed that some regions of temporal lobe are more active in MCI and AD as compared to CNT. Moreover, the most activated Brodmann areas obtained from the eLORETA source reconstruction are considered as regions deeply affected by Alzheimer's disease. This study could be further enlarged by combining source reconstruction with network connectivity measurement to analyze the evolution of the disease from two different but complementary points of view. In this way, the eLORETA method applied to HD-EEG could turn out to be a promising instrument for improving diagnosis of Alzheimer's disease.

3.2.5 Brain network analysis based on eLORETA active-source reconstruction applied to HD-EEG in Alzheimer's disease

The purpose of this work is to study the brain network parameters through the estimation of Lagged Linear Connectivity (LLC), computed by the LORETA-KEY software, for three groups of subjects: CNT, MCI and AD. In particular, the aim is to compare the results obtained using a 256-channel EEG, the corresponding 10–10 system 64-channel EEG and the corresponding 10–20 system 18-channel EEG, both of which are extracted from the 256-electrode configuration. The analysis of the results suggests that the small-world properties of MCI and AD patients are weakened only when the high-density electrode configuration is used. On the contrary, the results achieved by the analysis based on the standard low-density EEG are inconsistent with the cognitive decline in AD patients.

The subsection is organized as follows: first an overview of the findings about brain functional connectivity is presented; then, information about patients and EEG recordings are provided and the methodology is described; finally the results are presented and discussed.

Brain functional connectivity: a review

Graph theory represents a very useful tool to study complex brain network. According to graph theory, nodes (vertices) denotes the brain regions that are linked by edges, representing structural or functional connection [97]. Brain functional connectivity refers to the functionally integrated relationship between spatially separated brain regions and is defined in terms of statistical dependencies in the time domain (correlation) and in the frequency domain (coherence) among neurophysiological measurements. Coito et al. [98] investigated connectivity in temporal lobe epilepsy (TLE) in the absence of interictal epileptiform discharges (IEDs). Their study revealed a reduced connectivity from regions concordant with the default-mode network and a different network pattern in TLE patients compared to healthy controls. Astolfi et al. [99] employed graph theory for studying HD-EEG and fMRI of healthy subjects during the execution of the Stroop task. Recently, it has been shown that brain networks are characterized by a small-world architecture [97,100]. The small-world property of a normal brain network combines high levels of local specialization and global integration among nodes and can be measured , respectively, by the Clustering Coefficient (CC) [97] and the Characteristic Path Length (λ) [97]. The Connection Density (D) [101] is another index used to define the network's behavior: the more connections there are, the denser the network will be. Several studies reported that the EEG synchrony and the functional connections between regions decrease for AD [102–104]; it has also been proved that small-world properties extracted from EEG of AD patients are very weakened [105–107]. Mammone et al. [108] used the Permutation Disalignment Index (PDI) to obtain the connectivity matrices starting from HD-EEG of three groups: CNT, MCI and AD. HD-EEG were also compressed and reconstructed applying the Block Sparse Bayesian Learning (BSBL). It was shown that the three groups have network parameters significantly different and the compression does not alter the results of the network analysis.

The first step for an accurate connectivity analysis is the localization of the brain active sources. Starting from cortical electrical activity estimated with LORETA, functional connectivity measurements can be performed by a toolbox recently introduced in the LORETA-KEY software. To date, this tool was employed in research about Alzheimer's disease, above all, in the case of low-density EEG. In particular, Hata et al. [109] reported a decreased lagged phase synchronization in delta band between most cortical regions in AD subjects in comparison to healthy controls. Moreover, Babiloni et al. [110] showed that brain functional connectivity is lower in MCI patients compared to healthy elderly subjects.

Methodology

The experimental setup was arranged as follows:

1. EEG data were collected from three groups of patients (CNT, MCI and AD) by a high-density acquisition system. Starting from that, three different electrodes configurations were considered. The signals preprocessing was performed by means of MATLAB;
2. the preprocessed EEGs were used as input signals for the LORETA-KEY software. In order to quantify the functional connectivity, the Lagged Linear Connectivity (LLC) matrix was computed for each couple of regions of interest (ROIs), for a given frequency range;
3. starting from the LLC, the small-world properties of the brain networks were measured by three parameters: λ, CC, and D, estimated through a MATLAB toolbox.

Data acquisition system and preprocessing

EEG signals were recorded by the 256-channel HydroCel Geodesic Sensor Net, already described in Subsection 3.2.4. The 18-channel and 64-channel configurations were obtained based on the 10-10 position equivalence for the HydroCel GSN [111].

The dataset consists of HD-EEG recorded at IRCCS Centro Neurolesi Bonino-Pulejo of Messina (Italy). The research was performed as stated in a protocol approved by the local Ethics Committee (Approved N. 003/17). All the subjects involved or their caregivers signed an informed consent form. EEGs were acquired during eyes-closed resting conditions, for three groups of subjects: 10 CNT, 21 MCI and 9 AD. The demographic data of the subjects are reported in Table 3.6. The sampling rate was 250 Hz. The EEGs were filtered at 1 Hz low cut-off (high-pass) and at 40 Hz high cut-off (low-pass). After filtering, artifactual data segments were detected by visual inspection and rejected [112]. Moreover, only 173 channels from the starting 256 were considered because the signals from electrodes placed on the face and the neck were too noisy. Two minutes of cleaned EEGs were considered for each subject. EEGs were finally transformed to a common average reference montage.

Table 3.6: Demographic data for each group of subjects.

Patients	**Female**	**Male**	**Age**
CNT	5	5	61±5
MCI	13	8	68±8
AD	6	3	72±13

Lagged Linear Connectivity

In this work, the computation of brain connectivity was performed starting from the active source reconstruction by means of eLORETA algorithm, implemented in the LORETA-KEY software (v20181107). Moreover, Pascual-Marqui et al. proposed a new method for functional connectivity measurements [113, 114]. They decomposed the total connectivity into instantaneous and lagged contributions: the first one takes into account the potentials generated by distant cortical regions and conducted across head volume (the so-called "volume conduction"), while the lagged component contains almost pure physiological information.

The linear dependence between time series X and Y at frequency ω is defined as:

$$F_{X,Y}(\omega) = \ln \frac{\left| \begin{pmatrix} \mathbf{S}_{Y,Y}(\omega) & \mathbf{0} \\ \mathbf{0}^T & \mathbf{S}_{X,X}(\omega) \end{pmatrix} \right|}{\left| \begin{pmatrix} \mathbf{S}_{Y,Y}(\omega) & \mathbf{S}_{Y,X}(\omega) \\ \mathbf{S}_{X,Y}(\omega) & \mathbf{S}_{X,X}(\omega) \end{pmatrix} \right|} \tag{3.1}$$

where $\mathbf{S}_{X,X}$, $\mathbf{S}_{Y,Y}$, $\mathbf{S}_{X,Y}$, $\mathbf{S}_{Y,X}$ denote the complex valued covariance matrices and $|\mathbf{M}|$ is the determinant of $\mathbf{M}$.

Linear dependence can be expressed as the sum of the lagged linear dependence $F_{X\rightleftarrows Y}(\omega)$ and the instantaneous linear dependence $F_{X\cdot Y}(\omega)$:

$$F_{X,Y}(\omega) = F_{X\rightleftarrows Y}(\omega) + F_{X\cdot Y}(\omega) \tag{3.2}$$

The instantaneous linear dependence is defined as:

$$F_{X\cdot Y}(\omega) = \ln \frac{\left| \mathrm{Re} \begin{pmatrix} \mathbf{S}_{Y,Y}(\omega) & \mathbf{0} \\ \mathbf{0}^T & \mathbf{S}_{X,X}(\omega) \end{pmatrix} \right|}{\left| \mathrm{Re} \begin{pmatrix} \mathbf{S}_{Y,Y}(\omega) & \mathbf{S}_{Y,X}(\omega) \\ \mathbf{S}_{X,Y}(\omega) & \mathbf{S}_{X,X}(\omega) \end{pmatrix} \right|} \tag{3.3}$$

where $\mathrm{Re}(\mathbf{M})$ denotes the real part of $\mathbf{M}$.

Finally, the measure of lagged linear dependence is:

$$F_{X\rightleftarrows Y}(\omega) = F_{X,Y}(\omega) - F_{X\cdot Y}(\omega) = \ln \frac{\left\{ \left| \mathrm{Re} \begin{pmatrix} \mathbf{S}_{Y,Y}(\omega) & \mathbf{S}_{Y,X}(\omega) \\ \mathbf{S}_{X,Y}(\omega) & \mathbf{S}_{X,X}(\omega) \end{pmatrix} \right| \Big/ \left| \mathrm{Re} \begin{pmatrix} \mathbf{S}_{Y,Y}(\omega) & \mathbf{0} \\ \mathbf{0}^T & \mathbf{S}_{X,X}(\omega) \end{pmatrix} \right| \right\}}{\left\{ \left| \begin{pmatrix} \mathbf{S}_{Y,Y}(\omega) & \mathbf{S}_{Y,X}(\omega) \\ \mathbf{S}_{X,Y}(\omega) & \mathbf{S}_{X,X}(\omega) \end{pmatrix} \right| \Big/ \left| \begin{pmatrix} \mathbf{S}_{Y,Y}(\omega) & \mathbf{0} \\ \mathbf{0}^T & \mathbf{S}_{X,X}(\omega) \end{pmatrix} \right| \right\}} \tag{3.4}$$

All these measures are non-negative. They are equal to zero only when there is independence (lagged, instantaneous, or both). They can also be transformed into a "squared coherence", with values in the $[0 \ldots 1]$ range.

In this work, the Connectivity Toolbox implemented in the LORETA-KEY software was used. In particular, the Lagged Linear Connectivity (LLC) was computed by means of Equation (3.4). LLC gives a measurement of the statistical dependence among active sources, estimated by eLORETA, for each pair of cortical ROIs, at a given frequency range. Specifically, we estimated LLC for the all 84 possible ROIs defined by the LORETA-KEY software. The ROIs corresponds to distinct Brodmann areas, 42 for each hemisphere. The analysis was conducted for three different electrode configurations for the frequency range 1–40 Hz. EEG were segmented into artifact-free non-overlapping epochs of 250 samples (1s) [5]. LLC was evaluated for windows of 3 epochs, so we obtained 40 connectivity matrices for each patient. The choice of such a window length allows to perform a statistical analysis also in the event that EEG recordings are short and the number of patients is limited.

Complex network analysis

A network is defined in graph theory as a set of nodes and the links (edges) between them, which can be directed or undirected. In our case every ROI represents a node and the graph is weighted undirected. A weighted graph provides a measure of the connection strength between nodes, so it can be used to distinguish strong connections from weak ones.

Brain functional integration is the capacity to fast combine information from distributed brain regions. The Characteristic Path Length (λ) represents a measure of functional integration of a network [115]. λ is defined as the average shortest path length between all pairs of nodes [97]:

$$\lambda = \frac{1}{n}\textstyle\sum_{i\in N}\frac{\sum_{j\in N, j\neq i} d_{ij}^{w}}{n-1} \tag{3.5}$$

where n is the number of nodes and d_{ij}^{w} is the shortest weighted path length between the nodes i and j.

Functional segregation refers to the ability to create interconnected groups of brain regions (*clusters*). The Clustering Coefficient (CC) is an important parameter to quantify the presence of such groups within the network [115]. It provides a measure of the probability that the neighbors of one node become neighbors each other. The weighted Clustering Coefficient is defined as [97]:

$$CC^{w} = \frac{1}{n}\sum_{i\in N} CC_{i}^{w} = \frac{1}{n}\sum_{i\in N}\frac{2t_{i}^{w}}{k_{i}(k_{i}-1)} \tag{3.6}$$

where CC_i is the Clustering Coefficient of node i, t_i is the number of triangles around the node i and k_i is the number of links connected to a node i, so that $k_i(k_i-1)/2$ is the maximum number of possible edges can exist between neighbors of node i.

The Connection Density (D) of a network is the fraction of actual number of edges in the graph to the total number of possible edges [101]:

$$D = \frac{2k}{N(N-1)} \tag{3.7}$$

where N is the number of all nodes and k is the actual number of links.

A complex network characterized by high Clustering Coefficient, high Connection Density and short average path length has small-world properties.

Data processing and network analysis were conducted in a MATLAB environment (R2018a). In particular, the above-mentioned network parameters were computed by means of the *Brain Connectivity Toolbox*, a MATLAB toolbox for complex network analysis of structural and functional brain connectivity datasets [97].

Results

The methodology explained was applied to the HD-EEG database. Figure 3.14 displays the boxplots of the Characteristic Path Length and the Clustering Coefficient of the three groups of patients for each electrode configuration. Each boxplot is made up of 1600 parameters, 40 for each patient. Figure 3.14a shows that there is no clear difference of λ between the three groups for 18 and 64 electrodes, whereas the difference becomes evident only with the HD configuration (173 electrodes).

In particular the λ median value increases for MCI and even more for AD as compared with CNT. Figure 3.14b highlights that the median CC decreases when 64 electrodes are used, becoming more evident for 173 electrodes. For the low-density EEG the trend is completely different and does not correspond to the expected behavior. In order to validate the results, a statistical analysis was performed. First, a Kruskal–Wallis test [70] was carried out to determine if the samples of groups come from different distributions. Next, the post-hoc Tukey's Honestly Significant Difference (HSD) test [71] was used to perform multiple pairwise comparison of the group means and identify which groups are statistically different. The significance level was set at 5%, so that the differences between groups are statistically significant when $p < 0.05$. Table 3.7 and Table 3.8 show the outcome of the above-mentioned statistical analysis. In regard to λ, there is a significant difference between the all three groups only for 173 electrodes. A significant difference can be also found between CNT and AD groups when 64 sensors are considered. As for CC, it was found a statistically significant difference between CNT-MCI groups and MCI-AD groups when 18 electrodes are employed. It could seem that low-density configuration is able to detect the variations between the groups but, actually, this is not consistent with the expected trend of the parameter: in fact the median value in AD is higher than MCI and CNT whereas it should be lower. Finally, a statistical significant difference arises from the comparison between CNT and AD for both 64 and 173 electrodes. It is important to underline that only the results from HD-EEG are consistent with the expected behavior of the brain network, which is the weakening of small-world properties of MCI and AD patients in comparison to healthy subjects. It is noted that the variation of the network parameters was not detected correctly when the standard 10–20 configuration was employed.

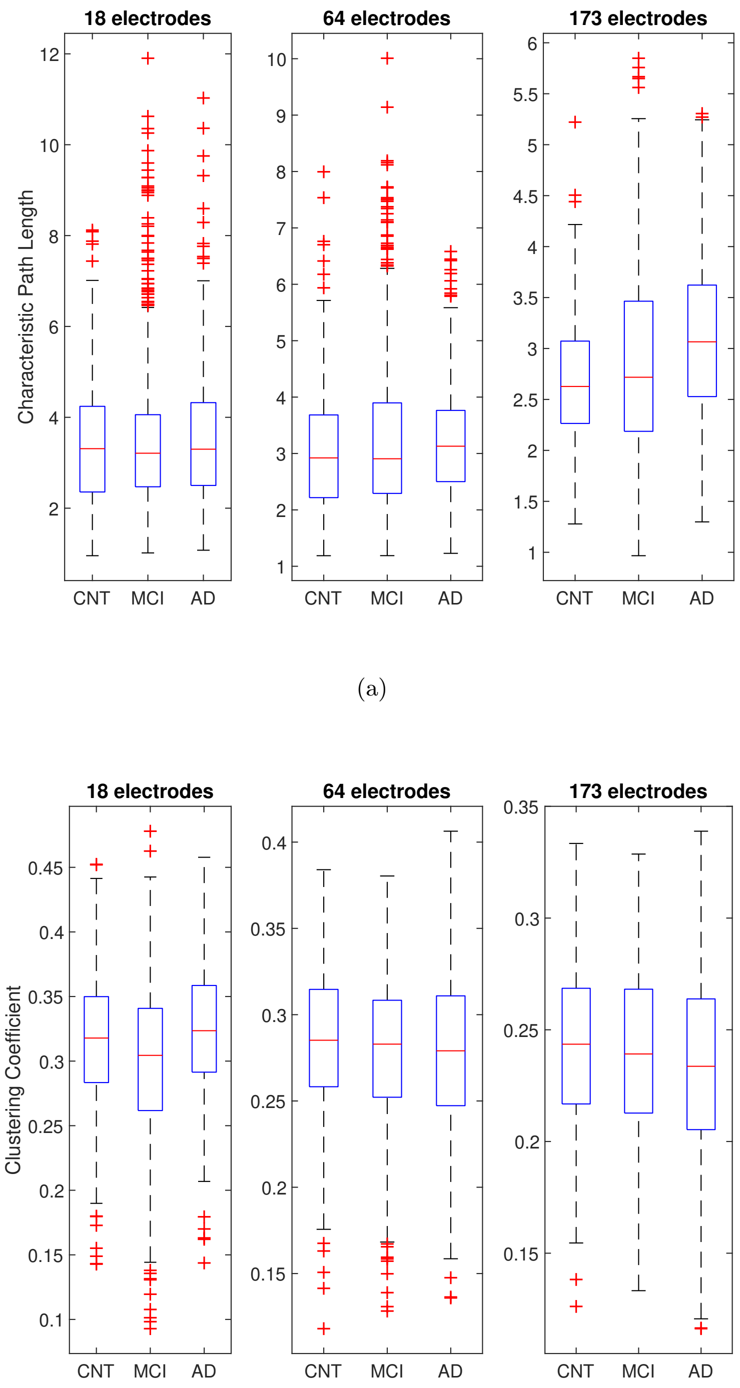

(a)

(b)

Fig. 3.14: (**a**) Boxplot of the Characteristic Path Length of CNT, MCI, and AD; (**b**) boxplot of the Clustering Coefficient of CNT, MCI, and AD. Both are computed for three electrode configurations. The bottom and the top edges of the boxes indicate the first and the third quartile, respectively; the segment inside the boxes represents the median and the "whiskers" below and above the boxes are the minimum and maximum values of the distribution. The stars outside the whiskers are considered outliers.

Table 3.7: Results of Kruskal–Wallis test.

Characteristic Path Length *p*-**Value**			**Clustering Coefficient** *p*-**Value**			**Connection Density** *p*-**Value**		
18	**64**	**173**	**18**	**64**	**173**	**18**	**64**	**173**
0.4345	0.0130	1.38×10^{-12}	6.24×10^{-10}	0.0282	0.0481	0.8780	0.9870	0.9965

Table 3.8: Results of Tukey's HSD post-hoc test.

Subjects	**Characteristic Path Length** *p*-**Value**			**Clustering Coefficient** *p*-**Value**		
	18	**64**	**173**	**18**	**64**	**173**
CNT-MCI	0.9974	0.1835	0.0101	2.8×10^{-4}	0.0613	0.3000
MCI-AD	0.4507	0.2054	8.6×10^{-8}	3.0×10^{-9}	0.7935	0.3353
CNT-AD	0.5132	0.0091	9.5×10^{-10}	0.0918	0.0377	0.0368

The Connection Density was computed as a function of the threshold applied to the weighted connection matrix. Obviously, the network will be totally connected if the threshold is set to 0 and disconnected if the threshold is set to 1. Figure 3.15 shows the mean value of D of each group of subjects for the three sensors configurations. AD and MCI patients should have lower network density than healthy controls. This trend is visible only when we used at least 64 sensors and becomes more evident with 173 electrodes. The statistical analysis shows that the data of the three groups come from the same distribution, so there is not a significant statistical difference between them (Table 3.7). Nevertheless, if you consider some patients individually, there is a reduction of the connections between the brain regions when 173 electrodes were employed. As an example, Figures 3.16–3.18 display the links between the network nodes, representing the 84 ROIs, of one subject for each group, for the three electrode configurations. The images were obtained by thresholding the weighted connection matrix at 0.3: at this value the corresponding network is moderately connected (Figure 3.15). It is evident that there is a clear reduction in the network links for MCI and AD just when 173 sensors are used. Specifically, there are no connections in the posterior regions for MCI and AD. This outcome agrees with recent studies reporting a reduction in functional connectivity within posterior areas in Alzheimer's Disease [116, 117]. For 18 and 64 electrodes the pictures of the three groups are indistinguishable. It can be supposed that 64 sensors are not sufficient for a correct estimation of functional connectivity. This topic needs further investigation in the future.

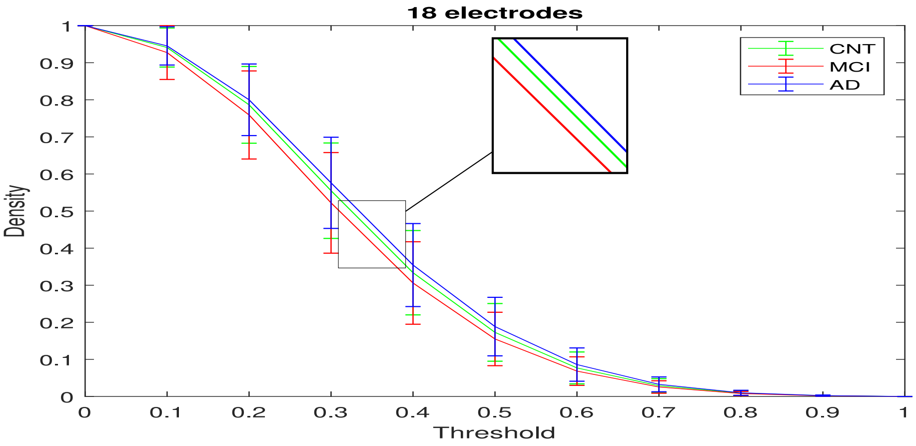

(a)

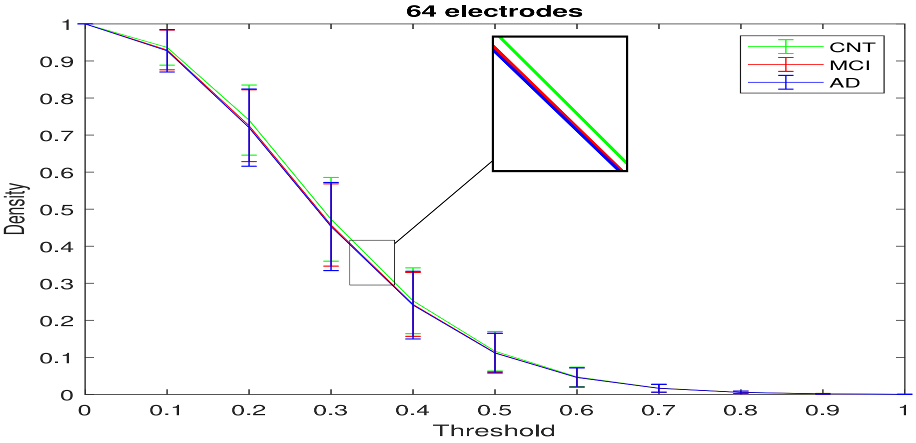

(b)

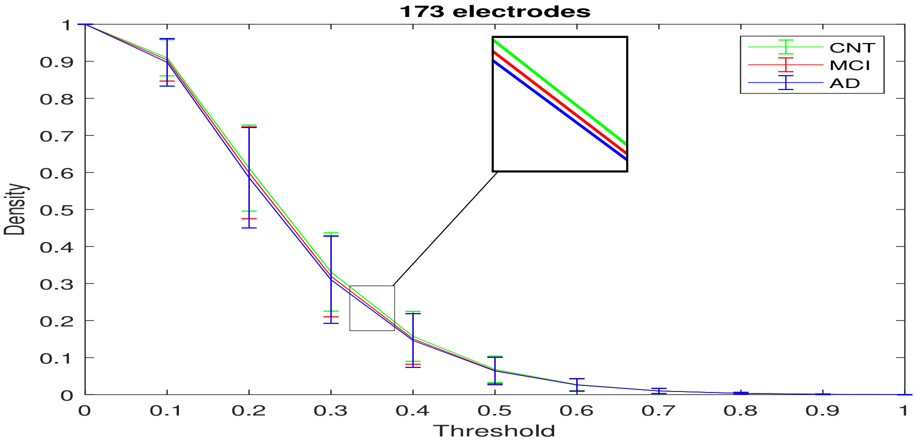

(c)

Fig. 3.15: Mean values of the Connection Density (D) computed by thresholding the connectivity matrix of CNT, MCI, and AD for: (**a**) 18 electrodes, (**b**) 64 electrodes and (**c**) 173 electrodes. The vertical segments represent the standard deviation of D.

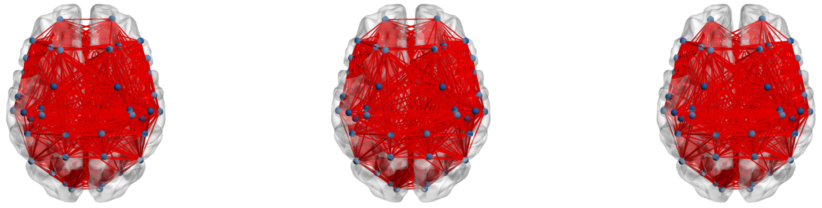

(a) (b) (c)

Fig. 3.16: Connections between ROIs for 18 electrodes of: (**a**) CNT, (**b**) MCI and (**c**) AD.

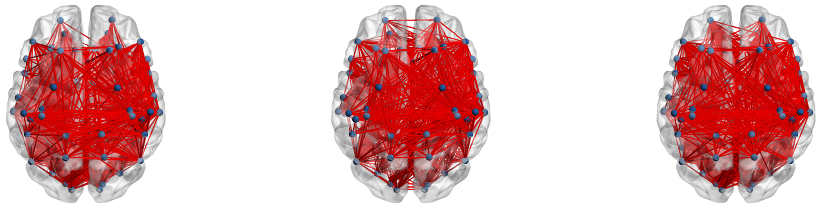

(a) (b) (c)

Fig. 3.17: Connections between ROIs for 64 electrodes of: (**a**) CNT, (**b**) MCI and (**c**) AD.

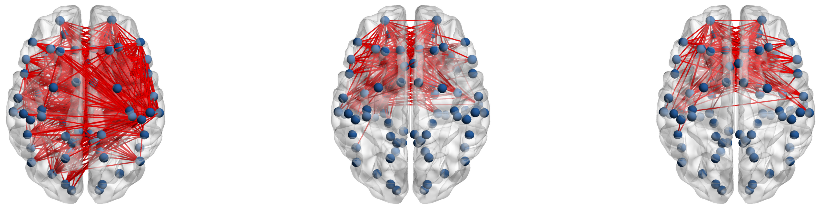

(a) (b) (c)

Fig. 3.18: Connections between ROIs for 173 electrodes of: (**a**) CNT, (**b**) MCI and (**c**) AD.

Conclusions

This study explored the brain network behavior for 10 healthy subjects (CNT), 21 MCI, and 9 AD patients. The brain functional connectivity was quantified by the computation of the Lagged Linear Connectivity parameter, which can be measured through the toolbox implemented in the eLORETA software. This index provides a measure of the true physiological connections, excluding instantaneous zero-lag contribution related to the volume conduction [114]. The novelty is the comparison between high-density EEG and low-density EEG results evaluated with this method: in particular, the network parameters were estimated for 84 ROIs considering 18, 64 and 173 electrodes, extracted by the starting 256-channel EEG. From the analysis of the three network parameters we focused on, arose that: the Characteristic Path Length of MCI and AD patients is higher than CNT for the 173 electrode configuration, whereas it does not show a clear difference between the three groups of patients for 18 electrodes; the Clustering Coefficient of MCI and AD decreases when 173 sensors are employed but it increases for AD with 18 electrodes; as reported in Table 3.9, which refers to Figure 3.15, the Connection Density decreases for MCI and AD with 173 electrodes; on the contrary it increases for AD when 18 sensors are used. The statistical analysis validated the results for λ and CC, according to which the small-world properties of MCI and AD patients are weakened just when the high-density electrode configuration is used. When the study was based on the standard low-density EEG, the results are not consistent with the behavior of the brain network affected by this pathology. Therefore, the current study suggests that it is advisable to use HD-EEG to achieve a better accuracy of results. These findings are also supported by the studies reported in [21, 22, 45, 46], according to which the localization accuracy of the epileptogenic zones, reconstructed by LORETA, improves when a high-density montage is used. As a consequence, the more the active-source localization is precise, the more the computation of the functional connectivity between brain regions is reliable. Although our results appear interesting, some limitations should be addressed. In particular, EEG recordings of a greater duration could be detected: in this case, it could be investigated if the EEG epochs and windows lengths affected the network parameters [118]. The methodology needs to be tested on a larger number of subjects, to confirm the results. Moreover, an intra-subject longitudinal study could be carried out to analyze the evolution of the disease in each single patient over time. The complex network analysis could also be performed together with the reconstruction of the brain active sources for each EEG frequency sub-band (delta, theta, alpha and beta). The integration of these analysis could provide a more complete vision of the brain behavior, resulting in a valid instrument for quantifying the loss of brain connections typical of Alzheimer's Disease. As a further development, future research could be performed, for example, with more advanced methodological improvements, combining the transcranial magnetic stimulation (TMS) with HD-EEG [119]. In conclusion, this study showed that HD-EEG seem to reveal resting-state connectivity alterations in AD patients, so this method could be a useful tool to predict the disease severity and improve diagnosis, clinical and therapeutic management.

Table 3.9: Mean Connection Density values of CNT, MCI, and AD for all electrode configurations for three threshold values.

THRESHOLD	**DENSITY**								
	18			**64**			**173**		
	CNT	**MCI**	**AD**	**CNT**	**MCI**	**AD**	**CNT**	**MCI**	**AD**
0.3	0.5549	0.5221	0.5761	0.4725	0.4572	0.4530	0.3312	0.3196	0.3101
0.5	0.1729	0.1551	0.1885	0.1164	0.1123	0.1114	0.0682	0.0651	0.0639
0.7	0.0290	0.0256	0.0327	0.0168	0.0165	0.0161	0.0101	0.0100	0.0099

3.3 Applications of LORETA for gliotic lesions

Gliosis is a nonspecific reactive modification of glial cells caused by a damage to the central nervous system (CNS). Specifically, gliosis is a process of proliferation or hypertrophy of several different types of glial cells, including astrocytes, microglia, and oligodendrocytes. The degree and type of the gliosis response change widely depending on the triggering insult. In its most severe form, gliosis leads to the formation of a glial scar. Gliosis arises from several acute conditions such as trauma, ischemia, and stroke. Moreover, gliosis occurs in a great variety of CNS pathologies, including Alzheimer's disease, multiple sclerosis, Parkinson's disease, amyotrophic lateral sclerosis and Huntington's disease [120]. In every case, gliosis implies an alteration in cellular activity which can affect neurons as well as other non-neural cells, causing either a loss of normal functions or a development of damaging ones [121]. In this light, gliosis can be considered not only as a distinguishing feature of many neuropathologies but also as a factor which takes part in several CNS disease mechanisms [122].

3.3.1 Effect of sensor density on eLORETA source localization accuracy

The purpose of this study is to examine the localization accuracy of the eLORETA method applied to HD-EEG of two patients with gliotic lesions. Starting from the 256-channel EEG, three different configurations were extracted. They consist of 18, 64, and 173 electrodes. The comparison of the results shows that an increasing number of electrodes improves the eLORETA source localization accuracy. The subsection is organized as follows: first the methodology is described; then, information about EEG recordings are provided; finally the experimental results are presented and discussed.

Methodology

The brain activity of each patient was computed by LORETA-KEY software (v20170220), using the eLORETA algorithm, for the following frequency bands: delta (0.5–4 Hz), theta (4–8 Hz), alpha1 (8–10.5 Hz), alpha2 (10.5–13 Hz), beta1 (13–18 Hz), beta2 (18–30 Hz), gamma (30–40 Hz), and total band (0.5–40 Hz). The three-dimensional current density distribution was evaluated for three different electrode configurations: 18, 64 and 173 sensors.

Data acquisition system and preprocessing

The dataset consists of two EEGs recorded by the 256-channel HydroCel Geodesic Sensor Net from two patients with gliotic lesions. The HD-EEG montage has been already described in Subsection 3.2.4. The EEGs were recorded during eyes-closed resting conditions. The data were cleaned from artifacts before being processed. The extraction of the three electrode configurations was carried out as explained in Subsection 3.2.5. The EEGs were filtered at 0.5 Hz low cut-off (high-pass) and at 48 Hz high cut-off (low-pass). The sampling rate was set at 100 Hz. The EEG recordings were segmented into artifact free non-overlapping epochs of 256 samples [5]. The EEGs were transformed to a common average reference montage. The data were recorded at IRCCS Centro Neurolesi Bonino-Pulejo of Messina.

Results

Figure 3.19 shows the current density field of patient 1 in beta1 band. All the images reveal that the most activated area is the frontotemporal region. In particular, the images obtained in the case of the 173-channel EEG (Figure 3.19c) best match the structural maps generated by the MRI of patient 1. The area near the gliotic lesions shows a greater activation. This could be caused by the mechanisms of neuroplasticity, according to which new neural connections could be created near the lesion and generate a growth of brain activity. These results suggest that the source localization accuracy improves significantly with the increase of the number of electrodes.

Figure 3.20 displays the current density field of patient 2 in delta band. The pictures show that the application of LORETA to HD-EEG allows to detect sources that are not revealed by the 10–20 configuration. In Figure 3.20a, only the frontotemporal area is active. In Figure 3.20b, a frontoparietal activity in both hemispheres appears. Finally, Figure 3.20c highlights a greater activation in the left frontoparietal area and the sources of the frontotemporal regions previously detected by the 10–20 electrode configuration become barely visible. Also in this case, the images obtained with the 173-channel EEG agree with the structural maps generated by the MRI of patient 2, whose gliotic lesions are placed near the left frontoparietal region.

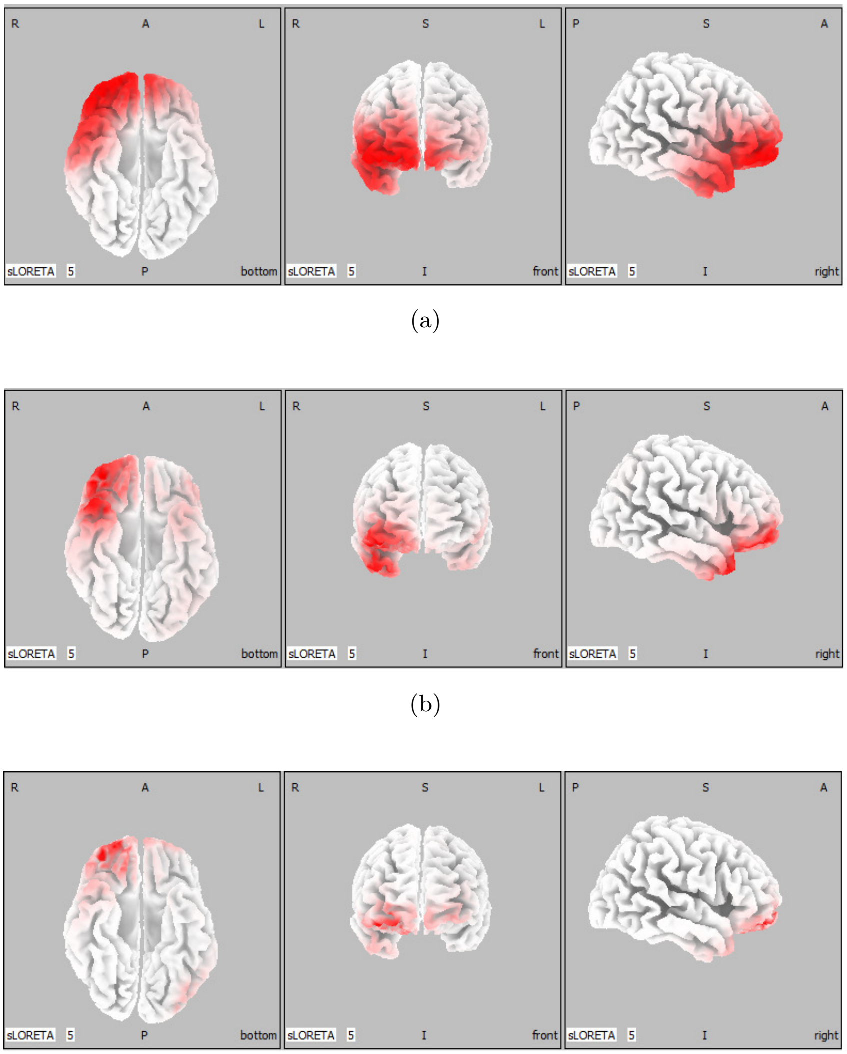

(a)

(b)

(c)

Fig. 3.19: Brain source distribution of patient 1 in beta1 band for (**a**) 18, (**b**) 64 and (**c**) 173 electrodes. On the left: a bottom view of the brain cortex. In the middle: a front view of the brain cortex. On the right: a lateral view of the brain cortex.

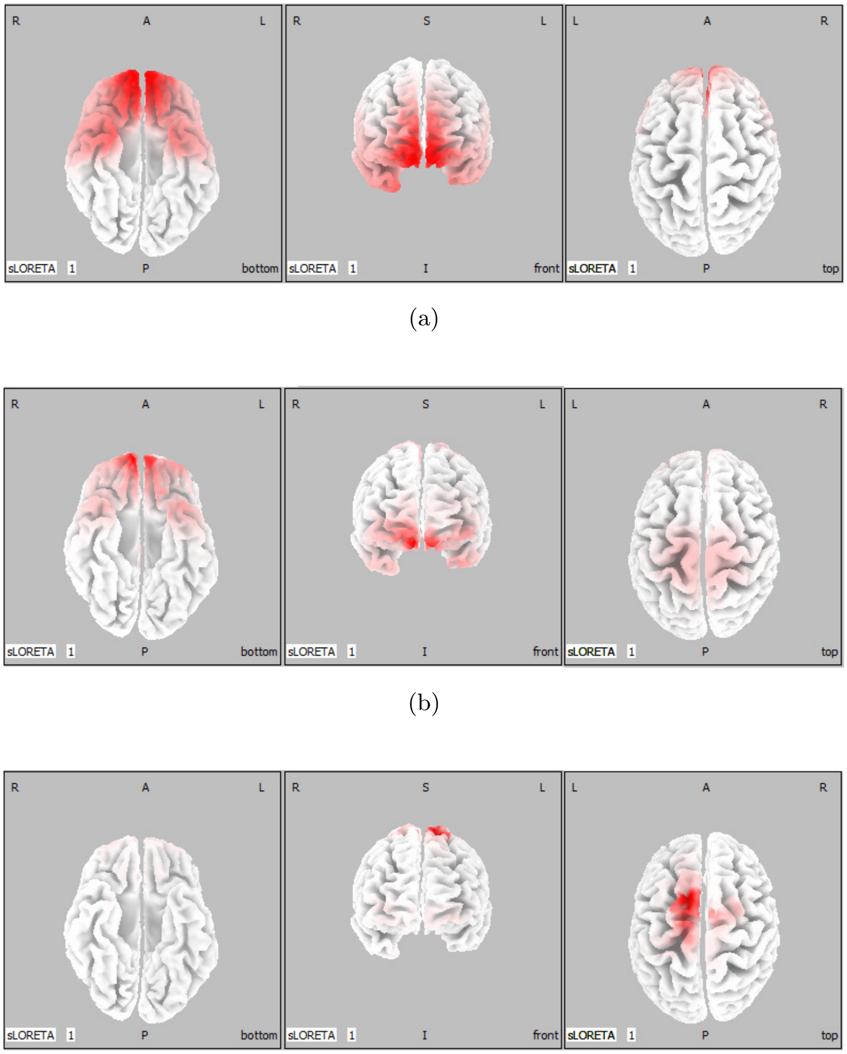

(a)

(b)

(c)

Fig. 3.20: Brain source distribution of patient 2 in delta band for (**a**) 18, (**b**) 64 and (**c**) 173 electrodes. On the left: a bottom view of the brain cortex. In the middle: a front view of the brain cortex. On the right: a top view of the brain cortex.

Conclusions

This study investigated if and how the localization accuracy of the most activated brain regions changes, depending on the number of electrodes. The simulations showed that LORETA improves its performance when the sensor density increases.
In particular, three important aspects arose from this study:

1. the regions with stronger activity detected by the 10–20 system configuration are defined in a better way when a greater number of electrodes are used;
2. a few number of sensors could be not sufficient to detect all active sources;

3. sources marked as significant when the 10–20 system configuration is used could turn out to be less significant when high-density sensor configurations are employed.

The limitation of the current study is that only two EEGs were analyzed. The matter of eLORETA source reconstruction accuracy needs further development using a larger database. In this way, it could be determined the minimum number of electrodes to reconstruct the active sources in an accurate way.

3.4 Applications of LORETA in stroke

Stroke is a leading cause of death and disability. Each year 14 million people suffer their first stroke worldwide and 80 million people living in the world have experienced stroke [123]. Stroke is defined by the World Health Organization as a neurological deficit of cerebrovascular cause that persists beyond 24 hours or is interrupted by death within 24 hours. The 24-hour limit differentiates stroke from transient ischemic attack (TIA), which is a temporary cerebral dysfunction related to stroke symptoms characterized by a swift resolution. Stroke can be classified into two main categories: ischemic, caused by a blockage of the blood flow to the brain, and hemorrhagic, due to the rupture of a blood vessel [124]. Both types leads to the dysfunction of the brain areas affected by the stroke. Signs and symptoms of stroke may include: numbness, confusion, difficulty in speaking or understanding speech, loss of balance or coordination. In most cases, the symptoms affect only one side of the body. The effects of stroke can be very different because they depend on the type, severity and location of the lesions. An early detection associated with a proper medical treatment are essential for reducing stroke outcomes. Finally, the post-stroke rehabilitation represents a very important process for recovering lost function and relearning the skills of everyday life. Even if complete recovery is unusual, rehabilitation can help the patient to regain independence and reintegrate in community life [125].

3.4.1 Effect of post-stroke rehabilitation on cortical reorganization

The purpose of this study is to investigate the cortical response in a sub-acute stroke patient, affected by conduction aphasia, before and after an intensive rehabilitation program. HD-EEG were recorded while the patient was performing language tasks at time T0 (baseline) and at time T1 (after a rehabilitative treatment of two months). The eLORETA active source reconstruction was performed at T0 and T1 for each task. The comparison of the results shows that an intensive rehabilitative therapy can improve inter- and intra-hemispheric cortical reorganization.

The subsection is organized as follows: first, conduction aphasia and the case study are described; then, the data acquisition process and the methodology are explained; finally the results are presented and discussed.

Conduction aphasia

Conduction aphasia is an acquired language disorder, first hypothesized by Carl Wernicke [126]. Conduction aphasia is characterized by normal comprehension, intact speech production, reading, writing, whereas speech repetition is impaired. Aphasic people produce paraphasic errors and show word-finding difficulty [127]. Conduction aphasia is considered as a disconnection syndrome because it is due to an interruption of communication between anterior and posterior language areas [128]. Lesions usually involve the left cerebral hemisphere, as reported in [129]. Several studies proved that the mechanisms of neuroplasticity leads to the recovery from aphasia [130,131]. Moreover, neurophysiological studies showed that the intra- and inter-hemispheric reorganization of the linguistic neural networks occurs after a stroke which involves linguistic areas [132,133]. Finally, the findings about neural reorganization in patients with conduction aphasia have proved the importance of the rehabilitation treatment [134–136].

Description of the case study

This study is concerned with a case of 50-year-old right-handed female affected by conduction aphasia following a left ischemic stroke involving white matter of fronto-parietal lobe and left temporo-occipital regions. One week before the acute cerebral event, she underwent surgical replacement of the aortic valve with mechanical prosthesis. She arrived at the rehabilitative unit of IRCCS Centro Neurolesi Bonino-Pulejo (Messina) one month after the stroke. Neurological, neuropsychological and logopedic assessments were performed. The patient was vigilant, collaborative, time and space oriented. Neurological examination showed right facio-brachio-crural hemiparesis. The patient was treated with a drug therapy of oral anticoagulants and antihypertensive. The rehabilitative treatment consisted of physiotherapeutic, neuropsychological and logopedic training. It was performed every day for a session of 60 min for each rehabilitative treatment.

Data acquisition and methods

EEG data were recorded by the 256-channel HydroCel Geodesic Sensor Net. The HD-EEG montage has been already described in Subsection 3.2.4. The sampling rate was 250 Hz. The EEG data were band-pass filtered between 1 and 40 Hz and cleaned from artifacts by visual inspection. Finally, the EEG recordings were average referenced and segmented into artifact-free non-overlapping epochs of 1 s. HD-EEG were acquired at baseline (T0) and after a rehabilitative treatment of two months (T1). HD-EEG were recorded while the patient was performing specific language tasks displayed on a computer screen in order to set time and use a standard method without the influence of external stimuli. The EEG recordings were carried out during time blocks consisting of five task periods alternating with rest periods. The task paradigm was built by means of E-prime 3.0 software and included the following tasks: naming, repetition, reading, writing, figure description. During the rest periods, the patient was instructed to stay at rest without moving. The naming task consisted in mentioning 24 images, each displayed on the computer screen for 3 s. The images were divided in two groups of 12 alternating to 10 s of rest. The repetition task consisted in repeating 16 words of 5 s, played by audio speakers. The words were divided in two groups of 8 alternating to 10 s of rest. The reading task consisted in reading 16 words of 3 s, displayed on the computer screen. The words were divided in two groups of 8 alternating to 10 s of rest. The writing task consisted of 16 words (6 s duration), displayed on the computer screen, which have to be written on paper. The words were divided in two groups of 8 alternating to 10 s of rest. Finally, the figure description task consisted in looking at a figure for 30 s and then illustrating it. The total duration of the paradigm was 6 min and 52 s.

The source reconstruction was performed by means of the eLORETA algorithm implemented in the LORETA-KEY software (v20200414) for the total band (1–40 Hz). The resting state analysis was conducted on a time segment resulting from the merging of the resting state segments of each task paradigm. The whole procedure was carried out in accordance with the relevant guidelines and regulations. As it is a case report, the ethical approval was not required. The patient signed an informed consent form.

Results

At baseline (T0), the patient suffered from conduction aphasia characterized by a fluent spontaneous language with stereotypes, circumlocutions and linguistic perseverations. Naming and writing were less compromised. After two months of daily speech rehabilitative therapy, the patient showed a significant improvement of aphasic deficit. Specifically, Figure 3.21 displays the difference of the power current density values between T1 and T0. Each image represents the cerebral cortex from six different perspectives. Red and yellow areas denote the most activated brain regions at T1.

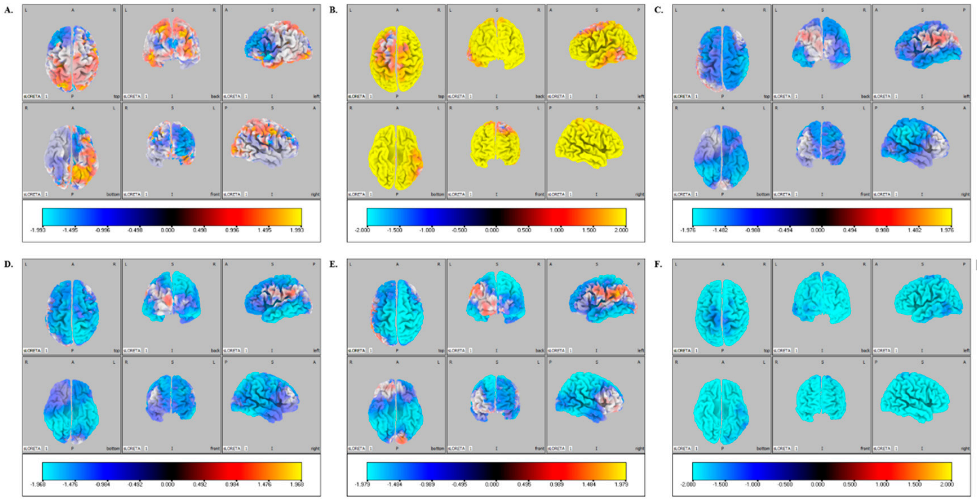

Fig. 3.21: Difference of the power current density values between T1 and T0 for: (**A**) resting state, (**B**) naming task, (**C**) repetition task, (**D**) reading task, (**E**) writing task, (**F**) figure description task. The red/yellow areas denote a greater activation at T1, the blue areas denote a greater activation at T0.

During the resting state, there is a greater activation in the parieto-occipital region at T1 (Figure 3.21A). As for the naming task, a widespread greater activation at T1 is detected (Figure 3.21B). Moreover, the images show a higher cerebral activity in the left parieto-temporo-occipital areas at T1, during the repetition (Figure 3.21C), reading (Figure 3.21D) and writing tasks (Figure 3.21E). Finally, during the figure description task, all brain regions are more active at T0 (Figure 3.21F). The results are consistent with the Aachener Aphasie Test (AAT), which highlighted an improvement in repetition, reading, naming and writing functions.

Conclusions

This study investigated the cortical response generated by speech therapy in a patient with conduction aphasia due to a left ischemic stroke. In fact, it is well known that the left hemisphere is specialized in language functions [137, 138]. The use of HD-EEG, as compared to standard EEG, allows to describe in more detail the asymmetry in the electrical brain activity in stroke patients, as reported in [139]. The results showed that, during the repetition, reading and writing tasks, the left parieto-temporo-occipital areas are more activated after the rehabilitative training. The mechanisms of neuroplasticity lead to the recruitment of new neural patterns to compensate the near injured area [140,141]. These findings revealed that an intensive rehabilitative training in subacute stroke is very useful for language deficit outcome. The results obtained from the HD-EEG recordings are also supported by motor, neuropsychological and speech improvement achieved by the patient after rehabilitation. In conclusion, this study proved that an intensive rehabilitation could contribute to an inter- and intra-hemispheric reorganization in sub-acute stroke patients affected by extensive brain damage involving language areas.

4

Conclusions

EEG is a useful diagnostic tool for recording brain electric signals. The research activity conducted during the PhD course focused on the resolution of the EEG inverse problem by means of the LORETA method. In particular, the brain source localization was performed on EEG recordings collected from subjects affected by the following pathologies: AD, gliosis and stroke. Moreover, it was investigated the effect of the sensor density on the LORETA source localization accuracy. To this purpose, some of the studies reported here provided a comparison between results from HD-EEG vs standard EEG data.
Specifically, the research activities are summarized below.

1. *Active source reconstruction and brain functional connectivity in AD.*
   In this regard, a longitudinal study and two cross-sectional ones were reported:
   - the computation of the power current density by means of the eLORETA algorithm, applied to standard EEG, was carried out to analyze the evolution of the disease. In particular the research involved eight subjects, who were diagnosed with MCI at time T0 and mild AD at time T1 (four months later). Five patients out of eight exhibited an increasing power in delta and theta bands. Seven patients revealed a lower activation in alpha 1 and beta 2 bands. Finally, the power decreased for six patients in alpha 2 and beta 1 bands.
   - the active source localization was performed by the eLORETA method applied to HD-EEG for three groups of subjects: 12 CNT, 23 MCI, 16 AD. The results revealed that EEG recordings of MCI and, even more, of AD were marked by a power increase in delta and theta bands as compared with CNT. It has also been shown that the most activated sources belonged to Brodmann areas typically affected by this pathology and were consistent with it.
   - starting from cortical electrical activity, estimated with eLORETA, the brain functional connectivity was estimated for three groups of subjects: 10 CNT, 21

MCI, 9 AD. The connectivity matrices were computed by means of a toolbox included in the LORETA-KEY software. Then, the small-world properties of the brain networks were evaluated for 84 ROIs considering three different electrode configurations: 173 channels, 64 channels and 18 channels, which were extracted from the HD-EEG configuration. The comparison of the results revealed that the small-world properties of MCI and AD patients were weakened only when HD-EEG were considered. Conversely, the results obtained from the standard low-density EEG were inconsistent with the behavior of the brain networks in AD patients.

2. *Active source reconstruction accuracy in the case of gliosis.*
   In this study two patients with gliotic lesions were considered. The active brain regions were reconstructed by eLORETA for three different configurations, made up of 173, 64 and 18 electrodes. For both patients, the most active sources detected in the case of the HD configuration best match the structural maps generated by the MRI. In fact, because of the mechanisms of neuroplasticity, the areas near the lesions showed an increase in their electrical activity.
3. *Active source reconstruction for investigating the effect of post-stroke rehabilitation.*
   This research proposed a study of pre- and post-rehabilitation brain activity in a sub-acute stroke patient affected by conduction aphasia. HD-EEG data were recorded while the patient was performing several language tasks before and after the therapy. The comparison between the eLORETA images showed that an intensive rehabilitative program can improve inter- and intra-hemispheric cortical reorganization.

Future research involving a larger cohort of subjects, would provide a further validation of the results. It would also be interesting to carry out comparative methodological studies between the LORETA family algorithms.

In conclusion, the findings of the above-mentioned works have shown that LORETA is a powerful method for the resolution of the EEG inverse problem. Finally, it has also been proved that the combination of LORETA with HD-EEG improves the brain source localization accuracy and, consequently, the diagnostic potential of this method in clinical applications.

References

1. A Lenartowicz and RA Poldrack. Brain imaging. 2010.
2. Mario Tudor, Lorainne Tudor, and Katarina Ivana Tudor. Hans berger (1873-1941)–the history of electroencephalography, 2005.
3. Carsten H Wolters, Alfred Anwander, Xavier Tricoche, D Weinstein, Martin A Koch, and Robert S Macleod. Influence of tissue conductivity anisotropy on eeg/meg field and return current computation in a realistic head model: a simulation and visualization study using high-resolution finite element modeling. *NeuroImage*, 30(3):813–826, 2006.
4. Md Kafiul Islam, Amir Rastegarnia, and Zhi Yang. Methods for artifact detection and removal from scalp eeg: A review. *Neurophysiologie Clinique/Clinical Neurophysiology*, 46(4-5):287–305, 2016.
5. Paul L Nunez, Ramesh Srinivasan, Andrew F Westdorp, Ranjith S Wijesinghe, Don M Tucker, Richard B Silberstein, and Peter J Cadusch. Eeg coherency: I: statistics, reference electrode, volume conduction, laplacians, cortical imaging, and interpretation at multiple scales. *Electroencephalography and clinical neurophysiology*, 103(5):499–515, 1997.
6. Federico Chella, Vittorio Pizzella, Filippo Zappasodi, and Laura Marzetti. Impact of the reference choice on scalp eeg connectivity estimation. *Journal of neural engineering*, 13(3):036016, 2016.
7. O Bertrand, F Perrin, and J Pernier. A theoretical justification of the average reference in topographic evoked potential studies. *Electroencephalography and Clinical Neurophysiology/Evoked Potentials Section*, 62(6):462–464, 1985.
8. William O Tatum IV. *Handbook of EEG interpretation*. Demos Medical Publishing, 2014.
9. Herbert H Jasper. The ten-twenty electrode system of the international federation. *Electroencephalogr. Clin. Neurophysiol.*, 10:370–375, 1958.
10. Plonsey Malmivuo, Jaakko Malmivuo, and Robert Plonsey. *Bioelectromagnetism: principles and applications of bioelectric and biomagnetic fields*. Oxford University Press, USA, 1995.
11. KH Levin and P Chauvel. High-resolution eeg. *Clinical Neurophysiology: Basis and Technical Aspects: Handbook of Clinical Neurology Series*, page 185, 2019.

12. Ramesh Srinivasan, Don M Tucker, and Michael Murias. Estimating the spatial nyquist of the human eeg. *Behavior Research Methods, Instruments, & Computers*, 30(1):8–19, 1998.
13. GE Chatrian, E Lettich, and PL Nelson. Ten percent electrode system for topographic studies of spontaneous and evoked eeg activities. *American Journal of EEG technology*, 25(2):83–92, 1985.
14. A Robert Spitzer, Leonardo G Cohen, Judy Fabrikant, and Mark Hallett. A method for determining optimal interelectrode spacing for cerebral topographic mapping. *Electroencephalography and clinical Neurophysiology*, 72(4):355–361, 1989.
15. Don M Tucker. Spatial sampling of head electrical fields: the geodesic sensor net. *Electroencephalography and clinical neurophysiology*, 87(3):154–163, 1993.
16. Walter J Freeman, Mark D Holmes, Brian C Burke, and Sampsa Vanhatalo. Spatial spectra of scalp eeg and emg from awake humans. *Clinical Neurophysiology*, 114(6):1053–1068, 2003.
17. Robert Oostenveld and Peter Praamstra. The five percent electrode system for high-resolution eeg and erp measurements. *Clinical neurophysiology*, 112(4):713–719, 2001.
18. Sylvain Baillet. Forward and inverse problems of meg/eeg. *Encyclopedia of computational neuroscience*, pages 1226–1233, 2015.
19. G Lantz, R Grave De Peralta, L Spinelli, M Seeck, and CM Michel. Epileptic source localization with high density eeg: how many electrodes are needed? *Clinical neurophysiology*, 114(1):63–69, 2003.
20. Christoph M Michel, Micah M Murray, Göran Lantz, Sara Gonzalez, Laurent Spinelli, and Rolando Grave de Peralta. Eeg source imaging. *Clinical neurophysiology*, 115(10):2195–2222, 2004.
21. Willeke Staljanssens, Gregor Strobbe, Roel Van Holen, Gwénaël Birot, Markus Gschwind, Margitta Seeck, Stefaan Vandenberghe, Serge Vulliémoz, and Pieter van Mierlo. Seizure onset zone localization from ictal high-density eeg in refractory focal epilepsy. *Brain topography*, 30(2):257–271, 2017.
22. Jasmine Song, Colin Davey, Catherine Poulsen, Phan Luu, Sergei Turovets, Erik Anderson, Kai Li, and Don Tucker. Eeg source localization: sensor density and head surface coverage. *Journal of neuroscience methods*, 256:9–21, 2015.
23. Roberta Grech, Tracey Cassar, Joseph Muscat, Kenneth P Camilleri, Simon G Fabri, Michalis Zervakis, Petros Xanthopoulos, Vangelis Sakkalis, and Bart Vanrumste. Review on solving the inverse problem in eeg source analysis. *Journal of neuroengineering and rehabilitation*, 5(1):25, 2008.
24. Matti S Hämäläinen and Risto J Ilmoniemi. Interpreting magnetic fields of the brain: minimum norm estimates. *Medical & biological engineering & computing*, 32(1):35–42, 1994.

25. Roberto D Pascual-Marqui, Christoph M Michel, and Dietrich Lehmann. Low resolution electromagnetic tomography: a new method for localizing electrical activity in the brain. *International Journal of psychophysiology*, 18(1):49–65, 1994.
26. J Talairach and P Tournoux. Co-planar stereotaxic atlas of the human brain. 1988. *New York: Theime*, 1988.
27. Roberto Domingo Pascual-Marqui. Review of methods for solving the eeg inverse problem. *International journal of bioelectromagnetism*, 1(1):75–86, 1999.
28. Shanbao Tong and Nitish Vyomesh Thakor. *Quantitative EEG analysis methods and clinical applications*. Artech House, 2009.
29. Andrej Nikolaevich Tikhonov and Vasiliy Yakovlevich Arsenin. Solutions of ill-posed problems. 1977. *WH Winston, Washington, DC*, 330, 1977.
30. Anders M Dale, Arthur K Liu, Bruce R Fischl, Randy L Buckner, John W Belliveau, Jeffrey D Lewine, and Eric Halgren. Dynamic statistical parametric mapping: combining fmri and meg for high-resolution imaging of cortical activity. *Neuron*, 26(1):55–67, 2000.
31. Roberto Domingo Pascual-Marqui et al. Standardized low-resolution brain electromagnetic tomography (sloreta): technical details. *Methods Find Exp Clin Pharmacol*, 24(Suppl D):5–12, 2002.
32. Manfred Fuchs, Jörn Kastner, Michael Wagner, Susan Hawes, and John S Ebersole. A standardized boundary element method volume conductor model. *Clinical Neurophysiology*, 113(5):702–712, 2002.
33. Roberto D Pascual-Marqui. Discrete, 3d distributed, linear imaging methods of electric neuronal activity. part 1: exact, zero error localization. *arXiv preprint arXiv:0710.3341*, 2007.
34. Munsif Ali Jatoi, Nidal Kamel, Aamir Saeed Malik, and Ibrahima Faye. Eeg based brain source localization comparison of sloreta and eloreta. *Australasian physical & engineering sciences in medicine*, 37(4):713–721, 2014.
35. Jun Shigemura, Aihide Yoshino, Yuji Kobayashi, Yoshitomo Takahashi, and Soichiro Nomura. Spatiotemporal differences between cognitive processes of spatially possible and impossible objects: a high-density electrical mapping study. *Cognitive brain research*, 18(3):301–305, 2004.
36. Young Youn Kim, Boreom Lee, Yong Wook Shin, Jun Soo Kwon, and Myung-Sun Kim. Activity of left inferior frontal gyrus related to word repetition effects: Loreta imaging with 128-channel eeg and individual mri. *Neuroimage*, 29(3):712–720, 2006.
37. Christopher A Brown, Ben Seymour, Yvonne Boyle, Wael El-Deredy, and Anthony KP Jones. Modulation of pain ratings by expectation and uncertainty: Behavioral characteristics and anticipatory neural correlates. *Pain*, 135(3):240–250, 2008.
38. Connie Lamm, Lauren K White, Jennifer Martin McDermott, and Nathan A Fox. Neural activation underlying cognitive control in the context of neutral and affectively charged pictures in children. *Brain and cognition*, 79(3):181–187, 2012.

39. Connie Lamm, Olga L Walker, Kathryn A Degnan, Heather A Henderson, Daniel S Pine, Jennifer Martin McDermott, and Nathan A Fox. Cognitive control moderates early childhood temperament in predicting social behavior in 7-year-old children: An erp study. *Developmental science*, 17(5):667–681, 2014.
40. Georg F Meyer, Neil R Harrison, and Sophie M Wuerger. The time course of auditory–visual processing of speech and body actions: Evidence for the simultaneous activation of an extended neural network for semantic processing. *Neuropsychologia*, 51(9):1716–1725, 2013.
41. Emmanuel Tremblay, Phetsamone Vannasing, Marie-Sylvie Roy, Francine Lefebvre, Damelan Kombate, Maryse Lassonde, Franco Lepore, Michelle McKerral, and Anne Gallagher. Delayed early primary visual pathway development in premature infants: high density electrophysiological evidence. *PloS one*, 9(9):e107992, 2014.
42. Anthoula Tsolaki, Vasiliki Kosmidou, Leontios Hadjileontiadis, Ioannis Yiannis Kompatsiaris, and Magda Tsolaki. Brain source localization of mmn, p300 and n400: aging and gender differences. *Brain research*, 1603:32–49, 2015.
43. Anthoula C Tsolaki, Vasiliki E Kosmidou, Ioannis Yiannis Kompatsiaris, Chrysa Papadaniil, Leontios Hadjileontiadis, and Magda Tsolaki. Age-induced differences in brain neural activation elicited by visual emotional stimuli: A high-density eeg study. *Neuroscience*, 340:268–278, 2017.
44. Commission on Classification and Terminology of the International League Against Epilepsy. Proposal for revised classification of epilepsies and epileptic syndromes. *Epilepsia*, 30(4):389–399, 1989.
45. Gang Wang, Gregory Worrell, Lin Yang, Christopher Wilke, and Bin He. Interictal spike analysis of high-density eeg in patients with partial epilepsy. *Clinical neurophysiology*, 122(6):1098–1105, 2011.
46. Abbas Sohrabpour, Yunfeng Lu, Pongkiat Kankirawatana, Jeffrey Blount, Hyunmi Kim, and Bin He. Effect of eeg electrode number on epileptic source localization in pediatric patients. *Clinical Neurophysiology*, 126(3):472–480, 2015.
47. Perrine Bocquillon, Kathy Dujardin, Nacim Betrouni, Valérian Phalempin, Elise Houdayer, Jean-Louis Bourriez, Philippe Derambure, and William Szurhaj. Attention impairment in temporal lobe epilepsy: a neurophysiological approach via analysis of the p300 wave. *Human brain mapping*, 30(7):2267–2277, 2009.
48. Gwénael Birot, Laurent Spinelli, Serge Vulliémoz, Pierre Mégevand, Denis Brunet, Margitta Seeck, and Christoph M Michel. Head model and electrical source imaging: a study of 38 epileptic patients. *NeuroImage: Clinical*, 5:77–83, 2014.
49. Rui Feng, Jie Hu, Li Pan, Jinsong Wu, Liqin Lang, Shize Jiang, Xin Gu, Jun Guo, and Liangfu Zhou. Application of 256-channel dense array electroencephalographic source imaging in presurgical workup of temporal lobe epilepsy. *Clinical Neurophysiology*, 127(1):108–116, 2016.

50. Gülsüm Akdeniz. Electrical source localization by loreta in patients with epilepsy: Confirmation by postoperative mri. *Annals of Indian Academy of Neurology*, 19(1):37, 2016.

51. Petros Nemtsas, Gwenael Birot, Francesca Pittau, Christoph M Michel, Karl Schaller, Serge Vulliemoz, Vasilios K Kimiskidis, and Margitta Seeck. Source localization of ictal epileptic activity based on high-density scalp eeg data. *Epilepsia*, 58(6):1027–1036, 2017.

52. Ching-Chang Kuo, Don M Tucker, Phan Luu, Kevin Jenson, Jeffrey J Tsai, Jeffrey G Ojemann, and Mark D Holmes. Eeg source imaging of epileptic activity at seizure onset. *Epilepsy research*, 146:160–171, 2018.

53. Charis Styliadis, Panagiotis Kartsidis, Evangelos Paraskevopoulos, Andreas A Ioannides, and Panagiotis D Bamidis. Neuroplastic effects of combined computerized physical and cognitive training in elderly individuals at risk for dementia: an eloreta controlled study on resting states. *Neural plasticity*, 2015, 2015.

54. Anthoula C Tsolaki, Vasiliki Kosmidou, Ioannis Yiannis Kompatsiaris, Chrysa Papadaniil, Leontios Hadjileontiadis, Aikaterini Adam, and Magda Tsolaki. Brain source localization of mmn and p300 erps in mild cognitive impairment and alzheimer's disease: a high-density eeg approach. *Neurobiology of aging*, 55:190–201, 2017.

55. Lihua Gu, Jiu Chen, Lijuan Gao, Hao Shu, Zan Wang, Duan Liu, Yanna Yan, Shijiang Li, and Zhijun Zhang. Deficits of visuospatial working memory and executive function in single-versus multiple-domain amnestic mild cognitive impairment: A combined erp and sloreta study. *Clinical Neurophysiology*, 130(5):739–751, 2019.

56. Luke Tait, George Stothart, Elizabeth Coulthard, Jon T Brown, Nina Kazanina, and Marc Goodfellow. Network substrates of cognitive impairment in alzheimer's disease. *Clinical Neurophysiology*, 2019.

57. Diego A Pizzagalli, Lauren A Peccoralo, Richard J Davidson, and Jonathan D Cohen. Resting anterior cingulate activity and abnormal responses to errors in subjects with elevated depressive symptoms: A 128-channel eeg study. *Human brain mapping*, 27(3):185–201, 2006.

58. Randy P Auerbach, Jeremy G Stewart, Colin H Stanton, Erik M Mueller, and Diego A Pizzagalli. Emotion-processing biases and resting eeg activity in depressed adolescents. *Depression and anxiety*, 32(9):693–701, 2015.

59. Randy P Auerbach, Colin H Stanton, Greg Hajcak Proudfit, and Diego A Pizzagalli. Self-referential processing in depressed adolescents: A high-density event-related potential study. *Journal of abnormal psychology*, 124(2):233, 2015.

60. Alexis E Whitton, Pragya Kakani, Dan Foti, Ashlee Van't Veer, Anja Haile, David J Crowley, and Diego A Pizzagalli. Blunted neural responses to reward in remitted major depression: a high-density event-related potential study. *Biological Psychiatry: Cognitive Neuroscience and Neuroimaging*, 1(1):87–95, 2016.

61. Alexis E Whitton, Stephanie Deccy, Manon L Ironside, Poornima Kumar, Miranda Beltzer, and Diego A Pizzagalli. Electroencephalography source functional connectivity reveals abnormal high-frequency communication among large-scale functional networks in

depression. *Biological Psychiatry: Cognitive Neuroscience and Neuroimaging*, 3(1):50–58, 2018.

62. ER Cuspineda, C Machado, T Virues, E Martínez-Montes, A Ojeda, PA Valdés, J Bosch, and L Valdes. Source analysis of alpha rhythm reactivity using loreta imaging with 64-channel eeg and individual mri. *Clinical EEG and neuroscience*, 40(3):150–156, 2009.
63. Yin Fang, Janis J Daly, Jeff Hansley, Wan X Yao, Qi Yang, Jiayang Sun, Ken Hvorat, Svetlana Pundik, and Guang H Yue. Hemispheric activation during planning and execution phases in reaching post stroke: a consort study. *Medicine*, 94(3), 2015.
64. Jacob G McPherson, Albert Chen, Michael D Ellis, Jun Yao, CJ Heckman, and Julius PA Dewald. Progressive recruitment of contralesional cortico-reticulospinal pathways drives motor impairment post stroke. *The Journal of physiology*, 596(7):1211–1225, 2018.
65. Hae-Jeong Park, Jun Soo Kwon, Tak Youn, Ji Soo Pae, Jae-Jin Kim, Myung-Sun Kim, and Kyoo-Seob Ha. Statistical parametric mapping of loreta using high density eeg and individual mri: application to mismatch negativities in schizophrenia. *Human brain mapping*, 17(3):168–178, 2002.
66. Ji Soo Pae, Jun Soo Kwon, Tak Youn, Hae-Jeong Park, Myung Sun Kim, Boreom Lee, and Kwang Suk Park. Loreta imaging of p300 in schizophrenia with individual mri and 128-channel eeg. *Neuroimage*, 20(3):1552–1560, 2003.
67. Jijun Wang, Ken-Ichi Hiramatsu, Hiroto Hokama, Hiroshi Miyazato, and Chikara Ogura. Abnormalities of auditory p300 cortical current density in patients with schizophrenia using high density recording. *International journal of psychophysiology*, 47(3):243–253, 2003.
68. Jijun Wang, Yunxiang Tang, Chunbo Li, Axel Mecklinger, Zeping Xiao, Mingdao Zhang, Yoshio Hirayasu, Hiroto Hokama, and Hui Li. Decreased p300 current source density in drug-naive first episode schizophrenics revealed by high density recording. *International Journal of Psychophysiology*, 75(3):249–257, 2010.
69. JD Gibbons and S Chakraborti. Nonparametric statistical inference springer. 2011.
70. Norman Breslow. A generalized kruskal-wallis test for comparing k samples subject to unequal patterns of censorship. *Biometrika*, 57(3):579–594, 1970.
71. Yosef Hochberg and Ajit C Tamhane. *Multiple comparison procedures*. John Wiley & Sons, Inc., 1987.
72. Robert McGill, John W Tukey, and Wayne A Larsen. Variations of box plots. *The American Statistician*, 32(1):12–16, 1978.
73. Sandra Weintraub, Alissa H Wicklund, and David P Salmon. The neuropsychological profile of alzheimer disease. *Cold Spring Harbor perspectives in medicine*, 2(4):a006171, 2012.
74. Reisa A Sperling, Paul S Aisen, Laurel A Beckett, David A Bennett, Suzanne Craft, Anne M Fagan, Takeshi Iwatsubo, Clifford R Jack Jr, Jeffrey Kaye, Thomas J Montine, et al. Toward defining the preclinical stages of alzheimer's disease: Recommendations

from the national institute on aging-alzheimer's association workgroups on diagnostic guidelines for alzheimer's disease. *Alzheimer's & dementia*, 7(3):280–292, 2011.

75. Marilyn S Albert, Steven T DeKosky, Dennis Dickson, Bruno Dubois, Howard H Feldman, Nick C Fox, Anthony Gamst, David M Holtzman, William J Jagust, Ronald C Petersen, et al. The diagnosis of mild cognitive impairment due to alzheimer's disease: recommendations from the national institute on aging-alzheimer's association workgroups on diagnostic guidelines for alzheimer's disease. *Alzheimer's & dementia*, 7(3):270–279, 2011.
76. Guy M McKhann, David S Knopman, Howard Chertkow, Bradley T Hyman, Clifford R Jack Jr, Claudia H Kawas, William E Klunk, Walter J Koroshetz, Jennifer J Manly, Richard Mayeux, et al. The diagnosis of dementia due to alzheimer's disease: recommendations from the national institute on aging-alzheimer's association workgroups on diagnostic guidelines for alzheimer's disease. *Alzheimer's & dementia*, 7(3):263–269, 2011.
77. PM Rossini, R Di Iorio, F Vecchio, M Anfossi, C Babiloni, M Bozzali, AC Bruni, SF Cappa, J Escudero, FJ Fraga, et al. Early diagnosis of alzheimer's disease: the role of biomarkers including advanced eeg signals analysis. an ifcn-sponsored panel of experts. *Clinical Neurophysiology*, 2020.
78. C Huang, L-O Wahlund, T Dierks, P Julin, B Winblad, and V Jelic. Discrimination of alzheimer's disease and mild cognitive impairment by equivalent eeg sources: a cross-sectional and longitudinal study. *Clinical Neurophysiology*, 111(11):1961–1967, 2000.
79. Davide V Moretti, Claudio Babiloni, Giuliano Binetti, Emanuele Cassetta, Gloria Dal Forno, Florinda Ferreric, Raffaele Ferri, Bartolo Lanuzza, Carlo Miniussi, Flavio Nobili, et al. Individual analysis of eeg frequency and band power in mild alzheimer's disease. *Clinical Neurophysiology*, 115(2):299–308, 2004.
80. K Van der Hiele, AA Vein, RHAM Reijntjes, RGJ Westendorp, ELEM Bollen, MA Van Buchem, JG Van Dijk, and HAM Middelkoop. Eeg correlates in the spectrum of cognitive decline. *Clinical neurophysiology*, 118(9):1931–1939, 2007.
81. Balázs Czigler, Dóra Csikós, Zoltán Hidasi, Zsófia Anna Gaál, Éva Csibri, Éva Kiss, Pál Salacz, and Márk Molnár. Quantitative eeg in early alzheimer's disease patients—power spectrum and complexity features. *International Journal of Psychophysiology*, 68(1):75–80, 2008.
82. Ursula Schreiter Gasser, Valentin Rousson, Frank Hentschel, Heribert Sattel, and Theo Gasser. Alzheimer disease versus mixed dementias: an eeg perspective. *Clinical Neurophysiology*, 119(10):2255–2259, 2008.
83. Fu-Jung Hsiao, Yuh-Jen Wang, Sui-Hing Yan, Wei-Ta Chen, and Yung-Yang Lin. Altered oscillation and synchronization of default-mode network activity in mild alzheimer's disease compared to mild cognitive impairment: an electrophysiological study. *PloS one*, 8(7), 2013.
84. Claudio Babiloni, Giuliano Binetti, Emanuele Cassetta, Daniele Cerboneschi, Gloria Dal Forno, Claudio Del Percio, Florinda Ferreri, Raffaele Ferri, Bartolo Lanuzza, Carlo

Miniussi, et al. Mapping distributed sources of cortical rhythms in mild alzheimer's disease. a multicentric eeg study. *Neuroimage*, 22(1):57–67, 2004.

85. Claudio Babiloni, Giuliano Binetti, Emanuele Cassetta, Gloria Dal Forno, Claudio Del Percio, Florinda Ferreri, Raffaele Ferri, Giovanni Frisoni, Koichi Hirata, Bartolo Lanuzza, et al. Sources of cortical rhythms change as a function of cognitive impairment in pathological aging: a multicenter study. *Clinical neurophysiology*, 117(2):252–268, 2006.
86. Claudio Babiloni, Giovanni B Frisoni, Michela Pievani, Fabrizio Vecchio, Roberta Lizio, Maura Buttiglione, Cristina Geroldi, Claudia Fracassi, Fabrizio Eusebi, Raffaele Ferri, et al. Hippocampal volume and cortical sources of eeg alpha rhythms in mild cognitive impairment and alzheimer disease. *Neuroimage*, 44(1):123–135, 2009.
87. Claudio Babiloni, Roberta Lizio, Filippo Carducci, Fabrizio Vecchio, Alberto Redolfi, Silvia Marino, Gioacchino Tedeschi, Patrizia Montella, Antonio Guizzaro, Fabrizio Esposito, et al. Resting state cortical electroencephalographic rhythms and white matter vascular lesions in subjects with alzheimer's disease: an italian multicenter study. *Journal of Alzheimer's Disease*, 26(2):331–346, 2011.
88. Claudio Babiloni, Filippo Carducci, Roberta Lizio, Fabrizio Vecchio, Annalisa Baglieri, Silvia Bernardini, Enrica Cavedo, Alessandro Bozzao, Carla Buttinelli, Fabrizio Esposito, et al. Resting state cortical electroencephalographic rhythms are related to gray matter volume in subjects with mild cognitive impairment and alzheimer's disease. *Human brain mapping*, 34(6):1427–1446, 2013.
89. Leonides Canuet, Ivan Tellado, Veronica Couceiro, Carmen Fraile, Lucia Fernandez-Novoa, Ryouhei Ishii, Masatoshi Takeda, and Ramon Cacabelos. Resting-state network disruption and apoe genotype in alzheimer's disease: a lagged functional connectivity study. *PloS one*, 7(9):e46289, 2012.
90. Lorena RR Gianotti, Gabriella Künig, Dietrich Lehmann, Pascal L Faber, Roberto D Pascual-Marqui, Kieko Kochi, and Ursula Schreiter-Gasser. Correlation between disease severity and brain electric loreta tomography in alzheimer's disease. *Clinical neurophysiology*, 118(1):186–196, 2007.
91. K Nishida, M Yoshimura, T Isotani, T Yoshida, Y Kitaura, A Saito, H Mii, M Kato, Y Takekita, A Suwa, et al. Differences in quantitative eeg between frontotemporal dementia and alzheimer's disease as revealed by loreta. *Clinical Neurophysiology*, 122(9):1718–1725, 2011.
92. PM Rossini, C Del Percio, P Pasqualetti, E Cassetta, G Binetti, G Dal Forno, F Ferreri, G Frisoni, P Chiovenda, C Miniussi, et al. Conversion from mild cognitive impairment to alzheimer's disease is predicted by sources and coherence of brain electroencephalography rhythms. *Neuroscience*, 143(3):793–803, 2006.
93. Claudio Babiloni, Giovanni B Frisoni, Fabrizio Vecchio, Roberta Lizio, Michela Pievani, Geroldi Cristina, Claudia Fracassi, Fabrizio Vernieri, Guido Rodriguez, Flavio Nobili, et al. Stability of clinical condition in mild cognitive impairment is related to corti-

cal sources of alpha rhythms: an electroencephalographic study. *Human brain mapping*, 32(11):1916–1931, 2011.

94. Claudio Babiloni, Roberta Lizio, Claudio Del Percio, Nicola Marzano, Andrea Soricelli, Elena Salvatore, Raffaele Ferri, Filomena II Cosentino, Gioacchino Tedeschi, Patrizia Montella, et al. Cortical sources of resting state eeg rhythms are sensitive to the progression of early stage alzheimer's disease. *Journal of Alzheimer's Disease*, 34(4):1015–1035, 2013.
95. Munsif Ali Jatoi, Nidal Kamel, Aamir Saeed Malik, Ibrahima Faye, and Tahamina Begum. A survey of methods used for source localization using eeg signals. *Biomedical Signal Processing and Control*, 11:42–52, 2014.
96. Electrical Geodesics. Geodesic sensor net technical manual. *Eugene: Electrical geodesics*, 2007.
97. Mikail Rubinov and Olaf Sporns. Complex network measures of brain connectivity: uses and interpretations. *Neuroimage*, 52(3):1059–1069, 2010.
98. Ana Coito, Melanie Genetti, Francesca Pittau, Giannina R Iannotti, Aljoscha Thomschewski, Yvonne Höller, Eugen Trinka, Roland Wiest, Margitta Seeck, Christoph M Michel, et al. Altered directed functional connectivity in temporal lobe epilepsy in the absence of interictal spikes: a high density eeg study. *Epilepsia*, 57(3):402–411, 2016.
99. Laura Astolfi, F De Vico Fallani, Febo Cincotti, D Mattia, MG Marciani, S Bufalari, S Salinari, Alfredo Colosimo, L Ding, JC Edgar, et al. Imaging functional brain connectivity patterns from high-resolution eeg and fmri via graph theory. *Psychophysiology*, 44(6):880–893, 2007.
100. Danielle Smith Bassett and ED Bullmore. Small-world brain networks. *The neuroscientist*, 12(6):512–523, 2006.
101. Ed Bullmore and Olaf Sporns. Complex brain networks: graph theoretical analysis of structural and functional systems. *Nature reviews neuroscience*, 10(3):186–198, 2009.
102. Jaeseung Jeong. Eeg dynamics in patients with alzheimer's disease. *Clinical neurophysiology*, 115(7):1490–1505, 2004.
103. Thomas König, L Prichep, Thomas Dierks, Daniela Hubl, LO Wahlund, ER John, and V Jelic. Decreased eeg synchronization in alzheimer's disease and mild cognitive impairment. *Neurobiology of aging*, 26(2):165–171, 2005.
104. Ziad Sankari, Hojjat Adeli, and Anahita Adeli. Intrahemispheric, interhemispheric, and distal eeg coherence in alzheimer's disease. *Clinical Neurophysiology*, 122(5):897–906, 2011.
105. Cornelis J Stam, BF Jones, G Nolte, M Breakspear, and Ph Scheltens. Small-world networks and functional connectivity in alzheimer's disease. *Cerebral cortex*, 17(1):92–99, 2007.
106. Yong He, Zhang Chen, Gaolang Gong, and Alan Evans. Neuronal networks in alzheimer's disease. *The Neuroscientist*, 15(4):333–350, 2009.

107. Ruofan Wang, Jiang Wang, Haitao Yu, Xile Wei, Chen Yang, and Bin Deng. Decreased coherence and functional connectivity of electroencephalograph in alzheimer's disease. *Chaos: An Interdisciplinary Journal of Nonlinear Science*, 24(3):033136, 2014.

108. Nadia Mammone, Cosimo Ieracitano, Hojjat Adeli, Alessia Bramanti, and Francesco C Morabito. Permutation jaccard distance-based hierarchical clustering to estimate eeg network density modifications in mci subjects. *IEEE transactions on neural networks and learning systems*, 29(10):5122–5135, 2018.

109. Masahiro Hata, Hiroaki Kazui, Toshihisa Tanaka, Ryouhei Ishii, Leonides Canuet, Roberto D Pascual-Marqui, Yasunori Aoki, Shunichiro Ikeda, Hideki Kanemoto, Kenji Yoshiyama, et al. Functional connectivity assessed by resting state eeg correlates with cognitive decline of alzheimer's disease–an eloreta study. *Clinical Neurophysiology*, 127(2):1269–1278, 2016.

110. Claudio Babiloni, Claudio Del Percio, Roberta Lizio, Giuseppe Noce, Susanna Lopez, Andrea Soricelli, Raffaele Ferri, Maria Teresa Pascarelli, Valentina Catania, Flavio Nobili, et al. Functional cortical source connectivity of resting state electroencephalographic alpha rhythms shows similar abnormalities in patients with mild cognitive impairment due to alzheimer's and parkinson's diseases. *Clinical Neurophysiology*, 129(4):766–782, 2018.

111. Phan Luu and Thomas Ferree. Determination of the hydrocel geodesic sensor nets' average electrode positions and their 10–10 international equivalents. *Inc, Technical Note*, pages 1–11, 2005.

112. Nadia Mammone and Francesco Carlo Morabito. Independent component analysis and high-order statistics for automatic artifact rejection. In *Proceedings. 2005 IEEE International Joint Conference on Neural Networks, 2005.*, volume 4, pages 2447–2452. IEEE, 2005.

113. Roberto D Pascual-Marqui. Instantaneous and lagged measurements of linear and nonlinear dependence between groups of multivariate time series: frequency decomposition. *arXiv preprint arXiv:0711.1455*, 2007.

114. Roberto D Pascual-Marqui, Dietrich Lehmann, Martha Koukkou, Kieko Kochi, Peter Anderer, Bernd Saletu, Hideaki Tanaka, Koichi Hirata, E Roy John, Leslie Prichep, et al. Assessing interactions in the brain with exact low-resolution electromagnetic tomography. *Philosophical Transactions of the Royal Society A: Mathematical, Physical and Engineering Sciences*, 369(1952):3768–3784, 2011.

115. Duncan J Watts and Steven H Strogatz. Collective dynamics of 'small-world'networks. *nature*, 393(6684):440–442, 1998.

116. Paul McCarthy, Lubica Benuskova, and Elizabeth A Franz. The age-related posterior-anterior shift as revealed by voxelwise analysis of functional brain networks. *Frontiers in aging neuroscience*, 6:301, 2014.

117. Meichen Yu, Alida A Gouw, Arjan Hillebrand, Betty M Tijms, Cornelis Jan Stam, Elisabeth CW van Straaten, and Yolande AL Pijnenburg. Different functional connectivity

and network topology in behavioral variant of frontotemporal dementia and alzheimer's disease: an eeg study. *Neurobiology of aging*, 42:150–162, 2016.

118. Katerina D Tzimourta, Nikolaos Giannakeas, Alexandros T Tzallas, Loukas G Astrakas, Theodora Afrantou, Panagiotis Ioannidis, Nikolaos Grigoriadis, Pantelis Angelidis, Dimitrios G Tsalikakis, and Markos G Tsipouras. Eeg window length evaluation for the detection of alzheimer's disease over different brain regions. *Brain sciences*, 9(4):81, 2019.

119. Carlo Miniussi and Gregor Thut. Combining tms and eeg offers new prospects in cognitive neuroscience. *Brain topography*, 22(4):249, 2010.

120. Michael K McMillian, Linda Thai, JS Hong, James P O'Callaghan, and Keith R Pennypacker. Brain injury in a dish: a model for reactive gliosis. *Trends in neurosciences*, 17(4):138–142, 1994.

121. Michael V Sofroniew and Harry V Vinters. Astrocytes: biology and pathology. *Acta neuropathologica*, 119(1):7–35, 2010.

122. Mary E Hamby and Michael V Sofroniew. Reactive astrocytes as therapeutic targets for cns disorders. *Neurotherapeutics*, 7(4):494–506, 2010.

123. World Stroke Organization. *Annual Report 2019*. `https://www.world-stroke.org`.

124. World Health Organization et al. *Cerebrovascular disorders: a clinical and research classification*. World Health Organization, 1978.

125. Glen E Gresham, William B Stason, and Pamela W Duncan. *Post-stroke rehabilitation*, volume 95. Diane Publishing, 2004.

126. Carl Wernicke. *Der aphasische Symptomencomplex: eine psychologische Studie auf anatomischer Basis*. Cohn & Weigert, 1874.

127. Alfredo Ardila. A review of conduction aphasia. *Current neurology and neuroscience reports*, 10(6):499–503, 2010.

128. Norman Geschwind. Disconnexion syndromes in animals and man. *Brain*, 88(3):585–585, 1965.

129. Gregory Hickok, Peter Erhard, Jan Kassubek, A Kate Helms-Tillery, Susan Naeve-Velguth, John P Strupp, Peter L Strick, and Kamil Ugurbil. A functional magnetic resonance imaging study of the role of left posterior superior temporal gyrus in speech production: implications for the explanation of conduction aphasia. *Neuroscience letters*, 287(2):156–160, 2000.

130. Alessandro Angrilli, Thomas Elbert, Stefano Cusumano, Luciano Stegagno, and Brigitte Rockstroh. Temporal dynamics of linguistic processes are reorganized in aphasics' cortex: an eeg mapping study. *Neuroimage*, 20(2):657–666, 2003.

131. Joshua I Breier, Eduardo M Castillo, Corwin Boake, Rebecca Billingsley, Lynn Maher, Gerard Francisco, and Andrew C Papanicolaou. Spatiotemporal patterns of language-specific brain activity in patients with chronic aphasia after stroke using magnetoencephalography. *Neuroimage*, 23(4):1308–1316, 2004.

132. Simone Sarasso, Sara Määttä, Fabio Ferrarelli, Rositsa Poryazova, Giulio Tononi, and Steven L Small. Plastic changes following imitation-based speech and language therapy for

aphasia: a high-density sleep eeg study. *Neurorehabilitation and neural repair*, 28(2):129–138, 2014.

133. Chiara Spironelli and Alessandro Angrilli. Brain plasticity in aphasic patients: intra- and inter-hemispheric reorganisation of the whole linguistic network probed by n150 and n350 components. *Scientific reports*, 5(1):1–14, 2015.
134. Cynthia K Thompson and Dirk-Bart den Ouden. Neuroimaging and recovery of language in aphasia. *Current Neurology and Neuroscience Reports*, 8(6):475, 2008.
135. Flavia Mattioli, Claudia Ambrosi, Lorella Mascaro, Cristina Scarpazza, Patrizia Pasquali, Marina Frugoni, Mauro Magoni, Laura Biagi, and Roberto Gasparotti. Early aphasia rehabilitation is associated with functional reactivation of the left inferior frontal gyrus: a pilot study. *Stroke*, 45(2):545–552, 2014.
136. James D Stefaniak, Ajay D Halai, and Matthew A Lambon Ralph. The neural and neurocomputational bases of recovery from post-stroke aphasia. *Nature Reviews Neurology*, 16(1):43–55, 2020.
137. Gregory Hickok, Tracy Love-Geffen, and Edward S Klima. Role of the left hemisphere in sign language comprehension. *Brain and Language*, 82(2):167–178, 2002.
138. Mathieu Vigneau, Virginie Beaucousin, Pierre-Yves Herve, Hugues Duffau, Fabrice Crivello, Olivier Houde, Bernard Mazoyer, and Nathalie Tzourio-Mazoyer. Meta-analyzing left hemisphere language areas: phonology, semantics, and sentence processing. *Neuroimage*, 30(4):1414–1432, 2006.
139. Nadia Mammone, Simona De Salvo, Cosimo Ieracitano, Silvia Marino, Emanuele Cartella, Alessia Bramanti, Roberto Giorgianni, and Francesco C Morabito. Compressibility of high-density eeg signals in stroke patients. *Sensors*, 18(12):4107, 2018.
140. Ian H Robertson and Jaap MJ Murre. Rehabilitation of brain damage: brain plasticity and principles of guided recovery. *Psychological bulletin*, 125(5):544, 1999.
141. PM Rossini, C Altamura, F Ferreri, J Melgari, F Tecchio, M Tombini, P Pasqualetti, and F Vernieri. Neuroimaging experimental studies on brain plasticity in recovery from stroke. *Europa medicophysica*, 43(2):241, 2007.